Smart Wearable IoT and Multi-Sensor Fusion for Firefighting

Submitted July, 2024, in partial fulfillment of
the conditions for the award of the degree **Doctor of Philosophy.**

Xiaoqing Chai
20382385

Supervised by:

Dr Boon Giin Lee
Dr Matthew Pike
Dr David Chieng

School of Computer Science, University of Nottingham Ningbo China

Abstract

Human Activity Recognition (HAR) algorithms have shown promise in firefighter risk assessment and behaviour monitoring. However, existing studies on HAR had not adequately addressed several critical challenges specific to firefighting scenarios. While various deep learning (DL) methods were proposed to increase classification accuracy, the more pressing needs in firefighting contexts were fast computation and timely notification. In addition, current HAR solutions were found to be unsuitable for recognizing the complex activities involved in firefighting. This thesis utilises multi-sensory fusion methods to explore advanced IoT-based wearable firefighter risk assessment system (FRAS) deployed with fall detection system (FDS) and firefighting activity recognition (FAR) algorithms. The research work consists of three associated studies that aim to answer the formulated research questions. The first study focuses on improving the accuracy and efficiency of a multi-IMU-based FDS using a novel attitude feature extraction (AFE) method. The second study introduces a pre-impact FDS (PI-FDS) model, which employed a dynamic thresholding method to tackle the issue of class imbalance. This study also investigate the feasibility of utilizing ensemble learning (EL) methods at the edge to increase real-time FAR performance. The last study presents a design and implementation of Internet of Things (IoT)-based wearable FAR system (IoT-FAR) for FAR remote monitoring. IoT-FAR explores the significance of adopting surface electromyography (sEMG), heart rate, and IMU features on the complex FAR. Results demonstrate that the proposed hybrid machine learning (HML)-based model outperforms existing state-of-the-art approaches with a mean accuracy of 98.29%. The IoT-based wearable FAR extends the application of HAR from healthcare to firefighting and serves as an inspiration for further research in other fields.

Acknowledgements

I would like to start by expressing my profound gratitude to my team of supervisors, Dr. Boon Giin Lee, Dr. Matthew Pike, and Dr. David Chieng. Their invaluable guidance, unwavering support, and insightful advice have been crucial to my research journey. I want to extend my deepest appreciation to Dr. Boon Giin Lee for his patient, hands-on guidance in academic research and writing that helped me achieve publications. His passion for academic research has profoundly influenced and inspired me, instilling a greater sense of enthusiasm and dedication in my research.

I would also like to extend my sincere thanks to the collaborators for my research: Ting Jiang, the Director of the Huzhou Fire Department; all firefighters from Nantaihu Fire Brigade, Huzhou, Zhejiang, and their leader Pengfei Dou; and all firefighters from Haishu Fire Brigade, Ningbo, Zhejiang, and their leader Hangchao Jin. Their participation and assistance in data collection, experimentation, and professional guidance have been indispensable in this research.

I am also profoundly thankful to all members of the In-The-Wild Lab for the precious and enjoyable times we experienced together both in the lab and in daily life.

Finally, I owe my deepest gratitude to my beloved wife and parents. Your unconditional love, support, and sacrifices have laid the foundation for all my accomplishments. You have always been my greatest supporters and have instilled in me the values of hard work, perseverance, and dedication. Thank you for believing in me and always being there when I needed you the most.

To all of you, thank you from the bottom of my heart. This thesis would not have been possible without your support and encouragement.

Publications

Journals

1. **Chai, X.**, Lee, B. G., Hu, C., Pike, M., Chieng, D., Wu, R., & Chung, W. Y. (2024). IoT-FAR: A multi-sensor fusion approach for IoT-based firefighting activity recognition. Information Fusion, 2025, vol.113, 102650. https://doi.org/10.1016/j.inffus.2024.102650

2. Wu, R., Lee, B. G., Pike, M., Zhu, L., & **Chai, X.** (2024). Multi-INS: A Novel Approach Integrating Online Magnetic Fingerprints for Multi-Person Inertial Navigation Systems. IEEE Transactions on Systems, Man, and Cybernetics: Systems. (Under Review)

3. **Chai, X.**, Lee, B. G., Pike, M., Wu, R., Chieng, D., & Chung, W. Y. (2023). Pre-Impact Firefighter Fall Detection Using Machine Learning on the Edge. IEEE Sensors Journal, 23(13), 14997-15009. https://doi.org/10.1109/JSEN.2023.3279858

4. Wu, R., Lee, B. G., Pike, M., Zhu, L., **Chai, X.**, Huang, L., & Wu, X. (2022). IOAM: a novel sensor fusion-based wearable for localization and mapping. Remote Sensing, 14(23), Article 6081. https://doi.org/10.3390/rs14236081

5. **Chai, X.**, Wu, R., Pike, M., Jin, H., Chung, W. Y., & Lee, B. G. (2021). Smart Wearables with Sensor Fusion for Fall Detection in Firefighting. Sensors 2021, 21, 6770. https://doi.org/10.3390/s21206770

Conference Proceedings

1. Wang, Y., Lee, B. G., Pei, H., **Chai, X.**, & Chung, W. Y. (2024). Smart IoT-based Wearable Lower-Limb Rehabilitation Assistance System. Intelligent Human Computer Interaction. IHCI 2023. Lecture Notes in Computer Science, vol 14532. Springer, Cham. https://doi.org/10.1007/978-3-031-53830-8_24

2. Lee, B. G., Wu, R., Xu, F., Zhu, L., **Chai, X.**, & Pike, M. (2023). Comparative Analysis of Wireless Transmission Methods for Firefighting Communication in Challenging Indoor Environments. In 2023 IEEE Region 10 Conference (TENCON 2023), Chiang Mai, Thailand, 2023, pp. 1070-1075. https://doi.org/58879.2023.10322361

3. Wu, R., Lee, B. G., Pike, M., Zhu, L., **Chai, X.** & Wang, Y. (2023). Enhancing DF-INS for Accurate Zero-Velocity Detection in ILBS: A Dual Foot Synergistic Method. In 2023 IEEE SENSORS, Vienna, Austria, 2023, pp. 1-4. https://doi.org/10.1109/SENSORS56945.2023.10325168

4. Wu, R., Pike, M., **Chai, X.**, Lee, B. G., Chung, W. Y. & Nkenyereye, L. (2023). GA-PDR: Using Gait Analysis for Heading Estimation in PDR Based Indoor Localization System. In 49th Annual Conference of the IEEE Industrial Electronics Society (IECON 2023), Singapore, Singapore, 2023, pp. 1-6. https://doi.org/10.1109/IECON51785.2023.10312643

5. **Chai, X.**, Lee, B. G., Pike, M., & Chieng, D. (2023). Wearable Fall Detection System for Firefighters based on Gesture Feature Extraction. In 2023 8th International Symposium on Sensor Science-China, I3S-CN 2023.

6. **Chai, X.**, Lee, B. G., Pike, M., Wu, R., & Wu, X. (2023). A Novel Attitude Feature Extraction Method for Multi-IMU Based Fall Detection System. In 2023 IEEE 3rd International Conference on Power, Electronics and Computer Applications, ICPECA 2023, pp. 99-103. https://doi.org/10.1109/ICPECA56706.2023.10075997

7. Wu, R., Pike, M., **Chai, X.**, Lee, B. G., & Wu, X. (2022). SLAM-ING: A Wearable SLAM Inertial NaviGation System. In 2022 IEEE Sensors, Dallas, TX, USA, 2022, pp. 01-04. https://doi.org/10.1109/SENSORS52175.2022.9967255

8. **Chai, X.**, Lee, B. G., Pike, M., Wu, R., & Chung, W. Y. (2022). A Smart Wearable Fall Detection System for Firefighters Using V-RNN. Intelligent Human Computer Interaction. IHCI 2021. Lecture Notes in Computer Science, vol 13184. Springer, Cham. https://doi.org/10.1007/978-3-030-98404-5_12

Patents

1. Boon Giin Lee, Renjie Wu, **Xiaoqing Chai**, Yongfu Wang. A New Type of Infrared Thermal Imaging Surveillance Camera. Chinese Utility Patent 2023222326525, Feb. 23, 2024. Publication No. CN220528134U. (Granted) (一种新型热成像监控摄像机)

2. Boon Giin Lee, Yongfu Wang, **Xiaoqing Chai**. A Flexible Wearable Lower Limb Rehabilitation Assistance System and Its Analysis Method. Chinese Patent 2024101903593, Feb. 20, 2024. (Under Review) (一种柔性可穿戴下肢康复辅助系统及分析方法)

3. Boon Giin Lee, Renjie Wu, **Xiaoqing Chai**, Linzhen Zhu. A Novel Infrared Thermal Imaging Glasses. Chinese Utility Patent 2023210014950, Aug. 25, 2023. Publication No. CN219590611U. (Granted) (一种新型红外热成像眼镜)

4. **Xiaoqing Chai**, Boon Giin Lee, Matthew Pike. A Wearable Device for Fall Detection. Chinese Utility Patent 2022207836495, Mar. 24, 2023. Publication No. CN218684386U. (Granted) (一种用于跌倒检测的可穿戴设备)

5. Boon Giin Lee, Shuhe Zhang, Renjie Wu, **Xiaoqing Chai**, et al. A Method, Apparatus, Electronic Device, and Storage Medium for Multi-User Collaborative Positioning. China Patent 2023102744373, Mar. 21, 2023. (Under Review) (一种多用户协同定位方法、装置、电子设备及存储介质)

6. Boon Giin Lee, Renjie Wu, Matthew Pike, **Xiaoqing Chai**. Ultrasonic Wave-Based Indoor Inertial Navigation Mapping Method and System. US Patent 47560776 (7430), Feb. 21, 2023. (Under Review)

7. Boon Giin Lee, Renjie Wu, Matthew Pike, **Xiaoqing Chai**. A Method, Apparatus, and System for Motion Trajectory Determination. Chinese Patent 2022101129705,

Jan. 29, 2022. Publication No. CN114485647A. (Granted) (一种运动轨迹确定方法、装置及系统)

8. **Xiaoqing Chai**. Firefighter Safety Risk Evaluation System Software. Chinese Software Copyright 2022SR0363015, Dec. 23, 2021. (Granted) (消防员安全检测系统软件)

Awards

1. **Innovation and Entrepreneurship Award**. Ningbo Computer Federation, 2023. （2023年宁波计算机学会大学生计算机创新创业奖）(Project title: Advanced Wearable Firefighting Combat System with Sensor Fusion)

2. **Silver Medal** in the 7^{th} Ningbo National Selection Competition for Young College Student Entrepreneurship. （2023年第七届宁波面向全国青年大学生创业大赛银奖）(Project title: Advanced Wearable Firefighting Combat System with Sensor Fusion)

3. **Third Prize** in the 2023 "Maker China" SME Innovation & Entrepreneurship Competition Advanced Manufacturing Special Race. （2023年"农行杯"第八届"创客中国"宁波市中小企业创新创业大赛先进制造专题赛创客组三等奖）(Project title: Advanced Wearable Firefighting Combat System with Sensor Fusion)

4. **National Gold Medal** in the 8^{th} China International College Students' 'Internet+' Innovation and Entrepreneurship Competition in 2022. （2022年第八届中国国际"互联网+"大学生创新创业大赛研究生创意组金奖）(Project title: Firefighting Defender - The Initiative Multi-sensory Fusion Based Smart Firefighter's Safety System Supplier in China)

5. **Best Session Paper Award** at the 13^{th} International Conference on Intelligent Human Computer Interaction (IHCI 2021). (Project title: A Smart Wearable Fall Detection System for Firefighters Using V-RNN)

Contents

List of Figures

List of Tables

List of Abbreviations

ADL	Activity of Daily Living
AFE	Attitude Feature Extraction
AHRS	Attitude and Heading Reference System
BLE	Bluetooth Low Energy
BMV	Boyer-Moore Voting
DL	Deep learning
DoF	Degree of Freedom
EL	Ensemble Learning
EMG	Electromyography
FAR	Firefighting Activity Recognition
FDS	Fall Detection System
FRAS	Firefighter Risk Assessment System
HAR	Human Activity Recognition
IC	Incident Commander
IMU	Inertial Measurement Unit
IoF	Internet of Firefighting
IoT	Internet of Things
LoRa	Long-Range Radio
LSTM	Long-Short Term Memory
ML	Machine Learning
PASS	Personal Alert Safety System
PIFDS	Pre-Impact Fall Detection System
PPC	Personal Protective Clothing
RNN	Recurrent Neural Network
SCBA	Self-contained Breathing Apparatus
WBSN	Wireless Body Sensor Network

Chapter 1

Introduction

1.1 Overview

1.1.1 Firefighter Safety Risk Assessment Approaches

Firefighting, a demanding and hazardous profession, requires significant physical and mental fitness alongside professional competence to perform effective rescues. The Annual Firefighting Report in China [3] reported 111 firefighter casualties between 2010 and 2020, with an average age of only 27 years. Inadequate training and practical experience, leading to poor decision-making, significantly contributed to these injuries [4]. The 2019 annual report from the International Association of Fire and Rescue Services (CTIF) [5] indicated that, out of 7,630,000 firefighters in China, only 130,000 (1.7%) are career firefighters, while the rest are volunteers. In contrast, in the USA, approximately 33.2% of firefighters (370,000 out of 1,115,000) were professionals. These young volunteer firefighters in China, with limited training and experience, often struggle to master complex firefighting skills, especially in dangerous situations like burning floors or unstable building structures [6].

Specialised firefighting training is crucial for improving young firefighters' rescue skills, physical fitness, and tactical capabilities. Nonetheless, the scientific rigor of the training approach significantly influences firefighters' physical aptitude and combat effectiveness. Research reveals a lack of innovative physical fitness training within many fire brigades, with a reliance on traditional military methods, which poses challenges in

increasing the motivation of firefighters to conduct proper fitness training [7]. In addition, studies show that traditional training methods significantly contribute to firefighter fatigue [8].

Falling activities, including being struck, collapsing, and fainting, are primary causes of firefighter fatalities in China (see Figure 1.1a) [9]. In the United States in 2018, overexertion and stress are the leading causes of firefighter deaths, according to a US National Fire Protection Association (NFPA) report (see Figure 1.1b) [10]. One significant reason for this difference is the need for improvements in personal protective equipment (PPE) for fall detection to better ensure the safety of the firefighters [6].

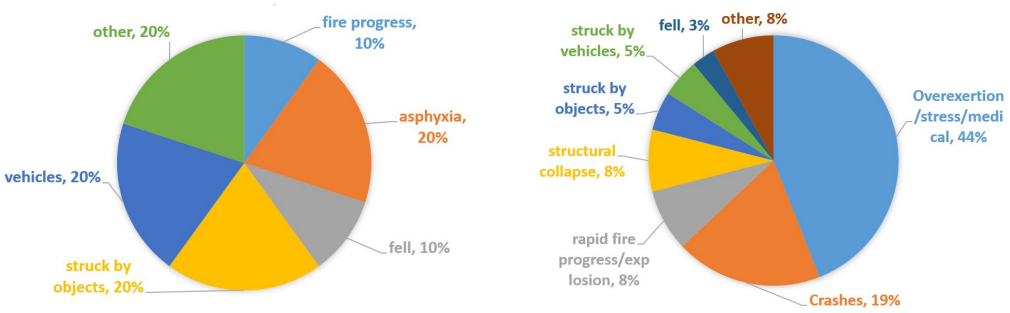

(a) (b)

Figure 1.1: Comparison of the causes of firefighter fatalities in 2018 in (a) China, and (b) the USA.

The current firefighter risk assessment system (FRAS) in use in China is a standard personal-alert safety system (PASS) device for detecting a firefighter's immobility (see Figure 1.2). This device emits a high-volume audible alert if no motion is detected after a short period, typically 30 seconds. Although the PASS device has been widely used globally, it has several drawbacks [11], including:

- A long delay (typically 30 seconds of motionlessness) before the alarm is raised,

increasing the rescue time and reducing the likelihood of a successful rescue.

- Lack of networking capability to notify the incident commander's (IC) in-time for coordinating resources effectively.

- Susceptibility to environmental factors that prevent other firefighters from hearing the alarm, further delaying the rescue.

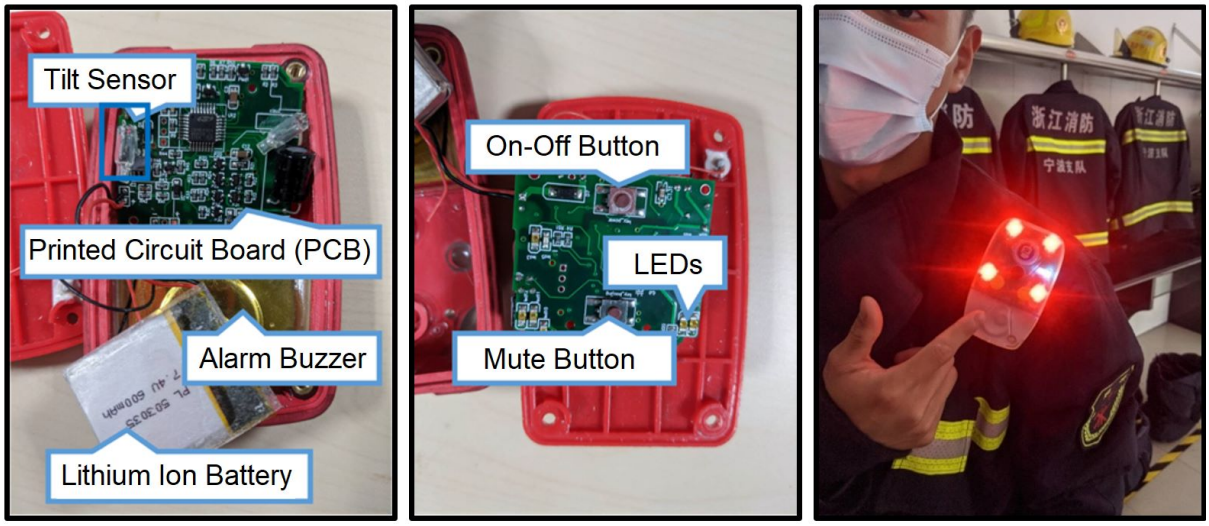

Figure 1.2: PASS device equipped by a firefighter in China.

In many recorded fatalities, the IC is unaware of a fallen firefighter, preventing timely rescue efforts. The smoke-filled environment also decreases firefighters' ability to identify a peer's injuries promptly. Generally, the principle of firefighter education in China emphasises learning and gaining experience through actual firefighting tasks, posing high risks to their life and safety [4], especially for those young and under-trained firefighters. These challenges underscore the importance of developing a smart FRAS to enhance firefighter safety during missions. In particular, FRAS with motion analysis can timely monitor firefighter activities, ensuring their safety and optimising their performance in firefighting scenarios.

1.1.2 Human Activity Recognition

Over the last decade, human activity recognition (HAR) has gathered significant interest within the research community, evolving into a crucial subject across various fields. It has been applied in many applications [12], such as healthcare for patient monitoring, sports for performance analysis, and high-risk occupations for danger recognition, surveillance, robotics and others. HAR adopts the sensor fusion method, which focuses on distinguishing human behaviour by analysing data gathered from distinct sensors [13]. Some HAR studies focus on classifying routine activities of daily living (ADLs), such as walking, running, and jogging [14]. Nevertheless, enhancing classification performance for more complex activities remains a significant challenge that continues to attract research attention.

The inertial measurement unit (IMU) is widely used in HAR, typically comprising an accelerometer, a gyroscope, and a magnetometer. There are tri-axial IMU with nine-degree-of-freedom (9-DOF), and bi-axial IMU with 6-DOF (without a magnetometer). Due to the form factor of IMUs, previous studies mostly focus on the IMUs designed as wrist or pocket devices [15, 16, 17], belts [18, 19, 20] and head-mounted systems [21]. These devices are mainly utilised for user motion analysis, location prediction, environmental information collection, and human-object interaction [22].

Fall detection systems (FDS) have developed rapidly over the past decades as part of the HAR. These systems aim to distinguish fall activities from ADLs, signaling abnormal or dangerous situations and triggering a warning alert to inform users or concerned parties [23]. Researchers have emphasised the importance of developing wearable FDS for firefighters to detect fall-related risks. Pham *et al.* [24] designed a waist-worn PASS

device equipped with a tri-axial accelerometer and a carbon monoxide sensor. They later enhanced the PASS device by embedding an additional barometer for fall detection [25]. However, the activities collected are still insufficient to realistically simulate falls, and the datasets are not publicly available.

Beyond fall detection, HAR has the potential to enhance firefighter safety in various ways. For instance, HAR can provide effective feedback to IC and command centres, enabling the monitoring of firefighters' behaviour during operations, thereby assessing their risks and enhancing their safety. Additionally, understanding specific firefighter activities helps IC allocate resources more effectively and make prompt adjustments, ensuring firefighters are supported efficiently. Furthermore, HAR can aggregate performance data over time, offering personalised post-mission feedback and evaluation. This helps firefighters understand their physical fitness limits and potentially develop customised training improvement plans.

1.2 Research Questions

Developing effective FDS and HAR models for wearable-based FRAS can significantly enhance risk assessment in firefighting contexts. Despite numerous studies on wearable HAR and FDS, most are designed for healthcare or Ambient Assisted Living (AAL) purposes. Several research challenges arise when applying HAR in firefighting contexts.

First, firefighting actions differ from ADLs due to their intensity and rapidity. This intensity results in similar motion data for normal and abnormal behaviours, leading to possible misclassification. For instance, existing FDSs target falls from stationary poses like standing or sitting, but perform poorly in distinguishing falls from fall-related be-

haviours in firefighting, such as walking with a stoop or crouching. Safety risk assessment in firefighting demands high accuracy since false alerts can reduce firefighting efficiency. Typical FDS with a single sensor may not meet this requirement, whereas multi-sensory approaches need further examination of the type of utilised sensor and the wearable design. In addition, achieving timely risk alerting is also crucial, which requires high-efficiency classification models to detect falls from different positions.

Second, recent research focused on the development of next-generation FDS, known as pre-impact FDS (PI-FDS), designed to detect the PI phase of a fall and initiate preventative actions. This advanced algorithm had the potential to improve fall risk detection, but several challenges remained. Effectively detecting the PI phase and promptly notifying the IC were critical tasks that required further attention. While previous studies on PI-FDS primarily executed algorithms on high-performance computers, few addressed the importance of processing time in real-time scenarios. In addition, the immediate transmission of information to the IC following PI-FDS detection posed significant challenges, particularly in maintaining stable and reliable wireless communication in large-scale fire scenarios, such as underground rescues and forest fires. For instance, the BLE transmission approach, while energy-efficient, could result in data transmission delays or losses over long distances in such scenarios. On the other hand, using Wi-Fi would provide more reliable connectivity but at the cost of higher power consumption.

Third, the application of HAR in firefighting missions presents distinct challenges compared to its application in ADLs. These challenges stem from the complexity of high-intensity and fast-paced firefighting activities. For instance, firefighters need to carry two reels of heavy hoses, increasing their burden in performing firefighting tasks. Although recent studies emphasise deep learning (DL)-based approaches for enhanced recognition

accuracy, these methods come with increased computational costs and are not applicable for time-critical firefighting applications [26].

In response to these challenges, this work targets on developing effective HAR models for the safety risk assessment of firefighters, through addressing the following three research questions (RQs), including:

RQ1: How can a reliable model be designed for assessing firefighter risk?

RQ2: How can the PI-FDS model be designed for practical firefighting scenarios?

RQ3: How can an efficient FAR model be designed to accurately distinguish between firefighting activities?

1.3 Research Objectives

This study aims to propose a wearable IoT-based FRAS using advanced sensing technologies to enhance the detection of safety risks, recognise firefighter activities, and provide timely information to the IC outside the fireground. The study focuses on three specific research objectives (ROs) to address the aforementioned RQs, as outlined below:

RO1: To Design a Fall Detection Model for Firefighters as Safety Risk Assessment

The primary goal is to develop a wearable motion recognition model that detects abnormal situation alerts rather than traditional immobility alerts from PASS devices. Considering that fall-related dangers are a leading cause of firefighter casualties, it is critical to develop a highly accurate safety risk assessment model targeting fall scenarios. This involves designing a robust FDS capable of distinguishing various types of fall events. Fall-like activities are considered in this study with the aim to

minimise false alerts. The focus of the study includes sensing approaches, sensor placement, data processing, and classification methods.

RO2: To Explore the Design of an Effective PI-FDS Framework for Firefighting Applications

The advanced PI-FDS model is designed to enhance fall risk detection response, yet current studies have proven inadequate for firefighting contexts, primarily due to the need for rapid response and the diverse nature of firefighting environments. This objective aims to investigate the practical application of the FRAS integrated with the PI-FDS algorithm by proposing an effective system framework suited to real-world firefighting scenarios. Key considerations included ensuring reliable wireless transmission from indoor to outdoor environments and developing a PI-FDS model capable of operating on lightweight hardware with minimal computational requirements to maintain efficiency.

RO3: To Identify Firefighter Activities through Behavioural Analysis Using a Multi-Sensor Fusion Approach

The final objective focuses on improving the FRAS by designing a HAR model capable of distinguishing firefighting activities. Through HAR, the IC could monitor firefighters' behaviour during operations, detect potential risks promptly, and assess task performance. For instance, observing firefighters as they ascend or descend stairs could provide indirect insights into the structural integrity of burning buildings. These high-intensity firefighting activities are markedly different from those commonly studied in HAR research, which typically focuses on ADLs.

1.4 Research Methodologies

To address the RQs, the proposed FRAS was designed, developed, and evaluated through a series of three studies, as shown in Figure 1.3. The first study (RS1) focuses on the development of a multi-sensor-based FDS to address RQ1, emphasizing the classification accuracy and efficiency of the system for firefighters. For RQ2, the second study (RS2) introduces an IoT-based firefighting framework (IoF) tailored to firefighting scenarios, where the PI-FDS algorithms are evaluated on an edge device. Finally, the third study (RS3) aims to develop a FAR algorithm using multi-sensor data to monitor firefighters' behaviours, specifically addressing RQ3.

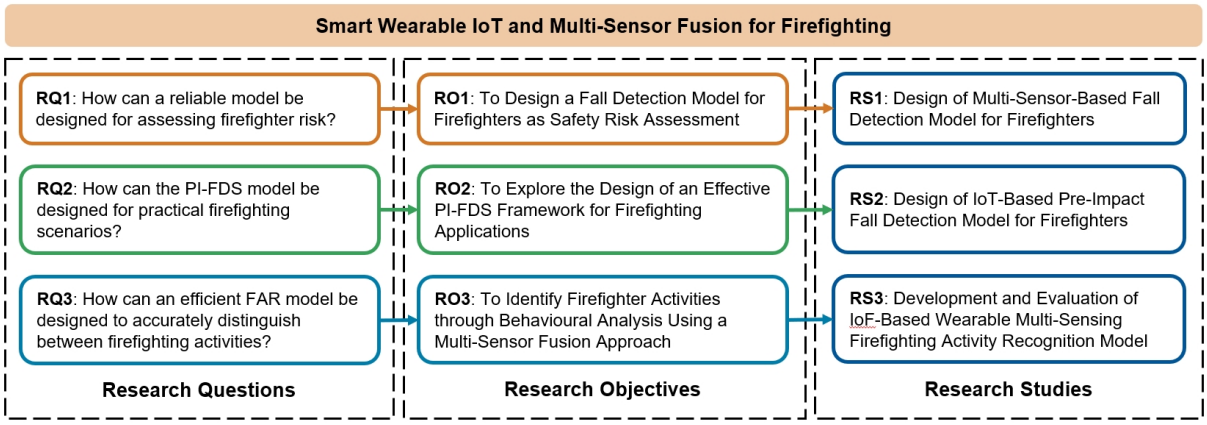

Figure 1.3: Overview of the research methodologies.

Figure 1.4 provides an overview of the three research studies conducted in this thesis, as described follows:

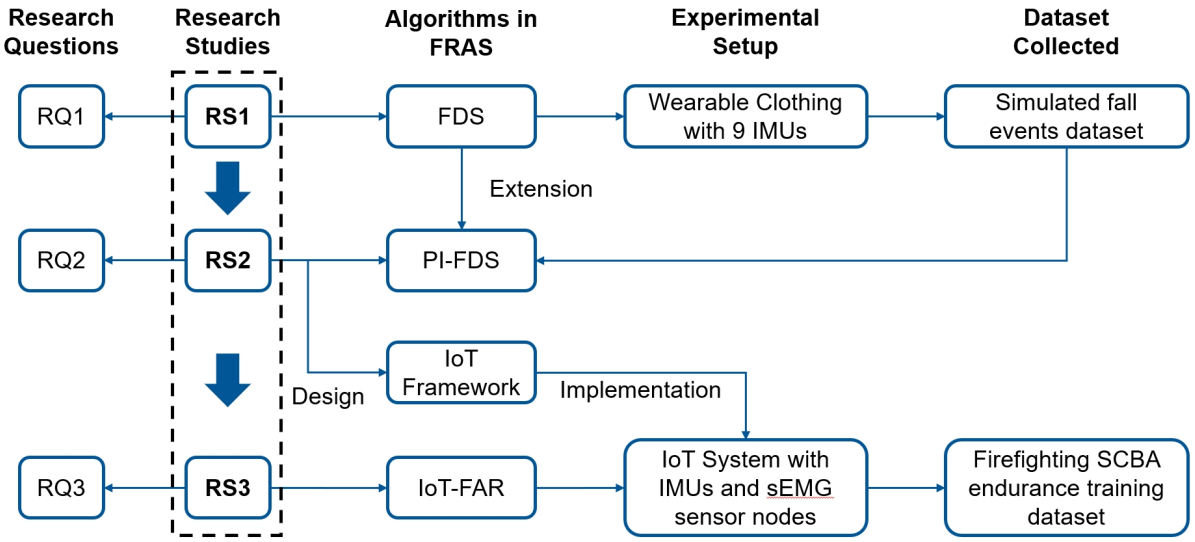

Figure 1.4: Overview of the research studies in the thesis.

RS1: Design of Multi-Sensor-Based Fall Detection Model for Firefighters

The first (preliminary) study aims to develop a FDS to recognise fall-related events of a firefighter and provide timely alerts. The study explores the integration of sensors into the personal protective clothing (PPC), which includes nine 9-DOF IMUs that collect motion data from different body parts, including the chest, elbows, wrists, thighs, and ankles. Experiments are designed by simulating fall events, performed by real firefighters, based on their experiences.

RS2: Design of IoT-Based Pre-Impact Fall Detection Model for Firefighters

Existing studies explored various fall prevention methods through early detection of imbalance motion behaviours, but mostly targeted on elders and ADLs. Using the dataset collected in RS1, this study further investigates the design of PI-FDS for firefighters to reduce safety risks. Unlike traditional FDS, the PI-FDS requires higher computational complexity to detect pre-impact fall events, which last between 300-500 milliseconds. In addition, the study proposes an IoT-based firefighting (IoF)

framework integrated with a Bluetooth Low Energy (BLE) wireless body sensor network (BLE-WBSN) to transmit sensor data to a Long-Range radio (LoRa) IoT cloud network (LoRa-IoT) for pre-impact fall prediction on the edge.

RS3: Development and Evaluation of IoF-Based Wearable Multi-Sensing Firefighting Activity Recognition Model

The final study concentrates on implementing the firefighting activity recognition (FAR) model using the proposed IoF-based framework and the multi-sensor approach. This research refines the proposed wearable design by reducing the number of IMUs from nine to five and introducing surface electromyography (sEMG) sensors to enhance the performance of the FAR model. This IoT-FAR model can accurately recognise eight specialised firefighting activities.

1.5 Chapters Outline

Chapter 2 offers a comprehensive review of existing research on HAR and FDS. The limitations and challenges specific to firefighting applications, such as motion analysis requirements, sensor placement, and sensor fusion techniques, are explored. The chapter concludes by highlighting the research questions derived from existing studies and outlines the contributions of this thesis.

Chapter 3 proposes a smart wearable FDS designed to detect falls in firefighters by integrating motion sensors into their PPC at various body parts. A multi-sensory recurrent neural network (RNN) is proposed to identify fall activities, and the impact of different combinations of IMUs on the FDS performance is analysed. A novel AFE method is introduced to reduce the computational complexity of the FDS.

Chapter 4 expands the aforementioned works by refining the design of the wearable PI-FDS for firefighters, which allows on-device prediction, thus reducing the processing burden. In addition, a moving thresholding method is proposed to address the class imbalance issue due to the minority rate of pre-impact fall event samples.

Chapter 5 extends the FDS by designing an IoT-FAR for recognising firefighting-related activities. The significance of sEMG, heart rate, and IMU features in activity recognition is assessed. In addition, the Specialized Firefighting Training Associated Activities (SFTAA) dataset, which includes self-contained breathing apparatus (SCBA) endurance training data from eighteen firefighters, is introduced. The proposed IoT-FAR model demonstrates its potential as a standardised metric for evaluating firefighting training performance.

Chapter 6 discusses the findings and contributions of the proposed IoF-FRAS. The limitations of the current work are addressed, and future research directions are proposed.

Chapter 2

Literature Review

In the past decade, there has been significant interest in HAR within the research community. FDS, as a subset of HAR, has also gathered extensive research attention. Various HAR algorithms have been proposed, utilising different wearable devices and sensing methods to capture motion data. This chapter mainly discusses and analyses the advancements of HAR, FDS and PI-FDS classifications with machine learning (ML) and deep learning (DL) approaches.

Section 2.1 provides an overview of typical sensing and classification methods used in HAR, followed by Section 2.2 reviews existing studies on conventional FDS and PI-FDS. Section 2.3 discusses the existing designs of IoT-based wireless sensor network. Lastly, Section 2.4 identifies the limitations of existing research and highlights the contributions of this study.

2.1 Sensor-Based HAR

HAR is generally divided into two primary types: vision-based and sensor-based approaches [27]. Vision-based HAR employs images and videos from optical sensors to identify activities [28]. Despite its simplicity and contactless advantages, this approach has several drawbacks, including privacy concerns, the requirement for pre-installed hardware, and the need for unobstructed views [29, 30]. These limitations make it unsuitable

for firefighting applications. As a result, the sensor-based HAR method is explored. This method uses various sensors to perform user motion prediction, location estimation, environment analysis, and human-object interactions [22]. Existing studies have proposed and discussed different sensing methods and sensor placements, as depicted in Figure 2.1. Commonly used sensors for HAR classification include IMU, EMG, RFID, and others.

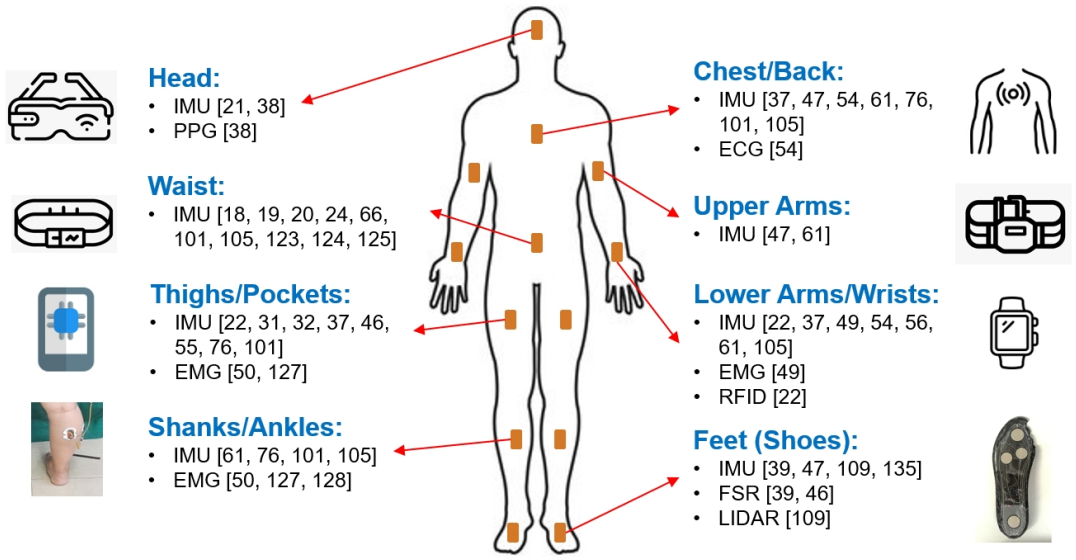

Figure 2.1: Overview of sensing methods utilised in existing studies on HAR.

2.1.1 IMU-based HAR

Numerous researchers have developed HAR models to classify ADLs using smartphones [31, 32, 33] and smartwatches [34] equipped with IMUs to analyse user motion data. These HAR systems are particularly beneficial in healthcare settings as they eliminate the need for additional devices, making them more suitable for long-term monitoring [35]. For instance, Ran *et al.* [36] proposed a DL-based HAR model that classified seven ADLs using 9-DOF IMU data from four smartphones placed at different body positions. Yande *et al.* [34] introduced a smartwatch-based HAR method to classify five activities, including stay, walk, run, upstairs, and downstairs. They emphasised that the perfor-

mance of smartphone-based HAR is significantly affected by the smartphone's placement compared to smartwatch-based HAR.

However, HAR using smartphones and smartwatches may struggle to efficiently distinguish complex activities, rendering them less suitable for firefighting applications. Barshan and Yurtman [37] indicated that uncertainty of the IMU placement on body parts was a leading cause of decreased classification accuracy. Thus, a wearable system ensuring position and orientation invariance in IMU placement is crucial for optimal classification performance.

Some studies have focused on custom-developed on-body wearable devices using IMUs to achieve position invariance during wearing. For instance, Han *et al.* [38] proposed an earlobe-worn wearable device called the TRACE sensor, integrated with an accelerometer and a PPG sensor, to recognise four ADLs. Their experiments with static and dynamic activity patterns revealed that acceleration data was vital for classification accuracy, and fusion with heart rate data could significantly improve classification performance. Additionally, Ascioglu and Senol [39] proposed a comprehensive HAR model comprising two smart insoles with force-sensitive resistors and two IMU sensors attached to each thigh. Their model achieved an average accuracy of 93.4% in distinguishing eight gait-based activities. Table 2.1 presents some publicly available benchmark datasets that have been widely utilised in HAR algorithm research.

2.1.2 HAR with EMG

In recent years, HAR models utilising multi-sensory approaches, such as integrating multiple Micro-Electro-Mechanical Systems (MEMS) IMU sensors or combining them

Table 2.1: Overview of publicly available benchmark datasets for IMU-based HAR

Dataset	Subject (Activities)	Method	Sensors
UCI-HAR [40]	30 (6 ADLs)	A waist-mounted smartphone.	ACC, GY
WISDM [41]	29 (6 ADLs)	A smartphone in front pants leg pocket.	ACC
PAMAP2 [42]	9 (18 PAs)	3 IMUs on chest, wrist, and ankle; HR strap on chest.	ACC, GY, MAG, HR
DSADS [43]	8 (19 ADLs and PAs)	5 IMUs on chest, wrists, and knees.	ACC, GY, MAG

Note: PAs: physical activities; ACC: accelerometer; GY: gyroscope; HR: heart rate; MAG: magnetometer.

with other sensor technologies, were widely proposed [44, 45, 46, 47]. Fu *et al.* [30] indicated that integrating various sensing methods benefits the recognition of human activities because each sensor type provides unique contextual information. For instance, sEMG signals gained popularity for HAR due to their ability to distinguish subtle motions related to muscle contractions, such as making a fist [48].

Bangaru *et al.* [49] explored HAR using a Myo armband equipped with a 9-DOF IMU and sEMG sensors on the forearm. Performance analysis and long-term reliability tests showed that the combined model of sEMG and IMU achieved higher accuracy than individual sensor models. Furthermore, Vijayvargiya *et al.* [50] proposed a HAR method by measuring and analysing lower limb sEMG signals using explainable artificial intelligence (XAI). Despite these advancements, the practical performance of sEMG in activity recognition remained under discussion, as most prior experiments collected data in static positions, which facilitated consistent muscle contractions throughout the trials [51].

2.1.3 HAR with RFID

Alternatively, Tao *et al.* [22] proposed a HAR method based on human-object interaction. This method included three accelerometers positioned on both hands and the

waist, along with two RFID wristband readers on each hand. The RFID readers detected RFID tags attached to household objects, such as cups and spoons, enhancing classification performance. Zheng *et al.* [52] introduced a body RFID skeleton-based HAR system consisting of a reader, an antenna, and sixteen RFID tags attached to the body skeleton. By capturing features like Received Signal Strength Indicator (RSSI), Doppler Frequency, and Phase from the backscattered signals, changes in tag positions were used to differentiate human activities. One advantage of using RFID for HAR was that the RFID features were straightforward and more accessible to process than the triaxial motion data measured by IMUs. However, the RFID reader needed to be placed close to the user to measure the features, making it impractical in scenarios such as firefighting.

2.1.4 Applications of HAR

Most existing HAR studies have focused on Ambient Assisted Living (AAL) systems, primarily tracking ADLs among residents, especially the elderly [53]. Table 2.2 shows some recent studies that demonstrated effective HAR in various domains. For instance, Qi *et al.* [54] introduced a multi-sensory HAR model called GPARMF for classifying gym physical activities involving both free weight and non-free weight exercises. This model used a wrist-worn sensor with an accelerometer and a chest-worn sensor with both an electrocardiogram (ECG) and an accelerometer. Similarly, in the field of sports and fitness, Nguyen *et al.* [55] proposed a smartphone-based HAR system to ensure cyclists' safety by recognising activities such as standing, sitting, walking, cycling, and falling. In a different context, Mastakouris *et al.* [56] developed an LSTM-based HAR model to recognise five activities in production floor environments. However, this approach was impractical since it required workers to attach a smartphone to their wrists.

Table 2.2: Existing studies on HAR applications

Study	Application	Activities (Subjects)	Method	Classifier
Lasek Jan & Gagolewski (2015) [57]	Firefighting	19 FAs (10)	7 6-DOF IMUs placed at legs, hands, arms, and back	RF
Geng *et al.* (2016) [58]	Firefighting	7 ADLs (N/A)	4 RF transmitters at chest, forehead, right wrist, and right ankle	SVM
Qi *et al.* (2019) [54]	Gym setting	19 PAs (10)	Wrist sensor with ACC and Chest Sensor with ACC+ECG	SVM, HMM
Asuroglu (2022) [53]	Assisted Living	24 ADLs (52)	wrist worn ACC	RF
Mastakouris *et al.* (2023) [56]	Assembly Work	5 CAs (2)	Wrist worn smartphone	LSTM
Mekruksavanich *et al.* (2023) [59]	Construction Work	16 CAs (13)	3 9-DOF IMUs placed at hip, upper arm, and the rear of the shoulder	LSTM
Nguyen *et al.* (2023) [55]	Cycling Sports	5 ADLs (5)	Smartphone placed in pocket	CNN-BiLSTM

Note: N/A: not available; FAs: firefighting activities; CAs: complex activities; RF: radio frequency; ECG: electrocardiogram

Despite the extensive literature on HAR, few studies have specifically addressed HAR models in firefighting application. Among these, Geng *et al.* [58] proposed an innovative HAR system based on on-body radio frequency features to monitor firefighters' physiological conditions using sensors placed on the chest, forehead, right wrist, and right ankle. The proposed SVM model effectively classified seven common firefighter activities, including standing, walking, running, lying, crawling, climbing, and stair climbing. Additionally, Blecha *et al.* [60] proposed a functional wearable PPC for firefighters that monitored physiological status (HR and temperature), detected movements, and measured environmental information such as relative humidity and toxic gas concentrations. They also designed a commander control unit to receive data from the PPC and alert the commander to any safety risks detected. Furthermore, a significant data mining competition themed 'Tagging Firefighter Activities at a Fire Scene' took place in 2015, aiming to classify common firefighter activities using binary categories (posture and action) and twenty-one subcategories, highlighting the importance of HAR in firefighting activity classification. However, it should be noted that the data acquisition for this competition relied on multi-positional sensors with wired connections, which could impact user mobility, and the dataset is no longer available [61].

2.1.5 Classification Methods

Recently, many studies have focused on DL models combined with multi-modal network structures, particularly the Convolutional Neural Network with Long Short-Term Memory (CNN-LSTM) model [27, 62, 63] and the Bidirectional LSTM (BiLSTM) model [55, 64, 65]. CNNs can automatically extract features, and LSTM models, as a type of RNN, are well-suited for time-series data. Some studies replaced CNN with traditional fea-

ture extraction methods in data processing [66]. Additionally, attention mechanisms and residual blocks were applied to enhance performance, such as the 1DCNN-ResBLSTM-Attention [67], Multilevel Residual Network with Attention (Multi-ResAtt) [68], Transformer with Bidirectional GRU (TRANS-BiGRU) [13], Multi-Head Attention and Graph Neural Networks (MhaGNN) [69], and Channel Attention-based Deep Residual Network (ResNet-SE) [70].

Generally, DL approaches achieved superior performance in HAR [71], but their high computational cost made deployment on embedded systems or mobile devices challenging [72]. Therefore, recent studies [71, 72, 73] proposed lightweight CNNs to reduce computation costs. With the rapid development of systems-on-a-chip (SoC), enabling the deployment of ML models on the edge, many studies evaluated the performance of constructing real-time HAR using various ML methods. Commonly used methods included the K-nearest neighbour method (KNN) [74], decision tree (DT) [75], support vector machine (SVM) [58, 76], and random forest (RF) [53, 74, 77].

Some studies evaluated these ML and DL methods to find an optimal model for specific applications, though results varied depending on the activities and sensing methods. For instance, Yuan *et al.* compared DL models (CNNLSTM, ConvLSTM, LSTM) with four ML methods (SVM, KNN, DT, RF), revealing that CNNLSTM and SVM achieved the highest accuracy in classifying 36 activities, with 86.94% and 74.58%, respectively. Besides these supervised learning methods, several studies focused on self-supervised learning methods, which significantly reduced annotation costs and addressed the limitations of small labelled datasets in HAR, although with lower accuracy performance [78, 79].

Many researchers shifted their focus to classifying more complex activities than basic

ADLs, termed Complex HAR (CHAR). Consequently, they emphasised multi-modal approaches combined with various ML or DL methods to achieve competitive performance in CHAR. Hierarchical methods were proposed in [54, 80, 81], which first distinguished coarse-level categories and then fine-grained subcategories. For instance, Qi *et al.* [54] proposed utilising first layer of SVM to distinguish free or non-free weight activities, and in the second layer, a neural network (NN) classified detailed aerobic and sedentary activities. The hidden Markov model (HMM) was applied for further refinement of free weight activities. Alternatively, Jeya *et al.* [82] introduced a concept-based CHAR using DL models called X-CHAR, which modelled the activity as a sequence of concepts, achieving a more understandable and explainable DL model than previous approaches.

In general, while prior studies introduced diverse DL approaches, they often exhibited a data-intensive nature and encountered significant computational costs, making them unreliable and unsuitable for practical application in real firefighting scenarios.

2.2 FDS

Similar to HAR, fall detection methods were categorised into two approaches: vision-based and sensor-based. Vision-based approaches, which constituted the majority of documented solutions, relied on one or more cameras installed in specific locations [83, 84]. Using DL and other ML approaches, existing vision-based solutions required clear and unobstructed views of the subjects in the environment. For instance, Iazzi *et al.* [85] built a vision-based FDS to extract the subject's silhouette from images obtained from an RGB camera. The proposed FDS classified activities such as lying down, sitting, bending over, and standing upright utilising a posture analysis algorithm. Other vision-based approaches utilised RGB cameras with infrared projectors and detectors (e.g., Microsoft

Kinect) to generate a depth map of a scene, enabling more accurate skeletal trajectory modelling and tracking for detecting falls [85, 86, 87, 88, 89]. Other techniques combined vision-based approaches with wearable motion sensors [90, 91, 92]. In contrast, ambient-based techniques typically analysed variations in pre-existing Wi-Fi network signals to detect falls [93, 94, 95]. For instance, Nishio *et al.* demonstrated that a microwave Doppler sensor, when combined with a frequency distribution trajectory, could successfully capture fall events [96].

However, both approaches shared a common limitation in the context of fire rescue which highly relied on pre-existing infrastructure installed in the environment. In addition, firefighters operated in harsh environments typically filled with smoke and fallen obstacles [21], severely limiting the application of these approaches due to the restricted range of vision and radio-frequency interference [97]. Consequently, several studies examined the possibility of using non-vision-based techniques to address the limitations associated with vision-based approaches [98, 99]. The strengths of this technique included reduced costs for algorithm computing and image processing, increased privacy, mobility, and resistance to environmental effects [100].

2.2.1 Typical Wearable FDS

Falls were typically divided into three phases: 1) pre-impact, 2) impact, and 3) post-impact or stationary [101]. To detect a fall, typical wearable FDSs aimed to identify the stationary phase following a significant impact with a noticeable difference in IMU data. Many studies highlighted the application of typical FDSs deployed in mobile devices, particularly in healthcare areas for the elderly [16, 102, 103, 104]. These studies extracted motion data from a common 9-DOF IMU for classifying fall activities, assuming the

smartphone was stored in the pants pocket or a smartwatch was worn on the wrist [17, 105, 106]. Advancements in MEMS technology enabled the development of FDSs based on specialised wearable form factors, extensively used in previous studies [107]. For instance, some studies [18, 19, 20] proposed wearable belts for fall detection, primarily because the body trunk could directly reflect the fall event, and the belt type was more acceptable for the elderly. Moreover, Lin *et al.* [21] developed a head-mounted FDS with a typical eyeglasses appearance, achieving an overall accuracy of 97.75%.

Although a single IMU could be acceptable to recognise fall activities, sensor fusion techniques allowed for the designing of more robust measurements and improved classification performance, especially in differentiating falls from fall-like activities [108]. For instance, Chen *et al.* [19] developed a shoe integrated with a barometer and IMU for a stair-based fall-risk detection model by measuring foot movements. The study also revealed that the multi-sensory approach performed better than a single-sensor method. Moreover, Selvaraj *et al.* [109] identified foot clearance as a sensitive fall risk factor. Hence, the study proposed a sensor shoe with an IMU and two short-range LIDAR sensors to measure the distance between the shoe and the stairs. Table 2.3 presents an overview of benchmark public datasets for IMU-based FDS.

Table 2.3: Overview of publicly available benchmark datasets for IMU-based FDS

Dataset	Subject	Types of ADLs/falls	Method
MobiFall [15]	24	9/4	A SP (trouser pocket)
Cogent Labs [110]	42	8/6	2 6-DOF IMUs (chest and thigh)
UMAFall [111]	17	8/3	4 9-DOF IMUs (wrist, chest, waist, ankle)
SisFall [112]	38	19/15	A 6-DOF IMU (waist)
UP-Fall [113]	17	6/5	EEG on head & 5 6-DOF IMUs (ankle, thigh, waist, neck, wrist)
AnkFall [114]	21	8/4	An ACC (ankle)

Note: SP: smartphone; EEG: electroencephalograph

However, applying sensor-fusion techniques may result in higher computation due to the increased number of features. For practical application as a real-time wearable FDS, an effective feature extraction method should be investigated to reduce the number of features while maintaining performance. Raw feature extraction (RFE) from IMU data has been commonly used with DL-based methods in wearable FDSs [100, 115, 116, 117]. Metrics of raw feature extraction (RFEM) such as mean, standard deviation, median, maximum, minimum amplitude, and mean absolute deviation were frequently extracted in ML and threshold-based methods [23, 115, 118]. The input features used by classifiers determine overall fall detection performance, computational cost, and processing speed. For instance, Le *et al.* [119] proposed a feature extraction method computing 44 features in the time-domain, frequency-domain, and Hjorth parameters, highlighting the significance of features extracted from different domains. Similarly, Vallabh *et al.* [120] extracted six time-domain and six frequency-domain features in their ML-based FDS. However, most feature extraction techniques increased the number of input features compared to raw measurements, resulting in longer processing times and higher computations. Therefore, for an FDS to be considered high-performing, placement, quantity, data processing stages, and classification methods must be carefully considered [100].

Similar to HAR, most existing studies developed FDS for the healthcare or AAL fields, with only a few emphasising the use of wearable devices for fall detection in firefighters. Pham *et al.* [24] proposed a wearable FDS device worn on the waist, integrated with a triaxial accelerometer and a carbon monoxide (CO) sensor to monitor the falls of firefighters in fire environments. The CO sensor was specifically utilised for detecting falls caused by broken air-support devices. The model was further improved with a sensor-fusion approach using a 9-DOF IMU, a CO sensor, and a barometer [25]. Sim-

ilarly, Anania *et al.* [121] developed an innovative garment-based FDS for emergency operators with an accelerometer integrated into the shoulder position, though the study only experimented on ordinary youths.

The comprehensive literature review in this study revealed that only a few studies have contributed to the use of wearable sensing for firefighting applications, primarily focusing on monitoring purposes. This highlights the significant challenges in developing smart firefighting models.

2.2.2 PI-FDS

Traditional wearable FDSs identify falls after impact, indicating that preventable injuries may already have occurred by the time of detection [122]. Consequently, recent research has explored on developing next-generation FDSs, known as PI-FDS, which specifically detect the pre-impact phase of falling to initiate preventative actions. Several studies have explored PI-FDS, such as Ferreira *et al.*, who proposed a waist-worn PI-FDS that used three-axis acceleration measurements and considered the user's height [123]. This threshold-based technique accurately predicted the user's state just before losing balance by measuring the distance between the IMU and the user's head and feet. Such classification facilitates automated intervention, potentially reducing the risk of severe injuries. Zhong *et al.* developed an automatically inflating "airbag" jacket that inflates when the integrated IMU detects a pre-impact state [124]. Similarly, Jung *et al.* proposed a protective wearable PI-FDS using Euler angles and the magnitude of a vector sum [125]. Li *et al.* presented a PI-FDS that extracted zero moment points and assessed body balance using a Kinect sensor [126]. However, utilising airbags as protective measures could affect firefighters' mobility once inflated, and the gas tank poses an explosion risk near

fires. Thus, developing an appropriate PI-FDS for firefighters is essential.

Alternative PI-FDS approaches have been explored, such as analysing an individual's gait using an EMG sensor placed on the thigh or ankle [127, 128, 129]. EMG signals show noticeable differences during a fall compared to other activities, such as walking or running, enabling the classification of various falling stages. However, this approach is largely impractical in firefighting contexts due to the properties of fire-retardant clothing. Moreover, EMG-based solutions require firm and prolonged contact with the user's skin, which can cause discomfort, especially in the intense heat of fireground environments.

Most classification methods used by PI-FDSs employ threshold-based algorithms (TBAs), such as the classical threshold model [124, 125, 130, 131, 132] and the dynamic threshold algorithm (DTA) [133]. The advantage of TBAs is that by adjusting the threshold value, sensitivity can reach 100%, ensuring effective protective measures, but reducing the overall accuracy. Some studies have proposed ML or DL methods, such as SVM [134] and CNN [117]. For instance, Wang *et al.* introduced an ensemble multi-source CNN (MCNNE) structure to more efficiently extract data from multiple sensors [135].

2.3 IoT-Based Wearable Sensing

One critical aspect of the effectiveness of wearable sensing like FDS or HAR is the intercommunication between the indoor and outdoor of the fireground and the distribution of sensor data. Existing setups can be categorised into two distinct approaches: 1) wireless body sensor networks (WBSNs) and 2) Internet of Bodies (IoB) [136]. Table 2.4 presents a comparison of the key features of various wireless technologies used in PI-FDS.

Bluetooth Low Energy (BLE) and Wi-Fi are commonly used for establishing WBSNs

Table 2.4: Comparison of key features of wireless technologies used in PI-FDSs [1, 2]

	Wi-Fi	**BLE**	**Zigbee**	**NB-IoT**	**LoRa**
Network Type	WLAN	P2P	Mesh	LPWAN	LPWAN
Power Consumption	High	Very Low	Low	Very Low	Very Low
Range	1 km	100 m	10-100 m	18-25 km	10-40 km
Data Rate (bps)	10-100 M	1 M	0.25 M	160-250 K	0.3-250 K

[115, 122, 123, 124, 131, 135]. Each has distinct advantages and disadvantages. BLE is compatible with existing devices like smartphones and PCs but has a relatively short transmission distance. Wi-Fi offers a greater transmission distance and compatibility with existing devices but requires existing infrastructure, which is impractical in firefighting contexts.

Low-power wide-area networks (LPWANs) such as NB-IoT, Sigfox, and LoRa radio have been utilised in FDS application. For instance, Qian *et al.* proposed a wearable FDS using NB-IoT and an IoT cloud platform to remotely send alerts on fall risks [137]. The effectiveness of NB-IoT depends on GSM signals, which may be unreliable in some firefighting scenarios, such as forest fires, due to poor GSM signals or unavailable cellular networks. Therefore, this study utilised LoRa as the base transmission protocol due to its low power consumption, long-distance transmission capability, strong penetration of building materials, concurrent connections with a gateway, and lower cost [1, 138].

However, LPWANs can only transmit limited data, posing a challenge for real-time monitoring [139]. In China, each firefighting truck typically has six firefighters: one driver, one incident commander (IC), one who controls the water supply, and three responsible for executing the rescue mission. LoRa alone has difficulty to transmit large amounts of sensor data from the three firefighters performing the rescue mission. Consequently, to design a robust wearable device applicable in different firefighting scenarios, a heterogeneous

network framework is required to accommodate different wireless IoT technologies.

2.4 Limitations of Existing Works

Firefighting scenarios present unique challenges for HAR systems due to harsh environments, limited visibility, and high risk. While the HAR techniques can be categorised as vision-based or wearable-based, vision-based approaches are often impractical in firefighting contexts because factors like smoke and darkness impair camera visibility. Wearable-based solutions, particularly those using IMUs, are more feasible, offering real-time monitoring of firefighter activities and detection of critical events. Despite the effectiveness of IMUs in capturing motion data, there is a lack of comprehensive studies investigating the optimal number, placement, and orientation of IMUs for FDS performance. Addressing this gap is crucial for developing robust HAR models that can accurately detect and classify activities and events in real-time. This study aims to address such gap by proposing a multi-IMU-based FDS and evaluate its performance based on different number of IMUs placed at different body positions.

Multi-sensory fusion approaches enhance the robustness, accuracy, and reliability of FDS and HAR models by integrating data from multiple sensors. However, applying multi-sensory fusion also introduces challenges in data processing, feature extraction, and classification algorithms, necessitating further studies to improve efficiency while maintaining accuracy, which is the other main gap that to be addressed in this study. In addition to traditional FDSs, PI-FDS studies have significantly improved detection response times and achieved some protective measures before impact occurs. However, the real-time demands of PI-FDS are crucial, as timely detection and response are essential for minimising injury or fatality risks in firefighting scenarios. This highlights the importance

of a reliable PI-FDS classification model and a low-delay IoT-based network for real-time data transmission.

A critical limitation identified in current FDS research is the unrealistic data acquisition. Among the six benchmark datasets listed in Table 2.3, only SisFall [112] includes falls that commence from dynamic motions like walking, while most collect data starting from a standstill pose, which fails to accurately represent real-world fall scenarios where falls typically occur suddenly and unpredictably during movement. Additionally, the data were collected from young individuals with less vulnerable to injuries through simulated falls. This lack of realistic fall experience can affect the quality of the data collected. To address this issue, this study conducted experiment data collection with real firefighters, with the fall activities more fitted to their experiences and work nature.

On the other hand, achieving accurate and reliable activity recognition in dynamic and unpredictable firefighting environments presents significant technical challenges. To solve this challenge, this study proposed an IoT-FAR framework through exploring multi-sensory fusion technique, integrating sEMG with IMUs, as well as proposing a design of IoT-based wireless sensor network in real firefighting scenarios. Meanwhile, practical considerations such as wireless data transmission, system integration with existing firefighting equipment, and user acceptance are critical factors that must be carefully considered in the design and implementation of HAR for firefighting scenarios.

2.5 Chapter Summary

This chapter reviewed the current state of research on HAR and FDS across various applications, emphasising their limitations, challenges, and opportunities for future ad-

vancements. HAR plays a crucial role in monitoring firefighter activities by recognising different firefighting behaviours but currently exhibits poor performance in distinguishing complex activities. For FDS, achieving high accuracy while ensuring efficiency remains critical for firefighting applications. This chapter also examined the factors essential for constructing the IoT framework for firefighting scenarios. By addressing the identified gaps and issues in the literature, this research aims to develop a practical and reliable FRAS that enhances firefighter safety, operational effectiveness, and situational awareness in challenging firefighting conditions. The FRAS comprises the FDS for detecting fall-related dangers, the HAR for monitoring firefighting related activities, and the IoT-based wearable sensing network for achieving real-time remote sensor data transmission.

Chapter 3

Design of Multi-Sensor-Based Fall Detection Model for Firefighters

3.1 Introduction

This chapter presents our initial study addressing **RQ1**, aiming to develop a wearable FDS to alert fall-related dangers in firefighting scenarios. In this study, a PPC-based wearable FDS for firefighters integrated with nine IMU sensors for various types of fall detection is proposed. Although many studies have proposed FDSs, among the current available benchmark datasets of fall detection, most of the falling data were collected from a standstill to a fallen state, which is less realistic to actual falling. Therefore, this study collects falling sample data from firefighters, where the fall activities include an additional walking activity before and after falling. Then, the fall detection classification model is developed and evaluated. The key contributions of this study are summarised as follows:

- Develop a wearable PPC prototype integrated with 9 IMUs placed onto the chest, elbows, wrists, thighs, and ankles.
- Evaluate the FDS performance with different combinations of IMUs.
- Carry out a realistic data collection from firefighters with six types of falls and three types of fall-like activities.
- Propose the V-RNN model that improves the classification performance.

- Introduce a novel feature extraction approach known as Attitude Feature Extraction (AFE) for enhancing FDS efficiency.

This study is published as:

- [Journal] Smart Wearables with Sensor Fusion for Fall Detection in Firefighting, *Sensors*, 2021 (IF = 3.9, CAS Q3, JCR Q2).
- [Conference] A Smart Wearable Fall Detection System for Firefighters using V-RNN, *The 13th International Conference on Intelligent Human Computer Interaction (IHCI 2021)*, 2021 (Best Session Paper Award).
- [Conference] A Novel Attitude Feature Extraction Method for Multi-IMU Based Fall Detection System, *2023 IEEE 3rd International Conference on Power, Electronics and Computer Application (ICPECA 2023)*, 2023.
- [Patent] Firefighter Safety Risk Evaluation System Software, 2021. (Granted)

The rest of this chapter is organised as follows: Section 3.2 discusses the methodology of the proposed FDS models and Section 3.3 details the design of the proposed smart wearable PPC prototype used for data collection. Section 3.4 evaluates the FDS models with various combinations of IMUs, discusses fall detection performance in each activity, and compares the results with existing works. Section 3.5 concludes with a review of the presented work and suggests directions for future research.

3.2 Methodology

The proposed wearable FDS is composed of three modules: (1) sensing, (2) pre-processing, and (3) classification, as illustrated in Figure 3.1.

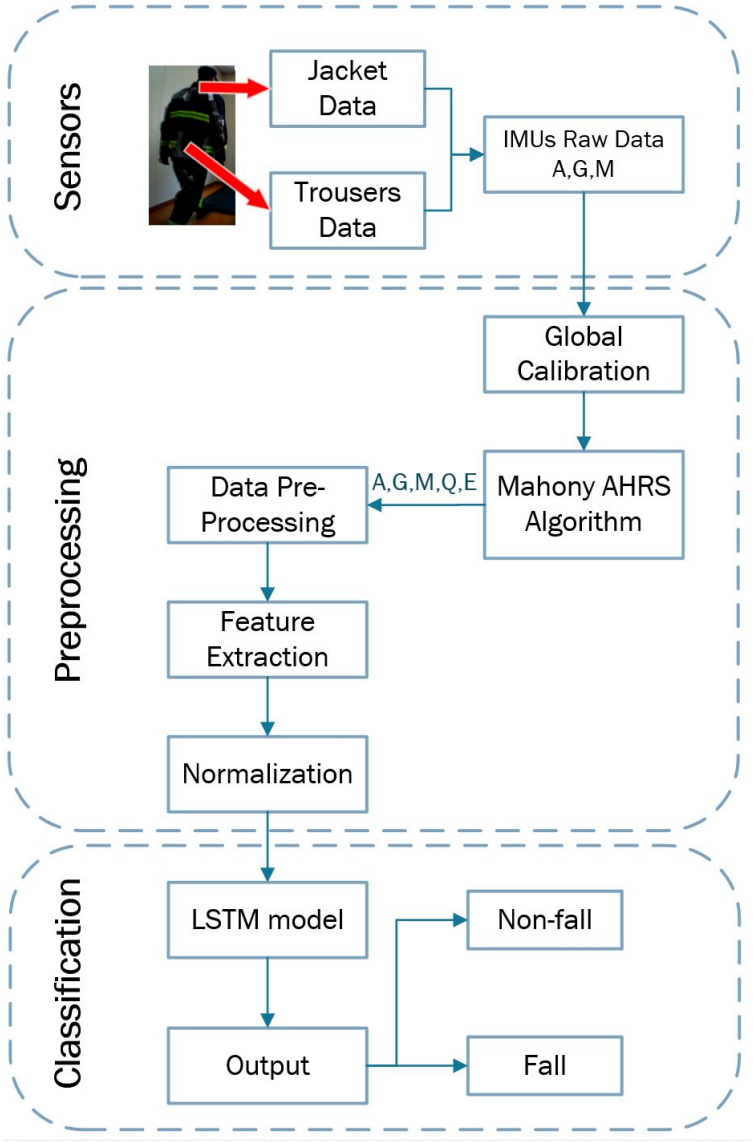

Figure 3.1: Flowchart of the FDS algorithm, where A is triaxial accelerometer data, G is triaxial gyroscope data, M is triaxial magnetometer data, Q is quaternion data, and E is Euler angles.

3.2.1 Global Calibration of IMUs

Each IMU has a tri-axial coordinate system, as depicted in Figure 3.2, which can be used to determine the position and orientation of an object. In fact, an FDS with multiple IMUs placed on different parts of the PPC needs further calibration to synchronise and unify the coordinate system as a single entity. To achieve a global calibration for IMUs on the PJ and PT, two common reference vectors are required [140].

The magnetic field vector (V_{mag}), which points to the north, is selected as one of the common reference vectors, assuming no magnetic interference and that the magnetic field in the vicinity of each IMU is the same. The other reference vector is the acceleration vector (V_{acc}) in a quasi-static condition; it can be regarded as the gravity vector pointing to the ground. The IMU local coordinates can thus be rotated to the north-east-up (NEU) earth coordinate system (right-hand rule). Figure 3.3 presents the local and global coordinate systems with two common reference vectors V_{mag} and V_{acc}. The calibration works in the way that the subject should stand still initially, and it will take 1 second (15 samples) to compute the average values of V_{acc} and V_{mag}. The main purpose of the calibration is to convert the local coordinate system of each IMU to the unified NEU system. With the values of V_{acc} and V_{mag} as the reference vectors, the rotation matrix of these two coordinate systems can be computed, and hence, update the collected raw data of each IMU referred to the NEU system.

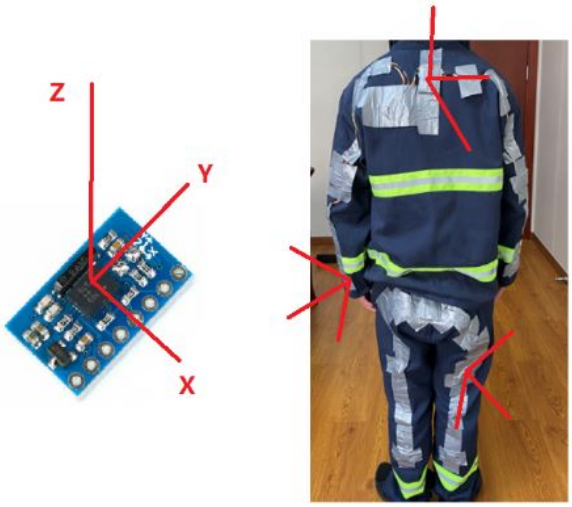

Figure 3.2: Local IMU coordinate system on PJ and PT.

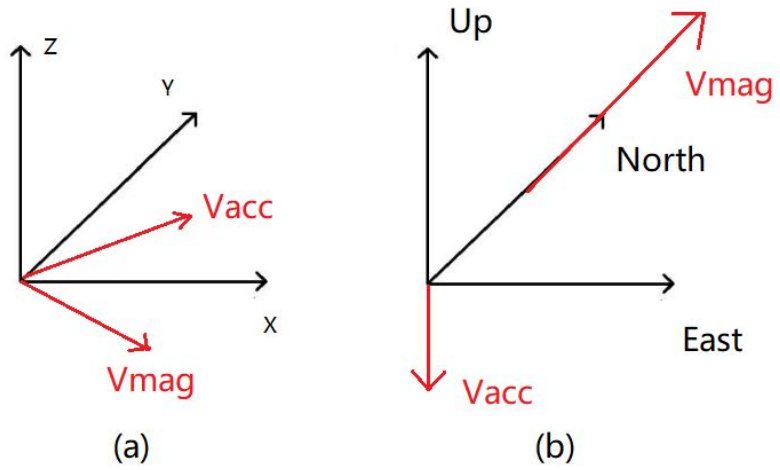

Figure 3.3: Global calibration which included (a) local coordinate system and vectors of Vacc and Vmag and (b) NEU coordinate system and vectors of Vacc and Vmag.

3.2.2 Data Pre-processing

The Mahony attitude and heading reference system (AHRS) [141] is utilised to compute the quaternion and Euler angles from the raw data received from the terminal. The rotation matrix of each IMU node can be derived as follows:

$$q = w + xi + yj + zk \tag{3.1}$$

$$R(q) = \begin{bmatrix} 2w^2 + 2x^2 - 1 & 2xy - 2zw & 2xz + 2yw \\ 2xy + 2zw & 2w^2 + 2y^2 - 1 & 2yz - 2xw \\ 2xz - 2yw & 2yz + 2xw & 2w^2 + 2z^2 - 1 \end{bmatrix} \tag{3.2}$$

where q, w, x, y, and z represent a quaternion value that consists of a real number (w) and imaginary values on three imaginary axes (i, j, k).

Each IMU delivered 13 outputs, including tri-axial acceleration (m/s^2), tri-axial angular rate (deg/s^2), four-point quaternion data, and the derived roll, pitch, and yaw angles. To represent the variation of the different movements of a firefighter, given a defined period, features including the mean (μ) (see Equation 3.3), range (R) (see Equation 3.4), standard deviation (σ) (see Equation 3.5), and mean absolute deviation (MAD) (see

Equation 3.6), are extracted from the 13 outputs, and calculated using 0.5 s of data each, with a window size of 0.1 s. As a result, each IMU generates 52 features (13 outputs × 4 arithmetic calculations), in which the total number of input features to the classifier is 468 features (52 features × 9 IMUs).

$$\mu = \frac{1}{N}\Sigma x[k] \tag{3.3}$$

$$R = \max x - \min x \tag{3.4}$$

$$\sigma = \sqrt{\frac{1}{N}\Sigma(x[k] - \mu)^2} \tag{3.5}$$

$$MAD = \frac{1}{N}\Sigma|x[k] - \mu| \tag{3.6}$$

3.2.3 RNN Classifier

Figure 3.4 illustrates the NN architecture, which includes three LSTM layers with 128 units, 32 units, and 16 units, respectively, one dense layer with an eight-unit rectified linear unit (ReLU) activation function (see Equation 3.7), and a Softmax activation function with two units (see Equation 3.8). This represents the probability of non-fall and fall activities using one-hot encoding. The adaptive moment estimation (Adam) algorithm with a learning rate of 0.01 is applied as the optimiser of the model, and the sparse categorical cross-entropy algorithm (see Equation 3.9) is used as the loss function in the model. The batch size is set to 10, representing the user's action in one second. The dataset is divided into 80% for training and 20% for testing.

$$ReLU = \max(0, x) \tag{3.7}$$

$$p(y_i) = \frac{e^{y_i}}{\Sigma^n{}_{j=1} e^{y_i}} \tag{3.8}$$

$$loss(y_i) = -\log p(y_i) \tag{3.9}$$

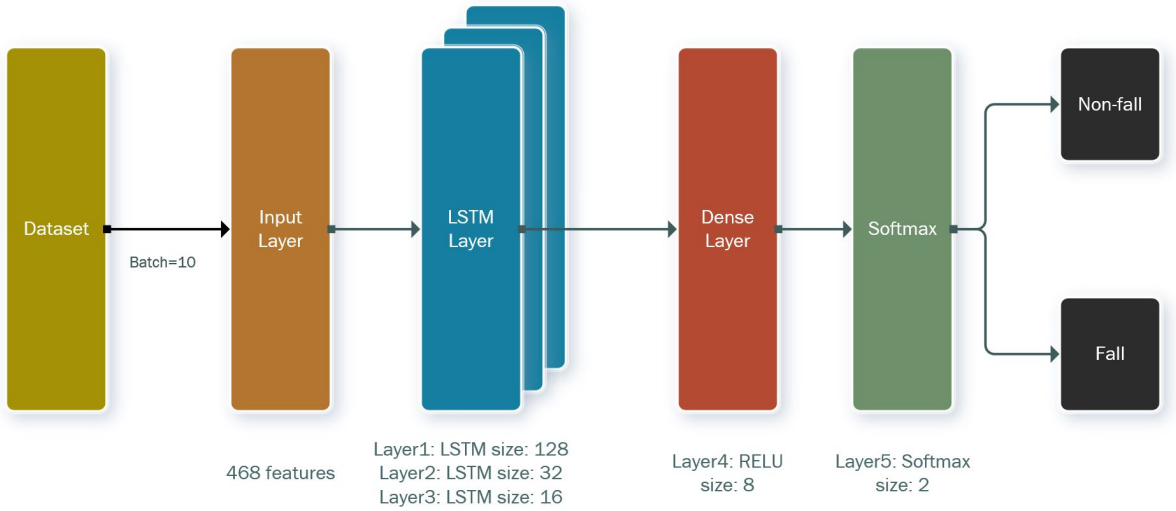

Figure 3.4: Utilised LSTM network architecture.

3.2.4 V-RNN FDS Algorithm

The proposed V-RNN algorithm (see Figure 3.5) consists of two parts: a front-end RNN model and a backend BMV algorithm. The RNN model is similar to the proposed LSTM network, while only the raw data are utilised here to evaluate if quaternion and Euler angles could improve the classification performance. Hence, the RNN model consists of three LSTM layers of 128 units, 32 units, and 16 units, followed by a RELU dense layer, and connected to the Softmax activation function of 2 units. The output of the RNN model indicated the probability of falling in every 0.1 s.

To further evaluate the falling occurrence at time t_m, a $W/20$ period of fall results before and after this moment are extracted. The fall results of this $W/10$ period with data length of W (0.1 s per result) are stored and added together to get the R_{sum}, representing the overall falling probability. Since each fall result is either one or zero, if the value is larger than a voting threshold T_v, the result at tm moment would be falling, and vice

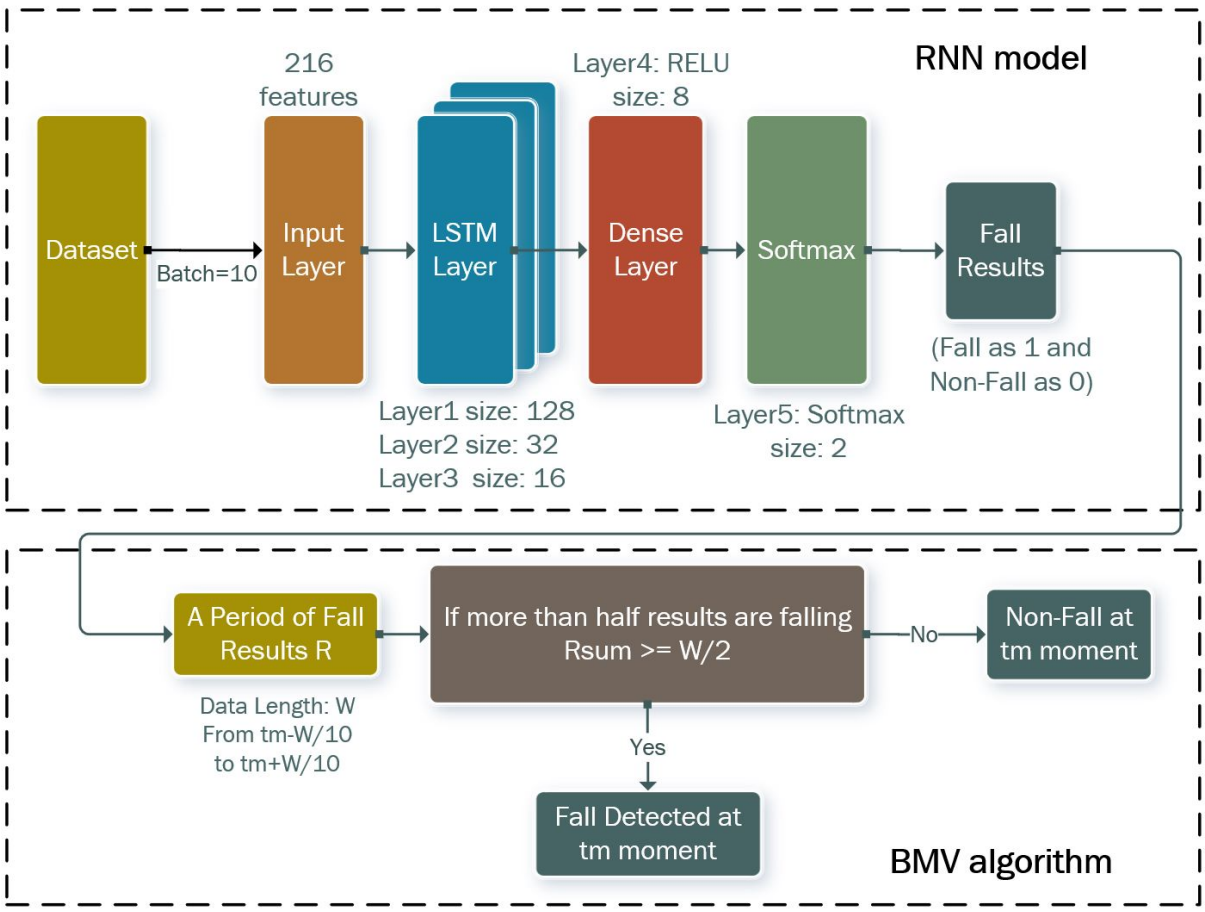

Figure 3.5: Overview of the structure of the proposed V-RNN algorithm.

versa. The threshold T_v is evaluated in the way that a larger value will classify the final result as not falling, but this may increase the false detection if the falling occurs within the time period. The T_v is set to half of the data length as 50 percent of falling occurrence, while we also evaluated the performance using the threshold with $\pm 10\%$ (or $\pm W/10$) of the half data length $W/2$. The proposed voting algorithm can overcome the false detection by introducing a time delay of $W/20$ as illustrated in Table 3.1. Therefore, to balance the detection accuracy and the response time of rescue, the parameter of data length W should not be too large. The performances are evaluated with various data lengths of W, and the maximum value of W is set to 60 as this is the maximum critical time for issuing a fall alert (a time delay within 3 seconds).

Table 3.1: Pseudocode of the proposed BMV

Boyer-Moore Voting Algorithm
Step 1: Extracting a window size of results with a data length of W
Step 2: Calculate the sum of the period results R_{sum}
Step 3: **if** R_{sum} is larger than the voting threshold T_v
The result will be 1 as falling
else
The result will be 0 as not falling
Step 4: Shift the window with one value (0.1 s) and repeat the Step.1

3.2.5 AFE Method

The flowchart of the proposed FDS with AFE method is shown in Figure 3.6. The red rectangle represents the AFE method. Firstly, the raw data of each IMU are inputted to estimate the quaternion value based on the attitude and heading reference system (AHRS). Then, by utilising the quaternions of all IMUs, a 3D skeleton that reconstructs the real motion can be achieved. Hence, the skeleton vectors and corresponding attitude features can be calculated as the input features of the fall detection classifier. In terms of the traditional naive FDSs, the raw data collected from IMUs will be directly used as the input features of the classification model.

For each IMU, the raw motion data from the triaxial-accelerometer and triaxial-gyroscope were collected. The simplified 6-DOF Madgwick AHRS was applied to estimate the quaternion from the raw measurements synchronously [142]. The quaternion of an IMU is defined in Equation 3.10, where n represents the discrete time data order. Initially, q_w^0 is 1, q_x^0, q_y^0, and q_z^0 are all 0, as shown Equation 3.11.

$$Q^n = q_w^n + q_x^n i + q_y^n j + q_z^n k \tag{3.10}$$

$$Q^0 = [q_w^0 \quad q_x^0 \quad q_y^0 \quad q_z^0] = [1 \quad 0 \quad 0 \quad 0] \tag{3.11}$$

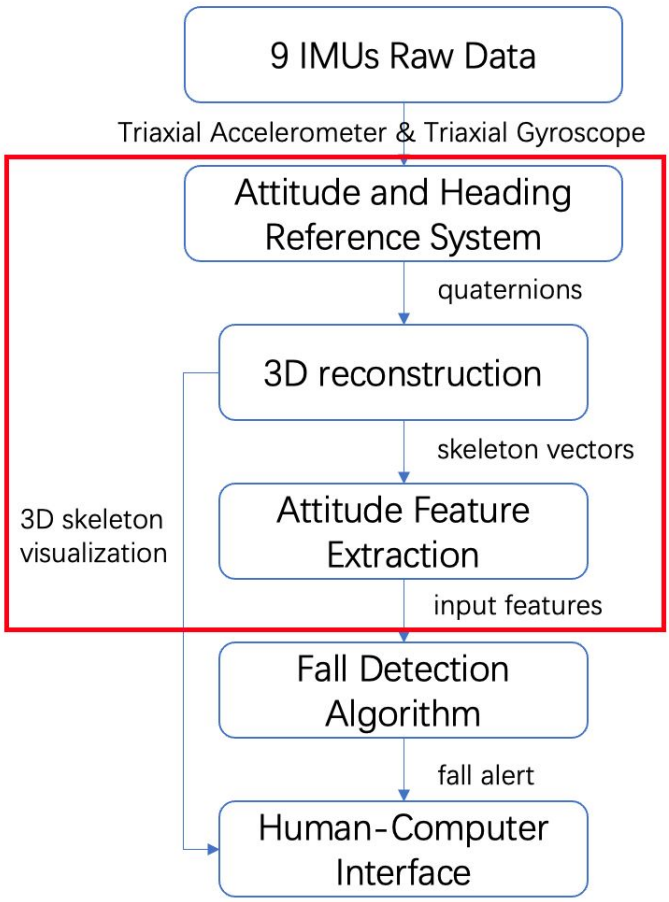

Figure 3.6: Flowchart of the FDS with AFE methods, represented by blocks in the red rectangle box.

Tri-axial accelerometer data $Acc_{x,y,z}$ was normalised using Equation 3.12.

$$NAcc_{x,y,z} = \frac{Acc_{x,y,z}}{\sqrt{Acc_x^2 + Acc_y^2 + Acc_z^2}} \tag{3.12}$$

The estimated direction of gravity $halfv_{x,y,z}$ was calculated using Equation 3.13 - 3.15, where $n-1$ represents the previous n.

$$halfv_x = q_x^{n-1} \times q_z^{n-1} - q_w^{n-1} \times q_y^{n-1} \tag{3.13}$$

$$halfv_y = q_w^{n-1} \times q_x^{n-1} - q_y^{n-1} \times q_z^{n-1} \tag{3.14}$$

$$halfv_z = (q_w^{n-1})^2 + (q_z^{n-1})^2 - 0.5 \tag{3.15}$$

The error $halferr_{x,y,z}$ can be computed through sum of the cross product between the

estimated and measured direction of gravity, as shown below:

$$halferr_x = NAcc_x \times halfv_z - NAcc_z \times halfv_y \tag{3.16}$$

$$halferr_y = NAcc_z \times halfv_x - NAcc_x \times halfv_z \tag{3.17}$$

$$halferr_z = NAcc_x \times halfv_y - NAcc_y \times halfv_x \tag{3.18}$$

Then, the gyroscope measurement $G'_{x,y,z}$ derived from the proportional feedback K_p and integral feedback K_i is updated as follows:

$$IF_{x,y,z} = K_i \times halferr_{x,y,z} \times (\frac{1}{F_S}) \tag{3.19}$$

$$G'_{x,y,z} = G_{x,y,z} + IF_{x,y,z} + K_p \times halferr_{x,y,z} \tag{3.20}$$

The updated quaternion is calculated as shown in Equation 3.21, where n represents the current time, and Q^n is the updated quaternion values.

$$Q^n = \begin{bmatrix} 1 \\ Gx' \\ Gy' \\ Gz \end{bmatrix}^T \times \begin{bmatrix} q_w^{n-1} & q_x^{n-1} & q_y^{n-1} & q_z^{n-1} \\ -q_x^{n-1} & q_w^{n-1} & q_w^{n-1} & q_w^{n-1} \\ -q_y^{n-1} & q_y^{n-1} & -q_x^{n-1} & q_x^{n-1} \\ -q_z^{n-1} & -q_z^{n-1} & q_z^{n-1} & -q_y^{n-1} \end{bmatrix} \tag{3.21}$$

Finally, the quaternion values of the current time n can be calculated by normalising the Q^n. Since each quaternion value represents the rotation of the subject in a 3D coordinate system, the 9 IMUs can be reflected into 3D points to construct a 3D skeleton model. The rotation of the 3D points is calculated according to its quaternion, as defined in Equation 3.22, where P is the point in the 3D plane before rotated, P_r is the point after rotated, Q is the quaternion, and Q' is its conjugate.

$$P_r = Q \times P \times Q' \tag{3.22}$$

The final five attitude features can be extracted using Equation 3.23, which represents the five angles between the vectors and the $x - y$ plane. The five vectors are the vectors

of chest-to-origin, left and right ankle-to-thigh, and left and right wrist-to-elbow. The angles can be calculated as:

$$\theta = arctan\frac{|V_z|}{\sqrt{V_x^2 + V_y^2}} \tag{3.23}$$

where V represents the attitude vector, and θ is the angle between the vector V and the $x - y$ plane.

3.3 Experiment Setup

3.3.1 Hardware Design for FDS

The placement of wearable sensors plays an essential role in recognising falls with a high accuracy rate [143]. The important motion data that contribute to fall-event detection are associated with the moving patterns of the chest, elbow, and wrist from the upper body, and the thigh and ankle from the lower part of the body. Hence, BNO055 IMUs [144], consisting of a triaxial accelerometer, triaxial gyroscope, and triaxial magnetometer, are integrated with wired connections on the back of the protective jacket (PJ) and protective trousers (PT), as shown in Figure 3.7. The angular velocity ranges from ±125 deg/s to ±2000 deg/s with a low-pass filter bandwidth from 523 Hz to 12 Hz, while the acceleration ranges from ±2 g to ±16 g with a low-pass filter bandwidth from 1 kHz to 8 Hz, and the measurement range of the magnetometer is about ±4800 uT with a resolution of 0.3 uT. The maximum output rate of 9-DOF fusion data is 100 Hz. However, considering fast data transmission can result in low data receiving efficiency, both the sampling rate of the 9-DOF data and the wireless transmission rate were set to 15 Hz in this study. This setting is supported by [145], which validated that a sampling rate between 15 and 20 Hz can optimise detection performance.. An IMU was not placed on the shoulder because shoulder movement is always associated with chest movement.

Figure 3.7: Placement of motion sensors that are mapped to the body parts where the motion data are critical for fall-detection computation.

Two processing units are placed on the chest and waist for receiving and transmitting IMU data from the PJ and PT, respectively. Each processing unit consists of a Seeeduino XIAO micro-controller unit (MCU) with a 20 $\times$ 17.5 mm^2 size and 3.3 V power consumption [146], a TCA9548A 1-to-8 I2C multiplexer [147] for multisensor connections, a Bluetooth low-energy (BLE) 4.2 module [148], and a 3.7 V 400 mAh lithium-ion battery [149], as illustrated in Figure 3.8. The IMU sensors are connected to a processing unit with wires soldered onto the PJ and PT.

Table 3.2 summarises the components of the sensing module with their respective specifications. To reduce the risk of damaging the components, such as IMUs, processing units, and wires, during the data collection, foam boards were placed on top of the components for protection, and rubber tape was used to secure the wire connections between the processing unit and IMUs, as depicted in Figure 3.9. Finally, the IMU data from the PJ and PT are transmitted to a terminal via BLE 4.2 for further processing, as shown in Figure 3.10.

Table 3.2: Components and their respective specifications in the sensing module

Component	Specification
IMU	Triaxial accelerometer Triaxial gyroscope Triaxial magnetometer Operating voltage: 3 V to 5 V
Seeeduino XIAO MCU	Operating voltage: 3.3 V / 5 V CPU: 40 MHz ARM Cortex-M0+ Flash memory: 256 KB RAM: 32 KB Size: 20 × 17.5 × 3.5 mm I2C: 1 pair
TCA29548A multiplexer	Operating voltage: 3 V to 5 V I2C: 8 pairs
JDY-18 BLE	Operating voltage: 1.8 V to 3.6 V BLE version: 4.2 Frequency: 2.4 GHz Size: 27 × 12.8 × 1.6 mm
Lithium-Ion battery	Power supply: 3.7 V Capacity: 400 mAh

3.3.2 Simulated Fall Events Dataset

Yan *et al.* [20] states that falls may be categorised into four distinct types: basic forward, backward, left, and right lateral falls. The fall-like activities can be further subdivided into basic forward, backward, left, and right lateral falls. However, a fall event is much more complicated during firefighting activities. Some specific activities, such as slipping, sliding, and fainting, can also result in falls [140]. Several existing studies [20, 150, 151] demonstrate the challenges of differentiating fall-like activities, such as sitting quickly, jumping onto a bed, and lying down slowly, from an actual fall. However, these existing fall datasets are not suitable for detecting the falls of firefighters because most of the recorded activities do not closely simulate realistic falling events in a fireground, such as jumping onto a bed.

This study initiated a collaboration with firefighters from the Haishu District Fire

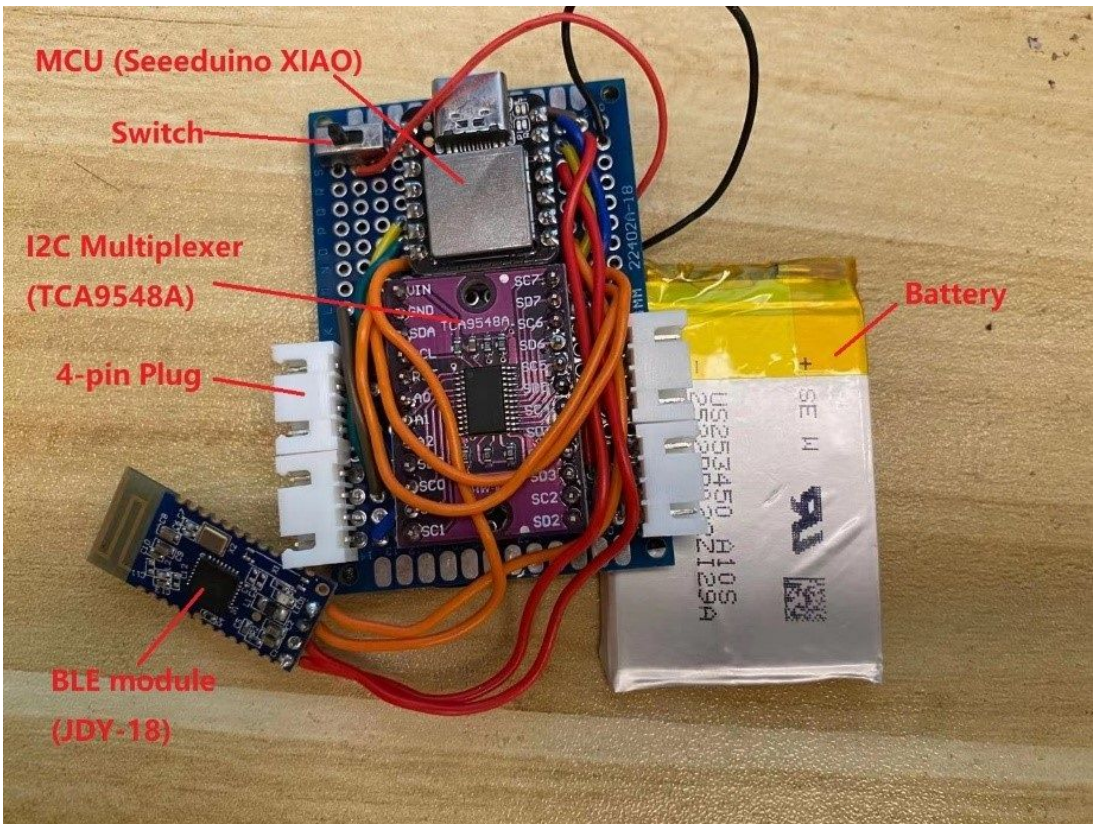

Figure 3.8: Processing unit that consists of an MCU, an I2C multiplexer, a BLE 4.2 module, and a lithium-ion battery.

Brigade from Ningbo City, Zhejiang Province, China, to obtain realistic fall events by firefighters, based on their experiences. Fourteen male firefighters (with one to three years of firefighting experience, ages between 21 and 24 years old, with heights between 1.7 and 1.88 m) voluntarily participated in the data collection. Six of them were career firefighters, and the other eight were volunteer firefighters.

Six types of fall activities were collected, including a forward fall with the knees, a forward fall with the hands, left and right sides of inclined falls, a backward fall, and a slow forward fall with a crouch. Three other activities, including crouching, sitting, and walking with a stoop, were also collected as fall-like activities. Each firefighter was requested to put on the developed PJ and PT and simulate falls and fall-like activities, based on their firefighting experience. Figure 3.11 illustrates the details of the falls and

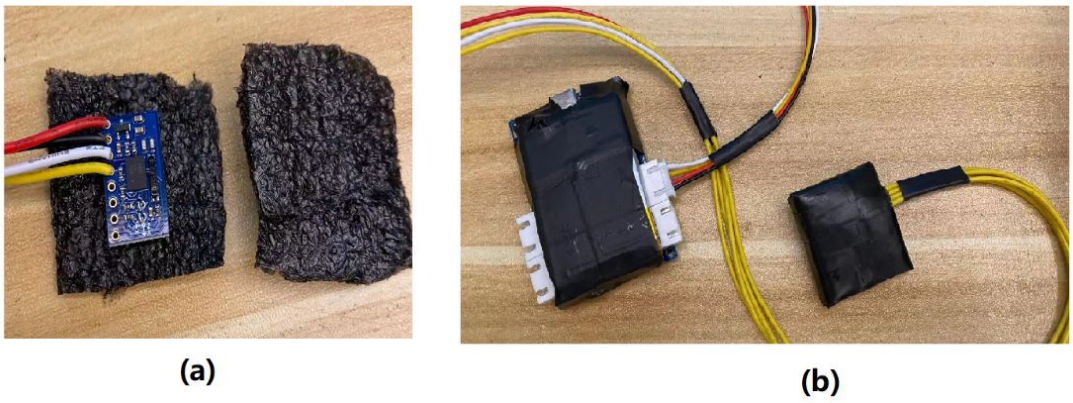

Figure 3.9: (a) Foam board is placed on the IMU for component protection and (b) rubber tape is used to secure the wire connections between the processing unit and IMUs.

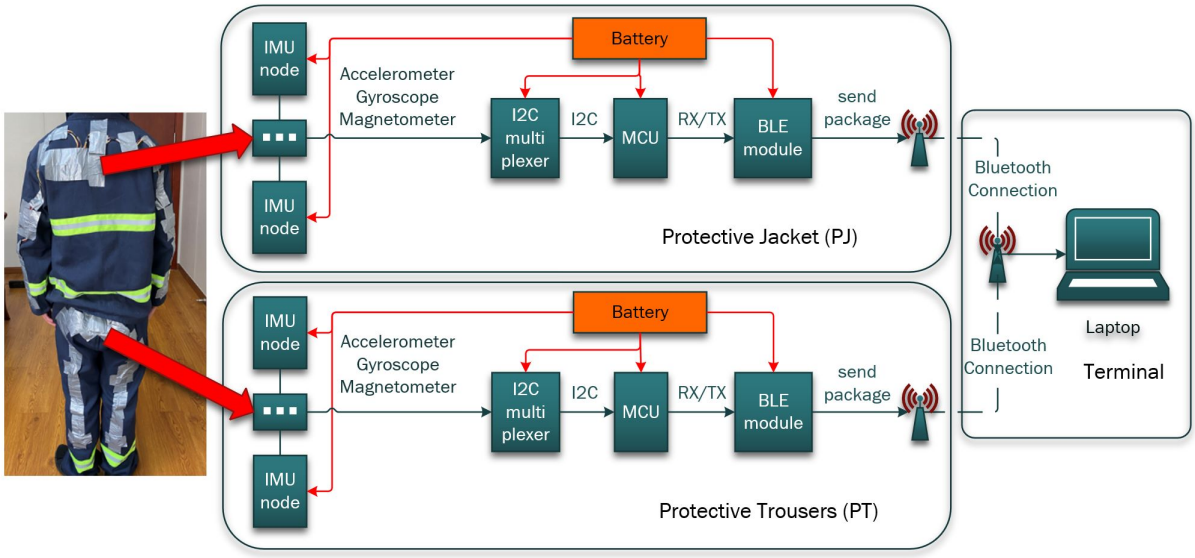

Figure 3.10: Overall design of the communication framework from the PJ and PT to a terminal via BLE 4.2 wireless transmission.

fall-like activities. The number of trials for each activity and total trials are summarised in Table 3.3.

IMU data from the PJ and PT are transmitted to a laptop via BLE 4.2 wireless communication with a 15 Hz sampling rate, as shown in Figure 3.12. A fall action consists of three phases: pre-impact, impact, and recovery [152]. As this study aims to target the falling event, the recorded data of the pre-impact and impact phases are labelled as fall, whereas the rest are labelled as non-fall. The total dataset comprises 221,820 samples,

Figure 3.11: Demonstration of a firefighter with the proposed PJ and PT performing different types of falls and fall-like activities, including (a) walking to a mat before falling, (b) forward fall with the knees, (c) forward fall with the hands, (d) left side of an inclined fall, (e) right side of an inclined fall, (f) slow forward fall with a crouch first, (g) backward fall, (h) fall-like crouching, (i) fall-like sitting, and (j) fall-like walking with a stoop.

Table 3.3: Details of activities recorded in the dataset

Code	Type	Activity	No. of Subject	Total trials
F1	Falls	forward falls using knees	5	70
F2		forward falls using hands	5	70
F3		inclined falls left	4	56
F4		inclined falls right	4	56
F5		slow forward falls with crouch first	3	42
F6		backward falls	3	42
FL1	Fall-like	crouch	4	56
FL2		walk with stoop	4	56
FL3		sit	3	42

distributed as follows: 33,092 in F1, 31,371 in F2, 26,256 in F3, 25,539 in F4, 17,479 in F5, 21,288 in F6, 26,670 in FL1, 13,965 in FL2, and 21,750 in FL3. The dataset is public available at `https://github.com/HCI-Laboratory/Smart-Firefighting/tree/main/Fall%20Detection`.

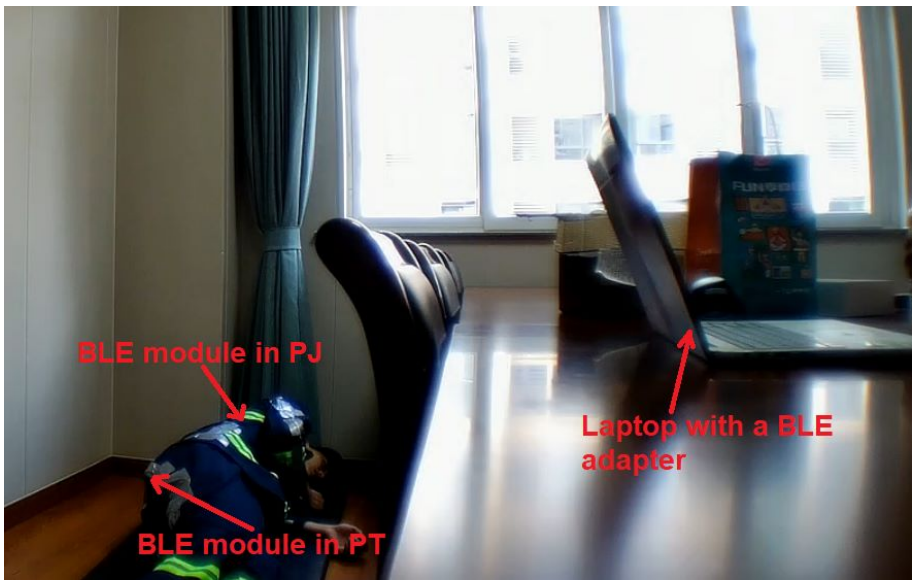

Figure 3.12: Data collection, via BLE 4.2 wireless transmission to a laptop, of IMU data from the PJ and PT.

3.4 Results

3.4.1 Performance Evaluation of Fall Detection with Multi-IMUs

First, the performance of the trained model with the proposed LSTM architecture is presented in Figure 3.13, trained with an RTX2060 6G RAM GPU with an Intel i7-9700 CPU (3.0 GHz). The results indicate a slow increment in the accuracy rate after 40 training epochs, with the highest accuracy of 99.95% obtained after 100 training epochs, using all the sensor data.

Meanwhile, this study has allocated 30 different combinations of sensor placements to further investigate the optimisation of the sensors' placements and the number of sensors allocated for the fall detection of firefighters. Five positions were coded, representing the placement of the IMU on the protective clothing, as listed in Table 3.4, including the chest, elbows, wrists, thighs, and ankles. The performance of each combination's model is evaluated with the metrics, including AUC, Specificity (Sp, see Equation 3.24), Sensitivity

(Se, see Equation 3.25) and Accuracy (Ac, see Equation 3.26).

$$Se = \frac{TP}{TP + FN} \tag{3.24}$$

$$Sp = \frac{TN}{TN + FP} \tag{3.25}$$

$$Ac = \frac{TP + TN}{TP + TN + FP + FN} \tag{3.26}$$

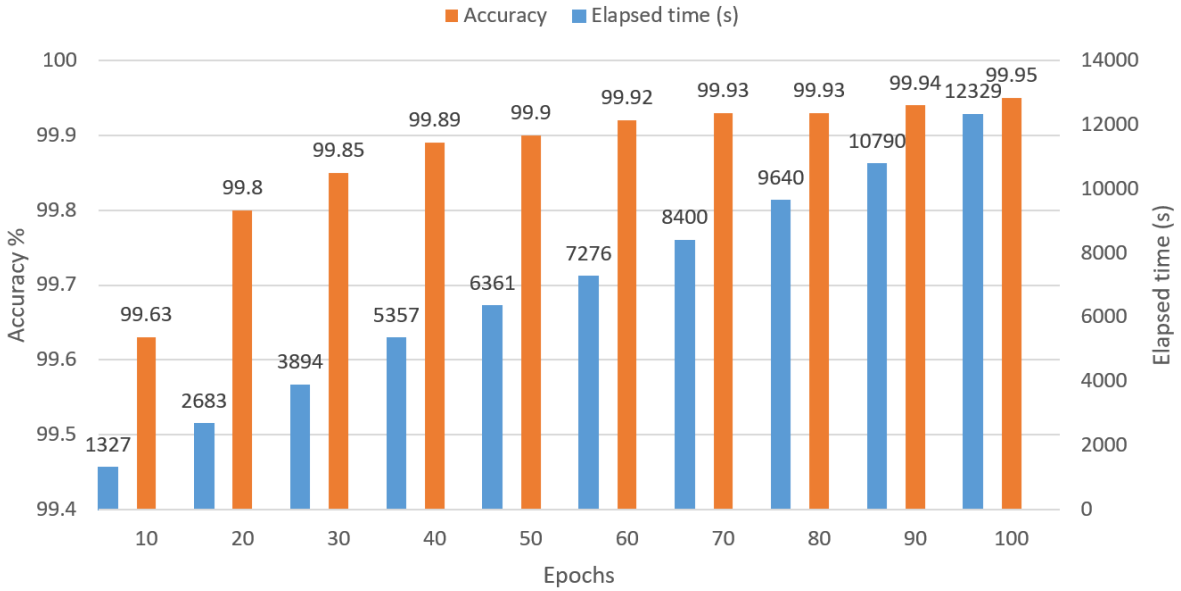

Figure 3.13: Training results of the LSTM model using different epochs.

Table 3.4: Codes for the IMU locations

Placement	Chest	Elbows	Wrists	Thighs	Ankles
Code	C	E	W	T	A

Table 3.5 illustrates the performance of these 30 models. The training accuracy of the models after 100 epochs is identical and mostly over 99.90%. In general, the best fall detection performance improved gradually with the addition of more IMUs placed on different sections of the cloth, with the highest Ac, Se, and Sp achieved at 94.10%, 92.25%, and 94.59%, respectively, for all IMUs included as proposed.

It is important to note that the IMU placed on the chest plays an important role in detecting the fall of the firefighter, as the combination of EWTA, where the chest part is

excluded, has the lowest Ac, Se, and Sp of 90.32%, 90.72%, and 90.21%, respectively. In addition, the IMU combinations of CET, CA, and a single C also achieved Ac of over 92% (Se over 90% and Sp over 92%). This further emphasised that the placement of an IMU on the chest is essential in detecting falls. In the group of two placements, combinations that involved the chest achieved fairly high Ac of over 90% and Sp of over 90%, but Se as low as 86.94%. Similarly, with only one IMU placement, the chest also presents a much higher efficiency than the others.

It is also interesting to note that the combinations of EA and ET, with IMUs placed on the elbows (PJ) and either the ankles or thighs (PT), also have Ac of over 90%, outperforming the rest of the IMU combinations. Moreover, the fall-detection performance based on PJ only (CEW) and PT only (TA) achieved Ac of 91.26% and 89.20%, respectively, indicating that adding IMUs from PT (either the thighs or ankles) can improve the overall fall-detection Ac by at least 2%. In summary, the results indicated that the IMU combinations of CEWTA, CEWT, and CET had the best performance among all metrics. Moreover, the chest position proves to be the most important placement of the IMU in fall detection for firefighters.

Furthermore, the most efficient combinations of each quantity group were evaluated. Figure 3.14 presents the results of the trained models in terms of accuracy and loss. The results illustrate that the fewer the placements, the lower the efficiency in the small-epoch training model, although the accuracy and loss were quite similar after training for 100 epochs. Moreover, Figure 3.15 illustrates the ROC curves and AUC values of these five models. The results show that all five models perform well and have similar ROC curves. To further evaluate the performance of these models, the efficiencies of each collected activity were compared.

Table 3.5: Performance of 30 IMU combinations

Quantity of IMU	Combination	AUC	Se	Sp	Ac
9	CEWTA	0.97	92.25%	94.59%	94.10%
7	CEWT	0.98	91.22%	94.72%	93.98%
7	CEWA	0.95	89.04%	94.25%	93.15%
7	CETA	0.95	88.01%	95.37%	93.82%
7	CWTA	0.95	90.35%	94.21%	93.38%
8	EWTA	0.94	90.72%	90.21%	90.32%
5	CEW	0.94	88.72%	91.94%	91.26%
5	CEA	0.95	88.39%	92.24%	91.43%
5	CWT	0.98	88.39%	92.24%	91.43%
6	EWA	0.93	85.06%	92.42%	90.87%
6	EWT	0.96	89.14%	91.42%	90.94%
5	CWA	0.96	90.84%	93.02%	92.56%
5	CET	0.97	91.61%	94.06%	93.55%
5	ETA	0.96	90.54%	92.30%	91.93%
5	WTA	0.93	90.54%	92.30%	91.93%
3	CE	0.96	92.88%	89.92%	90.54%
3	CW	0.95	90.96%	93.49%	92.96%
3	CT	0.95	86.94%	92.97%	91.70%
3	CA	0.94	90.23%	93.97%	93.18%
4	TA	0.92	83.92%	90.61%	89.20%
4	ET	0.91	85.34%	92.19%	90.75%
4	EA	0.95	87.40%	93.49%	92.21%
4	WT	0.91	85.99%	84.76%	85.02%
4	WA	0.90	81.98%	90.72%	88.88%
4	EW	0.94	83.01%	90.75%	89.14%
2	E	0.91	85.08%	88.70%	87.94%
2	W	0.84	71.99%	80.65%	78.83%
2	T	0.88	78.56%	86.56%	84.87%
2	A	0.89	73.97%	92.44%	88.55%
1	C	0.96	92.82%	92.43%	92.51%

Table 3.6 presents the detailed performance of these models for each activity. To clarify, the Se is zero for fall-like activities because no falling happens; hence, no true falling labels appear. According to the average results of these five models, F1 and F6 in the falling activities have lower Se than the other four types. This is mainly because these two activities have an action to reduce the impact before falling, while the others fall directly to the ground. In F1, the knees touch the ground first before falling, and the firefighter sits on the ground, when simulating a backward fall in F2.

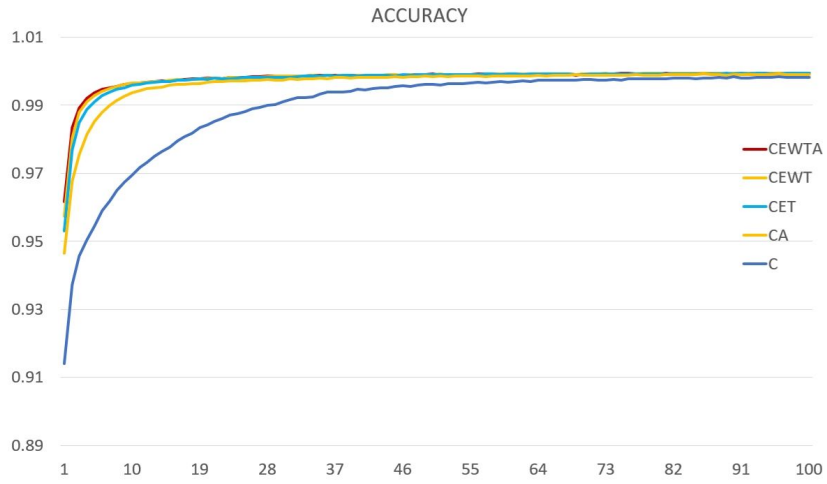

(a)

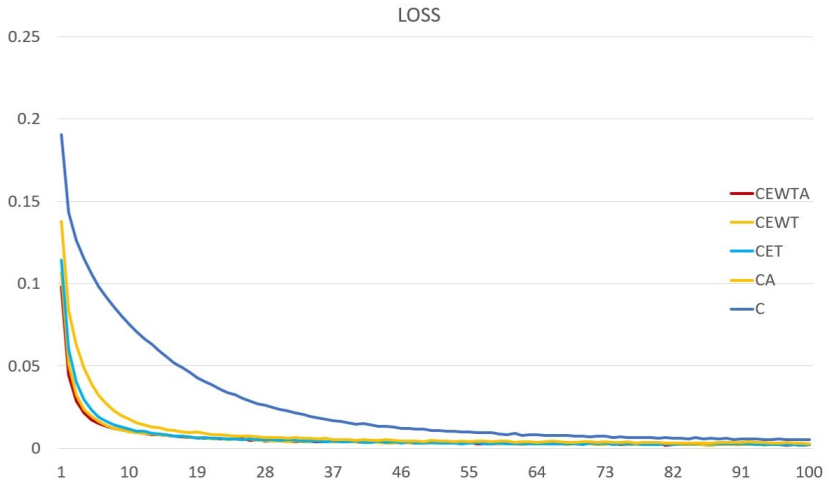

(b)

Figure 3.14: Illustration of the training performances of five trained models in (a) accuracy and (b) loss.

Meanwhile, for the fall-like activities, the model is incorrectly predict FL2 (walking with a stoop) as falling. This is because the physical status of the upper body is similar to a fall event; hence, it is more difficult to distinguish FL2, if fewer of the lower body's features are utilised. It is also important to notice that the Sp of the falls are much higher than those of the fall-like activities, which illustrates that fall-like motions indeed have some similarities with falling motions, while normal walking is very different from falling.

In terms of the each model performance, all five models are sufficient for fall detection

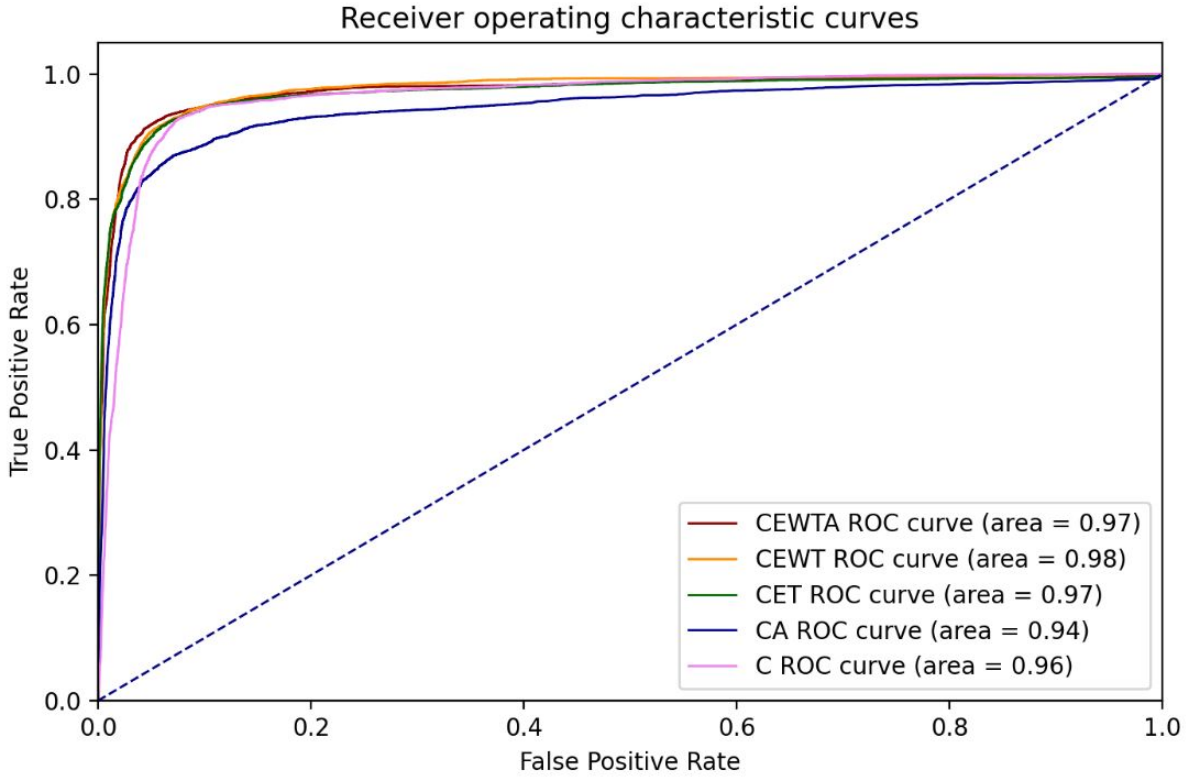

Figure 3.15: ROC and AUC results of the five models.

(Se over 90% and Ac over 92%); however, the CA and C models are insufficient for a specific fall activity (F2 and F4, respectively). This illustrates that it is difficult to detect some of the falling activities with fewer IMUs and fewer features. Moreover, CEWTA shows a better ability to distinguish falls and non-falls because the Sp of each activity is generally higher than that of the other models. This illustrates that the fall-detection system can indeed be improved by using more IMUs in different positions. In general, the IMU combinations of CEWTA, CEWT, and CET performed the best in each activity.

3.4.2 Performance Evaluation of V-RNN FDS

Table 3.7 illustrates the performance of proposed BMV in fall detection. The rank column presents the five best models and the five worst models according to the average value of Se, Sp, and Ac.

Table 3.6: Detection efficiency for each fall activity

Activity	CEWTA			CEWT			CET		
	Se(%)	Sp(%)	Ac(%)	Se(%)	Sp(%)	Ac(%)	Se(%)	Sp(%)	Ac(%)
F1	91.45	96.87	95.42	87.28	98.40	95.42	89.11	98.25	95.80
F2	94.48	98.34	97.15	93.54	98.26	96.81	95.22	98.38	97.41
F3	96.55	97.20	97.00	95.69	97.58	97.07	97.09	97.10	97.10
F4	95.02	98.72	97.62	94.91	99.02	97.79	95.37	98.72	97.72
F5	96.62	97.40	97.22	98.46	97.22	97.50	97.23	97.22	97.22
F6	78.38	99.05	92.80	80.70	99.27	93.66	76.71	99.11	92.33
FL1	0	90.31	90.31	0	90.06	90.06	0	89.38	89.38
FL2	0	89.92	89.92	0	84.17	84.17	0	82.21	82.21
FL3	0	87.79	87.79	0	89.87	89.87	0	87.60	87.60
Total	92.25	94.59	94.10	91.22	94.72	93.98	91.61	94.06	93.55
Activity	CA			C			Average		
	Se(%)	Sp(%)	Ac(%)	Se(%)	Sp(%)	Ac(%)	Se(%)	Sp(%)	Ac(%)
F1	91.25	94.31	93.49	90.84	95.31	94.11	89.99	96.63	94.85
F2	81.84	95.89	91.58	97.66	95.81	96.38	92.55	97.34	95.87
F3	93.64	97.44	96.27	99.68	95.80	97.00	96.53	97.02	96.89
F4	94.61	98.08	94.07	84.14	96.61	92.90	92.81	98.23	96.02
F5	98.46	96.32	96.80	96.61	97.04	96.94	97.48	97.04	97.14
F6	78.38	97.60	91.79	88.55	97.88	95.06	80.54	98.58	93.13
FL1	0	83.72	83.72	0	99.61	99.61	0	90.62	90.62
FL2	0	86.88	86.88	0	80.88	80.88	0	84.81	84.81
FL3	0	89.99	89.99	0	93.05	93.05	0	89.66	89.66
Total	90.23	93.97	93.18	92.82	92.43	92.51	/	/	/

The results indicate that the inclusion of BMV algorithm improved the overall fall detection. Based on the performances of M1 and M2-M21, most of the models with the proposed voting algorithm perform better than the M1 that has no voting algorithm in all aspects. It revealed that the BMV algorithm is effective in improving the fall detection results. Moreover, in comparison of the models with the same data length W, the Se is improved with lower voting threshold whereas Sp is higher with increased voting threshold. The results also stated that the threshold set as half of data length has a better performance according to the rank of these models. In addition, the ranks also indicated that the performances are improved significantly when the data length is increased from 4 to 30 but less significant when increased from 30 to 60. Since a longer data length

Table 3.7: Results of ablation study of the proposed fall detection models

Group	Models	Se	Sp	Ac	Rank
M1	Without BMV	96.32%	95.63%	95.73%	19(95.89%)
M2	W = 4, Tv = 2	97.04%	95.35%	95.60%	18(96.00%)
M3	W = 6, Tv = 3	97.09%	95.80%	96.00%	17(96.30%)
M4	W = 10, Tv = 4	98.58%	94.95%	95.50%	
M5	W = 10, Tv = 5	97.78%	96.43%	96.64%	
M6	W = 10, Tv = 6	95.74%	97.86%	97.54%	
M7	W = 20, Tv = 8	98.92%	96.15%	96.57%	
M8	W = 20, Tv = 10	97.76%	97.81%	97.80%	5(97.79%)
M9	W = 20, Tv = 12	95.52%	98.89%	98.38%	
M10	W = 30, Tv = 12	99.16%	96.37%	96.79%	
M11	W = 30, Tv = 15	97.78%	98.09%	98.05%	1(97.97%)
M12	W = 30, Tv = 18	93.67%	99.16%	98.32%	
M13	W = 40, Tv = 16	99.37%	96.14%	96.64%	
M14	W = 40, Tv = 20	97.62%	98.13%	98.05%	2(97.93%)
M15	W = 40, Tv = 24	91.50%	99.32%	98.13%	
M16	W = 50, Tv = 20	99.54%	95.56%	96.17%	
M17	W = 50, Tv = 25	97.47%	98.16%	98.05%	3(97.89%)
M18	W = 50, Tv = 30	89.09%	99.46%	97.88%	20(95.48%)
M19	W = 60, Tv = 24	99.64%	95.10%	95.79%	
M20	W = 60, Tv = 30	97.42%	98.12%	98.01%	4(97.85%)
M21	W = 60, Tv = 36	86.18%	99.53%	97.49%	21(94.4%)

Note: W is the window size (data length); Tv is the voting threshold.

would result in a longer time delay, as a result, M11 with W of 30 and T_v of 15 is the optimal model among others that showed 97.78%, 98.09%, and 98.95% in Se, Sp, and Ac, respectively.

3.4.3 Results Comparison with Existing Work

Table 3.8 illustrates a results comparison of the proposed CWETA, M1 and M11 models with existing studies. Firstly, the proposed method only utilised a low data sampling rate (15 Hz) to achieve higher performance in Se, Sp, and Ac, compared to the other studies (100 Hz), which indicates a cost reduction in the data-processing complexity and power consumption. In a comparison of the M1 (raw features) with the CEWTA model (including computed features of quaternion and Euler angles), which have the same

RNN model, the results revealed that the raw features are sufficient for fall detection, while the computed quaternion and Euler angles increased the complexity of input features, thus, influences the classification performance.

The study by [24] presented an acceleration-based algorithm and later further improved with four other algorithms [25]. These algorithms are threshold-based, while the four improved algorithms (A1-A4) have improved physical performance because of a double-check method used to reduce false detection. A1 utilised all features of different types of sensors, while the others used parts of the features. The results revealed that A5 performs worse than proposed three models in all aspects, and A2-A4 have a higher Se but the overall Ac is less efficient. Moreover, A1 showed a 100% Ac in fall detection, which highlighted the improvement approach of fall detection using a multi-sensory approach.

Besides, the FDS (with an IMU on the waist) proposed by [117] showed similar performance with the proposed M1 model, but less efficient than the proposed M11 with the BMV algorithm. In contrast, the results by [114] showed 76.8% Se, indicating that placing IMU on the ankle contributed less to fall detection. In general, the proposed 9-IMU-based wearable FDS using the V-RNN approach showed high Se and Ac in fall detection and significantly enhanced the classification performance compared with our previous work.

Table 3.8: Results comparison of fall detection with the proposed CEWTA, M1 and M11 models, and other existing work

Study	Application	Method	Algorithm	Sampling Rate (Hz)	Se (%)	Sp (%)	Ac (%)
Pham *et al.* (2018) [24]	Firefighters	1 3-DOF accelerometer and 1 barometer on the thigh pocket, and 1 CO sensor on the mask (they raised 4 algorithms in [24] and 1 algorithm in [25])	A1	100	100	100	100
			A2		100	94.44	95.83
			A3		100	90.74	93.05
			A4		100	91.67	93.75
Pham *et al.* (2018) [25]			A5		88.9	94.45	91.67
Shi *et al.* (2020) [117]	Elderly	1 IMU on waist	CNN	100	95.54	96.38	95.96
Luna-Perejon *et al.* (2021) [114]		1 IMU on ankle	LSTM	100	76.8	92.8	/
Kiprijanovska *et al.* (2020) [116]	Ordinary being	2 IMUs in 2 smartwatches	CNN-BiLSTM	100	90.6	86.2	88.9
Proposed CEWTA	Firefighters	9 9-DOF IMUs on the chest, wrists, elbows, thighs and ankles	LSTM	15	92.25	94.59	94.10
Proposed M1			LSTM		96.32	95.63	95.73
Proposed M11			V-RNN		97.78	98.09	98.05

3.4.4 Performance Evaluation of using ML with AFE Method

Table 3.9 presents the four different sets of input features extracted for fall detection. For metrics-based methods, the mean, range, standard deviation, and mean absolute deviation of each feature are further extracted based on the AFE or RFE, named AFEM and RFEM, respectively. The window size is defined as 0.5 seconds. Three of the most commonly used ML-based methods, including decision tree (DT), K-nearest neighbour (KNN), and support vector machine (SVM), were used to evaluate the impact different feature sets have on these classifiers and identify the optimal classifier for the proposed FDS.

Table 3.9: Extracted input features with different extraction methods

Features Set	Total Features for 9 IMUs FDS
AFE	5 attitude features
RFE	54 (6-DOF raw data $\times$ 9 IMUs)
AFEM	5 AFE $\times$ 4 metrics = 20
RFEM	54 RFE $\times$ 4 metrics = 216

Table 3.10 presents the fall detection performance of four feature extraction methods using KNN, DT, and SVM. The performance of the detection is evaluated using Se, Sp, and Ac.

SVM performed the best among the three ML methods for classification. According to the results of both AFE-SVM and RFE-SVM, although the Sp performance of both approaches is similar, the Se of AFE-SVM is much lower than that of RFE-SVMs. It is also important to note that the classification performance has significantly improved after applying the AFEM. Generally, RFEM-SVM had the best Ac performance, achieving 98.63%, while the AFEM-SVM model ranked second with 98.54%. The results of AFEM-SVM show that the proposed AFE method is effective for fall detection.

However, as shown in Table 3.11, the processing speed and feature size of the proposed AFE and AFEM present unique advantages with utlisation of SVM. The RFE-SVM testing time is 23.9 seconds, which impacts the practicality of this approach for real-time fall detection. AFE-SVM completes in only 1.185 seconds due to fewer features being processed. In summary, the proposed AFEM method has the similar performance to the RFEM method, but requires only a tenth of the features of RFEM, which significantly reduces the processing time.

Table 3.10: Results of fall detection performances of four types of feature extraction methods using KNN, DT, and SVM

Features Set	Classifier	Se (%)	Sp (%)	Ac (%)
AFE	KNN	91.38	99.51	96.98
	DT	92.15	99.46	97.19
	SVM	91.53	99.76	97.21
RFE	KNN	94.56	99.76	98.15
	DT	95.86	99.58	98.43
	SVM	96.72	99.46	98.52
AFEM	KNN	95.56	98.86	97.80
	DT	93.33	98.60	96.91
	SVM	97.01	99.25	98.54
RFEM	KNN	89.0	99.21	95.96
	DT	94.81	98.34	97.21
	SVM	97.04	99.39	98.63

Table 3.11: Results of processing time and feature size of four types of feature extraction methods using SVM

Features Set	Training		Testing	
	Time (s)	Size	Time (s)	Size
AFE	115.814	5×129113	1.185	5×25912
RFE	119.751	54×129113	23.9	54×25912
AFEM	2.350	20×16966	0.133	20×3414
RFEM	7.941	216×16966	0.447	216×3414

3.5 Summary

This chapter presented our preliminary study on FDS where a novel wearable FDS for firefighters is proposed, by embedding nine IMU sensors on the firefighting PPC. In this

study, the simulated falling events were designed based on the experiences and feedback collected from firefighters, and fourteen firefighters participated in the data acquisition. This preliminary study denoted the potential of wearable embedded motion sensors for identifying the falling activities of firefighters. Through evaluating the placements of IMUs, the results indicate that an IMU placed on the chest was critical for achieving the best fall detection performance. It also concluded that placing IMUs on the chest, elbows, and thighs could also achieve an acceptable fall detection performance with higher cost efficiency. Additionally, by utilising the proposed RNN and V-RNN, this study highlights the effectiveness of using DL methods in FDS, and presents an optimal V-RNN model with $W = 30$ and $Tv = 15$, which achieves a Se of 97.78% and a mean Ac of 98.05%. Compared with existing studies, our FDS outperforms others with a lower sampling rate, reducing computation costs and power consumption. Finally, the proposed AFE and AFEM methods demonstrated significant reductions in processing time and feature dimensionality, making them suitable for on-device fall detection classification within resource-constrained processing architectures.

Although the proposed 9-IMU-based FDS achieves high Ac in detecting fall-related dangers in firefighting, there are two issues we found during our experiments that should be addressed. First, during data collection, the wired connections with sensor nodes are found to be vulnerable to practical use for firefighters. An alternative design of wearable prototype with wireless connections is to be explored for improving the sensing stability. Besides, the coverage of BLE was identified to be highly affected by walls and other obstacles within the range of meters. Future work should also focus on improving the collection of sensor data approach through enhancement in the wireless network transmission framework.

Overall, this study contributes to the development of a highly accurate and efficient safety risk assessment model for firefighters, specifically targeting the detection of fall-related activities. However, two issues should be addressed: a reliable wireless network to ensure transmission efficiency and a PI-FDS to detect falls ahead. Therefore, the next study (see Chapter 4) will research the IoT-based PI-FDS for detecting the early imbalance phase of falls to improve the algorithm efficiency and provide a reliable network to transmit information effectively.

Chapter 4

Design of IoT-Based Pre-Impact Fall Detection Model for Firefighters

4.1 Introduction

PI-FDS is developed to enhance risk assessment by detecting falls before impact occurs, allowing for timely alerts and the activation of protective measures such as airbag systems or emergency signals. Designed for real-time applications, an ideal PI-FDS should operate on lightweight hardware and employ algorithms with minimal computational demands to ensure efficiency. Traditionally, micro-controllers implemented detection algorithms using classical threshold-based methods [153]. However, with the advancement of SoC technology and ML, edge computing has become feasible. Previous studies on FDS and PI-FDS often executed algorithms on high-performance computers, but few addressed the processing time required for detection algorithms.

Using datasets from prior FDS studies (Figure 3.11 and Table 3.3), this study explores integrating PI-FDS into FRAS. It evaluates pre-impact fall detection performance using ML and EL methods typical in HAR and FDS applications, identifying optimal approaches for edge deployment. Notably, effective networking is crucial for PI-FDS, as previous FDS prototypes faced challenges with long-range BLE transmission. To address this, an IoT network framework for firefighting (IoF) is designed to support distributed monitoring and coordinated rescue responses using advanced IoT techniques.

This study is published as:

- [Journal] Pre-Impact Firefighter Fall Detection Using Machine Learning on the Edge, *IEEE Sensors Journal*, 2023 (IF = 4.3, CAS Q2, JCR Q1).
- [Patent] A Wearable Device for Fall Detection, 2023, CN218684386U. (Granted)

The remainder of this chapter is structured as follows: Section 4.2 details the IoF framework's structure, the edge device used for algorithm deployment, and the ML-based PI-FDS algorithm utilising a class-imbalanced thresholding method. Section 4.3 presents the classification performance of candidate classifiers and discusses the optimal PI-FDS model, evaluating real-time performance on the edge. Finally, Section 4.4 concludes with a summary of this study and outlines future research directions.

4.2 Methodology

4.2.1 Hardware Design

This study designed an IoF transmission framework integrated with WBSN and IoT networks, which considered the sufficiency of transmission throughput and range for diverse firefighting missions. Figure 4.1 displays an overview of the system architecture, including the WBSNs using BLE in the fireground, which are linked to the IoT network (outside the fireground) via LoRa. The framework can be broadly divided into four modules: the sensor node (SN), the body node coordinator (BNC), the long-range wide-area network (LoRaWAN) gateway, and the command terminal device (tablet PC). The WBSN was constructed based on the existing firefighting equipment. For each firefighter, nine SNs integrated into the firefighting suit were placed at the chest, wrists, elbows, thighs, and ankles. The BNC, which was integrated into the helmet, transmitted the monitoring

information to the gateway installed on the firefighting vehicle outside.

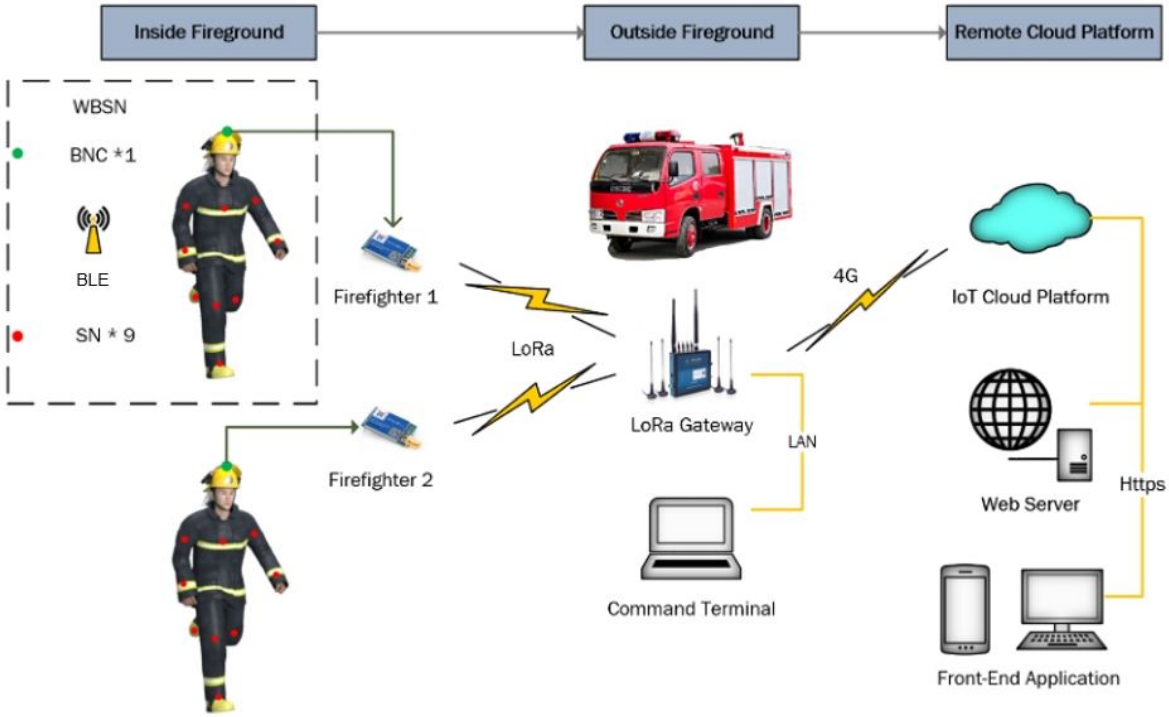

Figure 4.1: Overview of the IoF framework.

Table 4.1 specifies the main hardware components utilised in the IoF framework, and Figure 4.2 details the components utilised in the SN and BNC. The SN primarily consisted of a micro-controller unit (ESP32-D0WDQW6-V3) and an IMU (BNO055), which collected data and transmitted them over the WBSN. The IMU was configured to collect data on tri-axial acceleration and tri-axial angular velocity. To balance power consumption and accuracy, the IMU sampling rate was set to 15 Hz [145].

As for the BNC, a Raspberry Pi Zero 2W (RPI-2W) was utilised as the edge to deploy the detection algorithm. This micro-processor was used because it has sufficient external memory to store the pre-trained models and was compatible with MicroPython. Besides operating the PIFDS, the BNC also constructed a WBSN with BLE connection to receive data from nine SNs, and it sent the detection results and monitoring data to the LoRa gateway via the LoRaWAN module.

The USR-LG220 LoRaWAN gateway [154] was pre-installed on the firefighting vehicle. The Internet access is supported by the China Mobile 4G provider. The gateway transmits client data to the IoT cloud platform provided by the gateway vendor. The gateway was also connected to the terminal via LAN so that the terminal could receive data properly under extreme circumstances with no 4G network available.

Table 4.1: Hardware specification of IoF framework

Modules	Components	Specification
SN	BNO055	9-DOF IMU Sampling rate: 100 Hz
	ESP32-D0WDQ6-V3	Xtensa 32-bit dual-core CPU 448 KB ROM & 520 KB SRAM 2.4 GHz Wi-Fi & BLE 4.2 Operating voltage: 3.3 V
BNC	LoRaWAN terminal module	ASR6601 SoC Frequency range: 398-525 MHz Data rate: 0.814 Kbps
	Raspberry Pi Zero 2W	1 GHz quad-core Arm Cortex-A53 512 MB RAM 2.4 GHz Wi-Fi & BLE 4.2
Firefighting Vehicle	LoRaWAN Gateway	3 data channels WAN × 1 & Wi-Fi 4G LTE (support 2G/3G) Operating voltage: 5-36 V

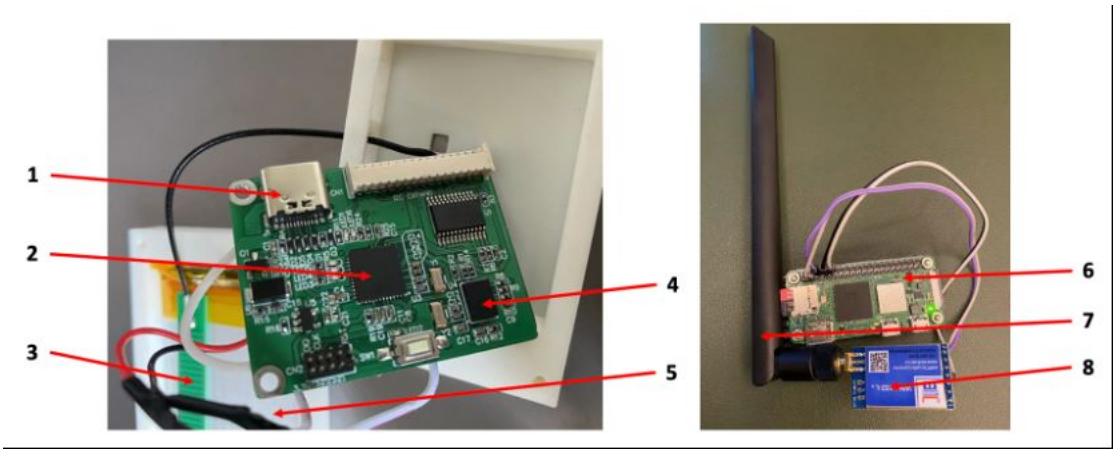

Figure 4.2: Major components integrated into the SN (left) and BNC (right), including 1: Charging port, 2: ESP32-D0WDQ6-V3, 3: PCB antenna, 4: BNO055, 5: battery, 6: Raspberry Pi Zero 2W, 7: antenna, and 8: LoRaWAN module.

4.2.2 Skeleton Reconstruction

In real firefighting scenarios, blindly relying on the detection results to carry out the rescue of a firefighter will result in lower firefighting efficiency. Studies by [155, 156, 157] showed that the most significant advantage of the proposed nine-IMU wearable system is the ability to 3D model the skeleton of firefighters as an alternative to computer vision technology for synchronously reconstructing the attitude of firefighters. The reconstructed attitude of firefighters can be derived through a manual double-check method to decrease the likelihood of a false alert.

MEMS based IMUs exhibit drift over time, particularly in the case of the gyroscope. Study by [158] stated that the drift observed after a one-hour test ranges between 0.04° and 1.08°. Consequently, prior to data collection, firefighters complete a 10-second initial calibration procedure while maintaining a stationary pose to counteract the drift. The calibration stage also serves to align all IMUs from their local coordinate systems to the standard east-north-up (ENU) system, utilising gravity and magnetic vectors (see Chapter 3.2.1). After calibrated data was collected, the Madgwick AHRS method was used in order to estimate the quaternions of the IMU based on the tri-axial acceleration and angular velocity [142]. Subsequently, these generated coordinates for each point could be calculated based on the previous coordinates and the quaternions, according to Equation 3.22.

Figure 4.3 illustrates the 3D skeleton plots and corresponding real motions performed in our previous data acquisition described in Chapter 3.3.2. A 3D skeleton model is initially plotted with 19 points, as shown in Figure 4.3a, which can be divided into trunk-related and IMU-related. IMU-related points, representing IMU locations placed on the

body, are updated according to the rotation of IMUs. The trunk-related points, referring to the kinematics of the firefighter, are assumed to have the same rotation of the chest IMU. The 3D visualisation allows the IC to monitor the motion of the firefighters and arrange a rescue if necessary.

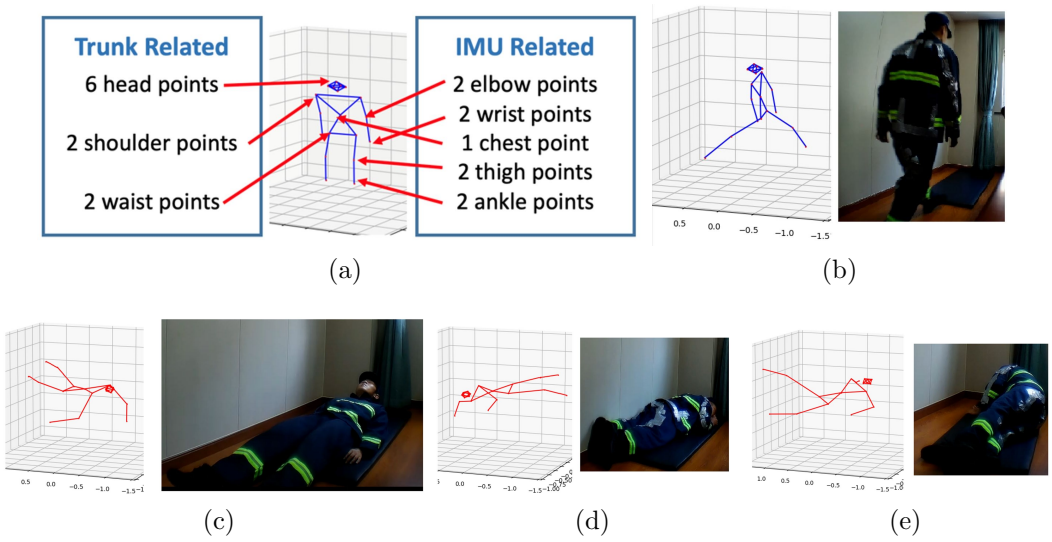

Figure 4.3: Illustration of the (a) 3D skeleton plots that represent (b) walking, (c) F6 event, (d) F3 event, and (e) F4 event (see Table 3.3).

4.2.3 Pre-impact Fall Detection Algorithm

Classifier and Hyperparameter Optimization

The raw motion data collected from the IMUs, including the tri-axial acceleration (in m/s^2) and the tri-axial angular velocity (in deg/s), are fed directly into the classifier model as feature inputs. Thus, the total number of columns required for the input features for all nine IMUs is 54. According to various studies in FDS and human activity recognition (HAR), TBA- and ML-based methods are more suitable for the edge node because they are less computationally expensive. However, DL-based methods commonly perform better in accuracy and sensitivity because high-level features can be automatically extracted [159].

Table 4.2: Hyperparameters in the ML and EL models

Classifier	Parameter Description
SVM	C = {1, 3} kernel = {'rbf','linear','poly'}
Decision Tree	max_depth = {1, 2, ..., 9, 10} criterion={'gini','entropy'}
AdaBoost	learning_rate = {1, 0.5, 0.2, 0.1, 0.05} n_estimators = {30, 40, ..., 100, 110, 150, 200, 300}
Random Forest	n_estimators = {40, 50, ..., 120, 130} criterion={'gini','entropy'}
KNN	n_neighbors = {5, 6, 7, 8, 9, 10, 11}
Logistic Regression	Default
Stacking	Combinations with the optimal models above

Even though various ML methods have been proposed in previous studies [160], no study has comprehensively compared these methods. In this study, DT, KNN, SVM, and logistic regression were evaluated to investigate their performance in pre-impact fall detection applications. In addition, EL is widely used in FDS and HAR to achieve higher accuracy by combining the results from certain weak learners. For instance, the study by [161] proposed the Stacked LSTM-Net model for HAR and proved that the ensemble DL model exhibited better performance than these base models. EL approaches can be categorised into three types: bootstrap aggregating (bagging), boosting, and stacking. In this study, three basic implementations were selected from each of these types, including RF, AdaBoost, and the stacking classifier with ML combinations. Table 4.2 depicted the hyperparameter setting for the ML methods utilised in this study.

Class-Imbalanced Thresholding

Given that the pre-impact phase typically lasts 200-400 ms [117], the class imbalance is identified with minority samples on the pre-impact (PI) class. To address this issue, the moving threshold method [162] is adopted to increase Ac of classification with imbalanced classes. The imbalance between the majority class and the minority class is represented by the ratio defined as follows:

$$\rho = \frac{samples\ in\ majority\ class}{samples\ in\ minority\ class} \tag{4.1}$$

The estimated threshold that matches the class contributions is computed as:

$$\hat{\lambda} = argmin_{\lambda}|f - f_{\lambda}| \tag{4.2}$$

where f is the frequency of the minority samples in the training dataset and f_{λ} is the frequency of the estimated minority samples with a given threshold λ. The relationship between the λ and the ρ is described by

$$\lambda^{*} = \frac{1}{N}(k \times e^{-\rho/10 \times k} + \frac{k}{10}) \tag{4.3}$$

where N is the number of classifiers and k is the classical threshold (set as 0.5). For a singular classifier, N is set to 1 by default, but the value is depending on the number of classifiers stacked in the stacking method.

The simulated fall events dataset described in Chapter 3.3.2 is utilised in this study. The data are relabelled by only identifying the pre-impact phase as the fall. Within the dataset of 221,820 samples, 27,885 samples are categorised as pre-impact labels. When training the models, 80% of the dataset was used for training and 20% for testing. To achieve a balance between processing speed and accuracy, the candidate models were first

trained and tested using a PC with an i7-9700 3.0 GHz CPU and NVIDIA RTX2060 6G RAM GPU. Next, to investigate the effectiveness of running the algorithm on the BNC, the candidate models were run on the RPI-2W. Then the trained models were deployed on the RPI-2W to validate the on-device performance.

4.3 Results

4.3.1 Evaluation of Candidate Classifiers

Firstly, the candidate classifiers with optimised hyperparameters that could be effective on the edge node was investigated. The performance of these binary classifiers was evaluated by calculating the area under the ROC curve (i.e., the AUC), and the processing time. The ideal candidate classifier should show equally high performances on both criteria, and the acceptable processing time for the testing dataset (18936 samples with 54 features) should be less than 1 second with an AUC of more than 0.98.

Figure 4.4 represents the performance and processing time of these models. Logistic regression was not included as the comparable of hyparameters is unlikely, but showed AUD of 0.9764 and an execution time of 0.0016 s. Among the ML and EL methods, KNN showed the lowest performance as the AUC only reached 0.941 and the processing time was over 12 s, which indicates that it is not suitable for the edge node. Hence, in the stacking implementation, the KNN was not used as a base classifier.

In terms of the classifier performance, the RF with 80 estimators and gini criterion outperformed the others with an AUC of 0.997, while the DT approach was much faster with an average execution time of 0.0019 s. Furthermore, increasing the depth value of the DT did not improve its performance, and the entropy function was more suitable than

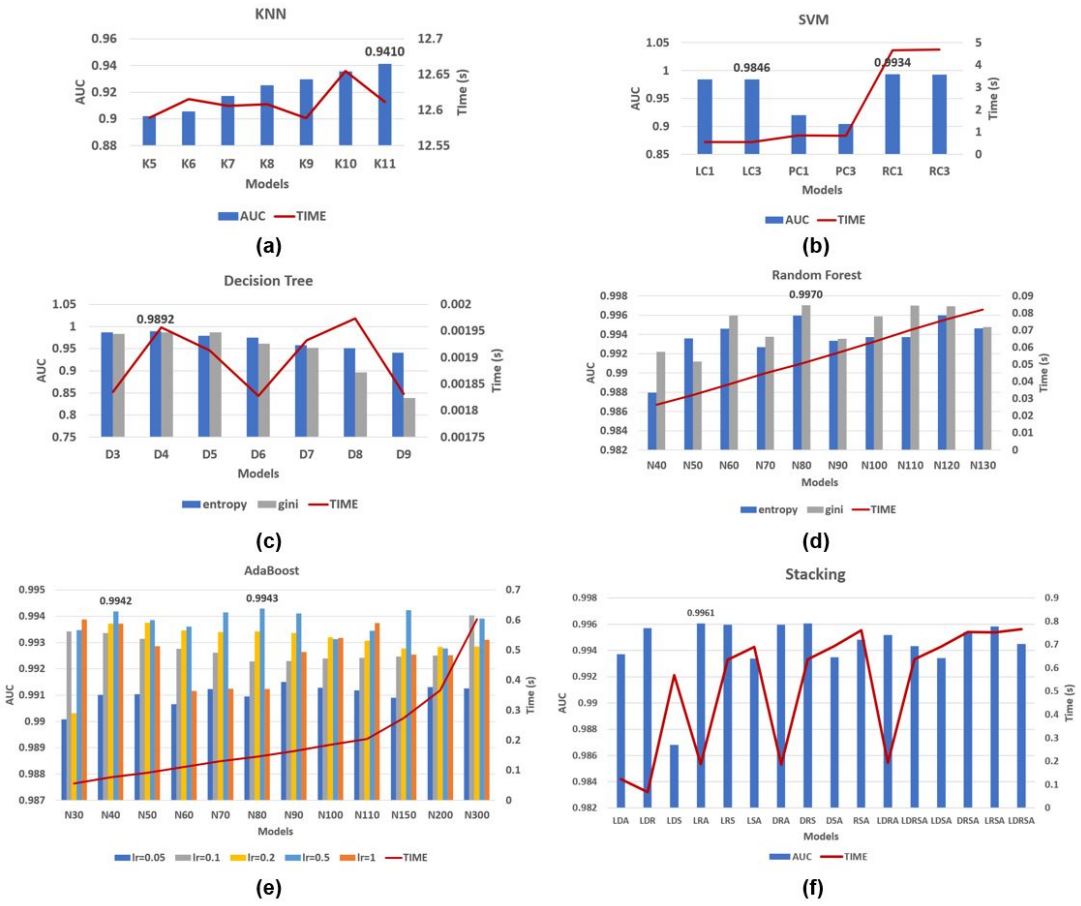

Figure 4.4: Performance evaluation with different hyparamater settings for (a) KNN, (b) SVM, (c) DT, (d) RF, (e) AdaBoost, and (f) stacking.

the gini. However, the variation of RF that used the gini criterion exhibited a superior performance. The processing time of the RF was proportional to the number of trees in the forest.

For the SVM, the linear kernel and rbf kernel achieved similar AUC results, but the processing time was significantly reduced with the linear kernel. In terms of overall performance, the SVM-LC3 was selected as one of the candidates.

For AdaBoost, there should be a trade-off between the learning rate and the n_estimators. Considering the execution time of these models, the model with 40 estimators and a learning rate of 0.5 was selected as the candidate. Moreover, the processing time of the stacking

classifiers is relevant to the base classifier utilised. Overall, LRA (which used logistic regression, RF, and AdaBoost as the base classifiers) was the optimal classifier, achieving an AUC of 0.9961 and an execution time of 0.188 s.

In summary, after evaluating these ML and EL methods, five classifiers, including SVM-LC3, DT-ED4, RF-GN80, AB-LR05N40, and STACK-LRA were selected to be further evaluated on the edge node.

4.3.2 Evaluation of the On-the-Edge Node

Apart from Ac, Se, and Sp, the lead time, which represents the time of the earliest occurrence detection before a collision, is also measured. To investigate the effectiveness of using the class-imbalanced thresholding method, the Youden index was also computed, as defined in Equation 4.4. In firefighting scenario, the Youden index assumes greater importance as it establishes a balance between Se and Sp, which not only ensures detection correctness but also considerably minimises the false alert rate.

$$J = Se + Sp - 1 \tag{4.4}$$

Table 4.3: Results of the five optimised classifiers with NT, CIT, and HST methods

Methods	Real-Time Execution Time in RPI-2W (ms)	Se (%)	Sp (%)	Ac (%)	J (%)	Lead Time (ms)
SVM-LC3 | w/ NT |		77.62	99.66	98.83	77.29	386.5
SVM-LC3 | w/ CIT |	2.1557	94.41	94.84	94.82	89.25	447.9
SVM-LC3 | w/ HST |		98.37	66.99	68.17	65.35	316.2
DT-ED4 | w/ NT |		82.75	99.56	98.93	82.31	423.7
DT-ED4 | w/ CIT |	0.6816	95.10	97.99	97.88	93.09	447.9
DT-ED4 | w/ HST |		98.13	94.87	95.00	93.01	375.1
RF-GN80 | w/ NT |		80.89	99.85	99.13	80.73	436.5
RF-GN80 | w/ CIT |	65.203	98.83	95.04	95.18	93.87	447.9
RF-GN80 | w/ HST |		100	91.95	92.22	91.95	370.7
AB-LR05N40 | w/ NT |		81.59	99.62	98.94	81.20	429.2
AB-LR05N40 | w/ CIT |	27.151	96.50	96.96	96.95	93.47	447.9
AB-LR05N40 | w/ HST |		99.77	69.76	70.88	69.52	316.2
STACK-LRA | w/ NT |		80.89	99.82	99.11	80.70	425.1
STACK-LRA | w/ CIT |	93.927	93.01	99.27	99.03	92.28	447.9
STACK-LRA | w/ HST |		99.30	89.23	89.61	88.53	357.4

Note: 'w/' represents 'with'.

Table 4.3 presents the experimental results for the five classifiers used by the RPI-2W with the normal thresholding (NT), class-imbalanced thresholding (CIT) method, and the highest Se thresholding (HST) method. The real-time execution represents the processing time required for the RPI-2W to collect the data and compute the detection results. The classical 0.5 threshold value caused the Se to be far lower than the Sp, which was to be expected for the class-imbalanced issue. Employing CIT, a decrease in Sp may result in the increasing demand of monitoring a firefighter's status. However, the improved Se and significant increase in the Youden index contribute to enhanced firefighter safety. These findings suggest that maximising Se with the HST approach leads to a considerable decline in Sp, Ac, and lead time. On the contrary, the CIT can contribute to the lead time because more samples could be correctly classified. In terms of real-time performance, these classifiers are adequate for this study with 15 Hz sampling rate except for the stacking implementation. DT-ED4 only required 0.6816 ms to execute the model, which is optimal for real-time PI-FDS. Overall, DT-ED4, RF-GN80, and AB-LR05N40 exhibited favourable detection performances, with Youden indices higher than 93%.

Previous study (see Chapter 3.4) showed that chest-mounted IMU was most vital in deciding FDS performance, and presented that a model incorporating all nine IMUs is more effective than alternative configurations. In this study, the performance of PI-FDS using various combinations of IMUs was further explored. Drawing on the earlier findings, five combinations of IMUs were investigated: CEWTA (9 IMUs), CEWT (7 IMUs), CET (5 IMUs), CA (3 IMUs), and C (1 IMU), where C, E, W, T, and A denote chest, elbow, wrist, thigh, and ankle, respectively. Figure 4.5 depcited that the CEWTA outperforms other configurations across all three classifiers according to the Youden index, and IMUs

with fewer than 5 showed significant decline in classification performance. Interestingly, for DT-DE4 and RF-GN80, the performance of CET configuration is highly close to that of CEWTA, whilst requiring less execution time due to a reduced number of features. Consequently, the PI-FDS utilising the CET combination of IMUs could represent an optimal choice in practice, with the full nine IMUs employed solely for pose reconstruction purposes.

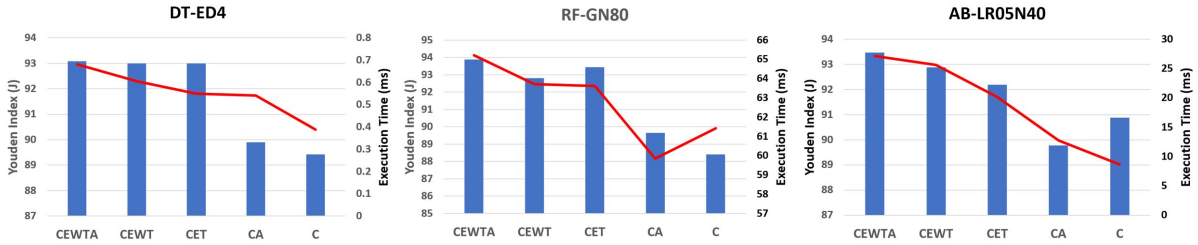

Figure 4.5: Results of the five combinations of IMUs using DT-ED4, RF-GN80, and AB-LR05N40 with CIT method.

Then, the performance of these three classifiers is evaluated for each activity, which is depicted in Table 4.4. The RF-GN80 achieved a Se of 100% for the F2, F3, F5, and F6 actions, but the Sp was quite low, which means the CIT shifted the balance more toward Se. Furthermore, all three classifiers exhibited poorer performances for the F5 action, which was a slow squat on the ground that simulated fainting. This is significant because the slow squat resulted in a smaller difference in acceleration than other fall actions. Moreover, these three classifiers performed well in distinguishing between the fall and fall-like actions. In summary, the results of a comprehensive evaluation of the processing speed and detection performance of the candidate classifiers revealed that DT-ED4 is more suitable for the PI-FDS as its execution time was short with 0.6816 ms and its Se, Sp, and Ac were 95.1%, 97.99%, and 97.88%, respectively.

Table 4.5 compares the performance of the proposed DT-ED4 with the CIT method

Table 4.4: Performance evaluation of DT-ED4, RF-GN80, and AB-LR05N40 models with the CIT method

Activity	Method	Se (%)	Sp (%)	Ac (%)
F1	DT-ED4	95.60	93.26	93.59
F1	RF-GN80	96.70	86.17	87.63
F1	AB-LR05N40	96.70	94.33	94.66
F2	DT-ED4	100.00	94.13	94.80
F2	RF-GN80	100.00	81.67	83.75
F2	AB-LR05N40	100.00	94.57	95.19
F3	DT-ED4	95.95	96.66	96.57
F3	RF-GN80	100.00	88.50	89.89
F3	AB-LR05N40	94.59	94.43	94.45
F4	DT-ED4	92.86	94.62	94.43
F4	RF-GN80	98.57	87.28	88.54
F4	AB-LR05N40	94.29	92.65	92.83
F5	DT-ED4	82.69	90.63	89.60
F5	RF-GN80	100.00	87.78	89.36
F5	AB-LR05N40	92.31	89.20	89.60
F6	DT-ED4	100.00	93.09	93.67
F6	RF-GN80	100.00	86.51	87.63
F6	AB-LR05N40	100.00	92.11	92.76
FL1	DT-ED4	-	99.61	99.61
FL1	RF-GN80	-	98.75	98.75
FL1	AB-LR05N40	-	97.65	97.65
FL2	DT-ED4	-	99.88	99.88
FL2	RF-GN80	-	98.95	98.95
FL2	AB-LR05N40	-	99.88	99.88
FL3	DT-ED4	-	99.89	99.89
FL3	RF-GN80	-	98.72	98.72
FL3	AB-LR05N40	-	99.52	99.52

to the results of other similar studies. Adjusting the threshold value to maximise the detection of fall events could achieve Se of 100% [152], but this resulted in an obvious decrease in Ac. The comparison indicates that the proposed method has a higher lead time and a better balance between Se and Sp. The overall results of this study revealed a slight improvement in the detection performance compared to [117, 122, 123], and the proposed method only require lower sampling rate for the IMU, exhibits greater power consumption for on-the-edge node.

Table 4.5: Performance comparison of PI-FDS with relevant studies

Study	Sampling Rate (Hz)	Se (%)	Sp (%)	Ac (%)	Lead Time (ms)
Wu *et al.* (2019) [122]	100	95.50	97.30	96.40	376-404
Ahn *et al.* (2019) [152]	100	100.00	83.90	90.30	Not specified
Shi *et al.* (2020) [117]	50	94.52	96.52	95.55	Not specified
Jung *et al.* (2020) [125]	100	96.10	90.50	92.40	280.25
Sousa *et al.* (2022) [123]	400	94.04	97.67	95.86	259
Proposed Method	15	95.10	97.99	97.88	447.9

4.4 Summary

This chapter explores the feasibility of applying ML and EL methods on edge devices to enhance the performance of proposed PI-FDS in real-time firefighting scenarios, as RQ2 mentioned. To ensure efficient sensor data transmission, the study proposed an IoT framework (IoF) for PI-FDS, facilitating remote monitoring and early warning mechanisms. To address the issue of imbalanced classifier contributions, a class-imbalanced thresholding method was introduced, which improved classification performance by balancing Se and Sp. The study also summarised the design of an efficient safety risk assessment model for firefighters by evaluating fall-related risks. It highlighted the need to carefully consider the trade-off between Ac and efficiency. However, an effective FRAS should achieve real-time monitoring of various activities, whilst the FDS can only distinguish fall-related risks. Therefore, the next study (see Chapter 5) will research the detailed firefighting activities beyond fall detection to provide a more reliable safety risk assessment model.

Chapter 5

Design of IoF-Based Wearable Multi-Sensing Firefighting Activity Recognition Model

5.1 Introduction

This chapter introduces an IoF-based multi-IMU wearable sensing model designed to enhance the FRAS with a FAR algorithm. This algorithm efficiently differentiates specialised firefighting activities. The main contributions of this study include:

- This work utilises fewer sensor nodes to reduce power consumption and ensure stable wireless transmission. Additional sEMG sensors are integrated to measure muscular exertions during firefighting activities, such as lifting hoses and rescuing victims. The BNC is redesigned to attach to the SCBA, facilitating data collection without interfering with firefighting missions.

- The study focuses on SCBA endurance training, resulting in the publicly available SFTAA dataset. This dataset includes data from eighteen firefighters engaged in SCBA endurance training activities. Activities are categorised into upper and lower body subcategories, including motion, HR, sEMG, and environmental data.

- A novel HML-based network is introduced to classify complex firefighting activities using the SFTAA dataset. The study emphasises the importance of sensor placement

by analysing its impact on the classification performance of firefighting activities.

This study is published as:

- [Journal] IoT-FAR: A multi-sensor fusion approach for IoT-based firefighting activity recognition, *Information Fusion*, 2024 (IF = 14.7, CAS Q1, JCR Q1).

The remaining sections are structured as follows: Section 5.2 introduces the proposed HML-based network for the FAR algorithm. Section 5.3 provides an overview of the hardware design of the IoT-FAR system architecture and details the experimental setup for data collection. Section 5.4 presents the experimental results and performance evaluations. Finally, Section 5.5 summarises key insights and outlines potential directions for future research.

5.2 Methodology

5.2.1 Data Pre-Processing

During the preliminary analysis, it was observed that trained firefighters consistently exhibited high HRs with low variability in HR data which resulting in low significance for FAR prediction based on firefighter conditions. Additionally, since SCBA endurance training was conducted in a controlled environment lacking realistic firefighting scenarios with actual fire and smoke, environmental and HR data were excluded from the FAR analysis in this study.

The time-series raw data from the IMU at time step t for the sensor node S are

represented as A_t^S, G_t^S, and E_t^S, which are defined as follows:

$$A_t^S = [Ax_t^S, Ay_t^S, Az_t^S] \in \mathbb{R}^3, \tag{5.1}$$

$$G_t^S = [Gx_t^S, Gy_t^s, Gz_t^S] \in \mathbb{R}^3 \tag{5.2}$$

where Ax_t^S, Ay_t^S, and Az_t^S represent the acceleration forces (m/s^2) along the x-, y-, and z-axis (including gravity), respectively. Similarly, Gx_t^S, Gy_t^S, and Gz_t^S represent the rotational rates (rad/s) around the x-, y-, and z-axis, respectively, and $S \in \{B, LA, RA, LS, RS\}$. The sEMG data collected from four nodes placed on the limbs, denoted by E_t^S, can be represented as the following sequence of raw data for S:

$$R^S = \begin{cases} ([A_t^S, G_t^S])_{t=1}^T \in \mathbb{R}^{6\times T}, S \in \{B\} \\ ([A_t^S, G_t^S, E_t^S])_{t=1}^T \in \mathbb{R}^{7\times T}, S \in \{LA, RA, LS, RS\} \end{cases} \tag{5.3}$$

where T is the sequence length, and no sEMG data is recorded for sensor node B, which is placed on the body trunk. The 6-DOF IMU data was then transformed into the signal magnitude vector (SMV) [163] and the angular axis of acceleration vector (AAV) [164]. The SMV is defined by Eqs. 5.4 to 5.5, and the AAV is defined by Eq. 5.6:

$$SMVa_t^S = \sqrt{(Ax_t^S)^2 + (Ay_t^S)^2 + (Az_t^S)^2} \tag{5.4}$$

$$SMVg_t^S = \sqrt{(Gx_t^S)^2 + (Gy_t^S)^2 + (Gz_t^S)^2} \tag{5.5}$$

$$AAV_t^S = \cos^{-1}(A_t^S / Av_t^S) \tag{5.6}$$

where Av_t^S denotes the three-axis acceleration force vector, and the processed data P_t^S is given by:

$$P^S = \begin{cases} ([SMVa_t^S, SMVg_t^S, AAV_t^S])_{t=1}^T \in \mathbb{R}^{5\times T}, S \in \{B\} \\ ([SMVa_t^S, SMVg_t^S, AAV_t^S, E_t^S])_{t=1}^T \in \mathbb{R}^{6\times T}, S \in \{LA, RA, LS, RS\} \end{cases} \tag{5.7}$$

The study evaluated various window sizes and selected a 2 s window (W) with a 1.5

s overlap (V) for feature extraction segmentation. In addition to the four features utilised in RS1 (Section 3.2.2), this study included a total of 31 features, comprising 25 time-domain features and 6 frequency-domain features. The SHapley Additive exPlanations (SHAP) method [165] was then employed to assess the importance of features associated with IMU and EMG data. Table 5.1 illustrates the final selected features $F^S_{a,n}$, denoted as:

$$F^S_{a,n} = f_a(P^S_n) = f_a(P^S_{(n-1)\times V+1:W+(n-1)\times V}) : n \in N \tag{5.8}$$

where a is the index of a feature, n is the segments of features, N represents the set of segments, and $f_a(P^S_n)$ represents the function for calculating the $a-th$ feature at $n-th$ segment.

In total, 654 features were extracted for each window segment across five sensor nodes (excluding one sEMG sensor node, as shown in Fig. 5.3). Fig. 5.1 shows the data pre-processing steps for EMG and accelerometer data on the LA node, including data segmentation and feature extraction.

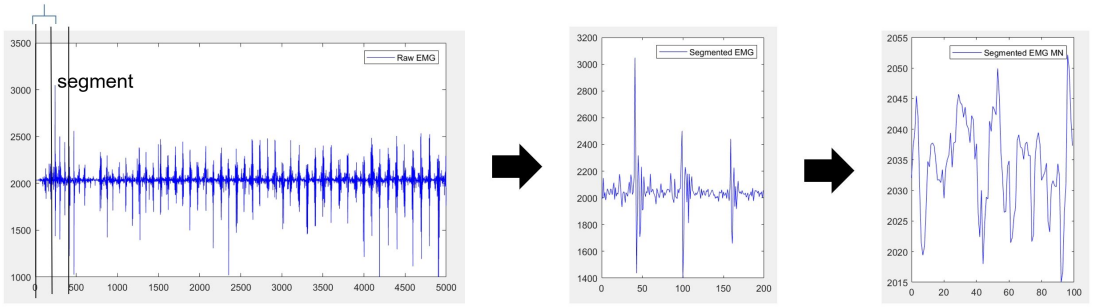

(a)

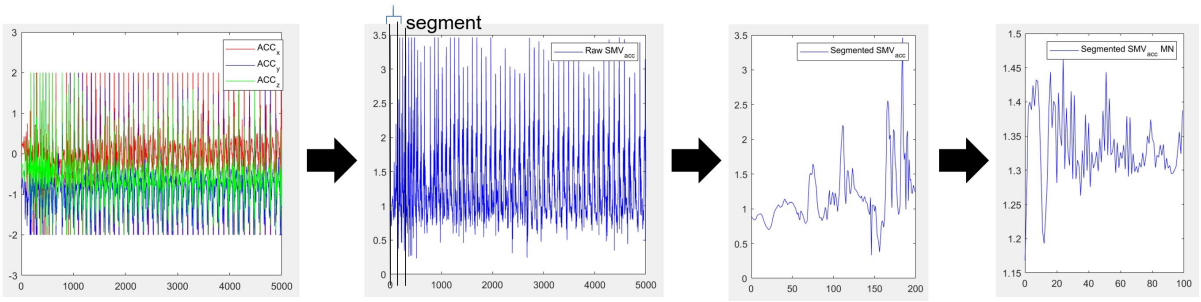

(b)

Figure 5.1: Data pre-processing stages for the LA node, illustrating (a) EMG and (b) ACC data segmentation and feature extraction.

Table 5.1: List of selected features, including 25 time-domain features and 6 frequency domain features

Domain	Feature	SMV_{acc}	SMV_{gyr}	AAV_x	AAV_y	AAV_z	EMG
Time	Mean (MN)	✓	✓	✓	✓	✓	✓
	Standard Deviation (STD)	✓	✓	✓	✓	✓	✓
	Range (RG)	✓	✓	✓	✓	✓	✓
	Mean Absolute Deviation (MNAD)	✓	✓	✓	✓	✓	✓
	Median Absolute Deviation (MDAD)	✓	✓	✓	✓	✓	✓
	Mean Absolute Value (MAV)	✓	✓	✓	✓	✓	✓
	Simple Square Integral (SSI)	✓	✓	✓	✓	✓	✓
	Root Mean Square (RMS)	✓	✓	✓	✓	✓	✓
	Average Amplitude Change (AAC)	✓	✓	✓	✓	✓	✓
	L2norm (L2N)	✓	✓	✓	✓	✓	✓
	L-Scale (LSC)	✓	✓	✓	✓	✓	✓
	Difference Absolute Standard Deviation (DASTD)	✓	✓	✓	✓	✓	✓
	Interquartile Range (IQR)	✓	✓	✓	✓	✓	✓
	Skewness (SKEW)	✓	✓	✓	✓	✓	✓
	Signal Magnitude Area (SMA)	✓	✓	✓	✓	✓	✓
	Kurtosis (KURT)	✓	✓	✓	✓	✓	✓
	Autocorrelation (CORR)	✓	✓	✓	✓	✓	✓
	Auto-Regressive Coefficient (ARC)	✓					✓
	Logarithm Base 10 (LOG)						✓
	Zero Crossing (ZC)						✓
	Sequential Segments Change (SSC)						✓
	Myopulse Percentage Rate (MYOP)						✓
	Willison Amplitude (WAMP)						✓
	Hjorth Mobility (HJM)	✓		✓	✓	✓	✓
	Hjorth Complexity (HJC)	✓		✓	✓	✓	✓
Frequency	Mean Frequency (MNF)	✓	✓				✓
	Median Frequency (MDF)	✓	✓				✓
	Spectral Peak Height (SPH)	✓	✓				✓
	Peak Frequency (PF)	✓	✓				✓
	Total Power (TP)	✓	✓				✓
	Variance of Central Frequency (VCF)	✓	✓				✓
	Total Features Per SN	26	23	19	19	19	31
	Total SN	5	5	5	5	5	4
	Total Features	130	115	95	95	95	124

5.2.2 Proposed HML-based Network

This study introduces an HML-based network tailored to the unique sensor placements on firefighters, as depicted in Fig. 5.2, comprising three distinct models: one integrating all selected features (MA), another focusing solely on upper body (UB) features (MU), and a third emphasizing lower body (LB) features (ML). The features for UB and LB are denoted as $FUB_{b,n}$ and $FLB_{c,n}$, respectively, and are represented by:

$$FA_{a,n} = \sum F^{S}_{a,n} = [FUB_{b,n}, FLB_{c,n}] \tag{5.9}$$

where b and c are the indices of the features for UB and LB, respectively.

The UB activities are further categorized based on muscle force usage into instantaneous force (UB1), continuous force (UB2), and irrelevant activities (UB3). Similarly, LB activities are classified based on leg movement patterns, including climbing (LB1), walking (LB2), and stationary positions (LB3).

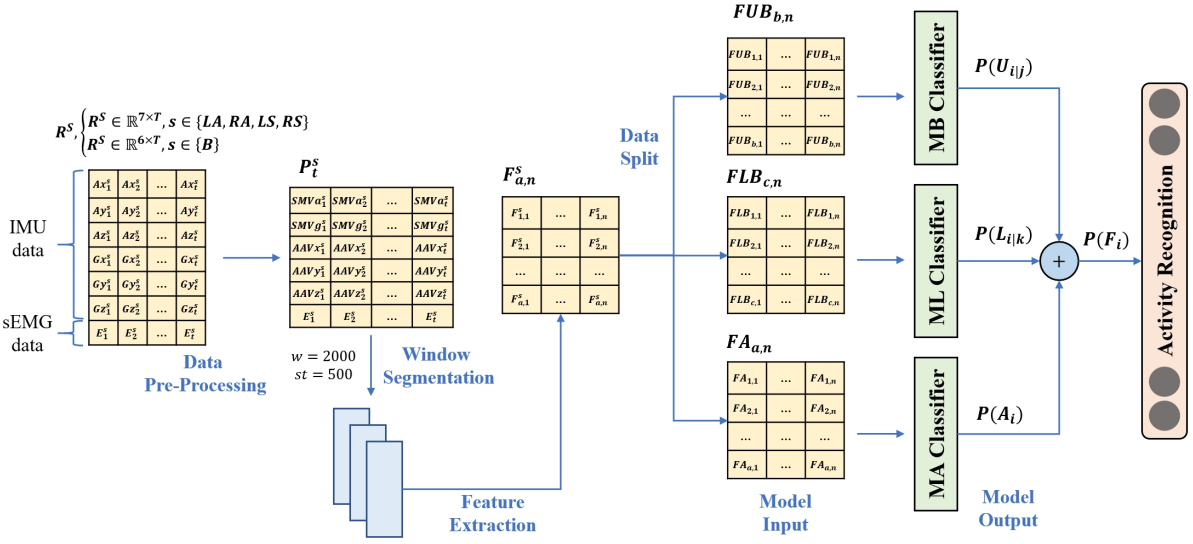

Figure 5.2: Overview of the proposed HML-based network flowchart.

Table 5.2 outlines the UB and LB sub-activities corresponding to main activities A1 to A8, alongside the number of segmented data instances obtained post data pre-

processing and validation via recorded videos, totaling 26,947 segmented data instances. Note that the activity durations vary among firefighters; for instance, activities involving climbing (A4) or descending stairs (A6) span longer durations, resulting in increased segmented data instances, as shown in Table 5.2. Despite this variance, data collection complied with an individual-centric approach, with all firefighters undergoing identical SCBA endurance training. While this approach may lead to slight class imbalances across the eight activities, it does not significantly impact the model's training and testing phases.

Table 5.2: Sub-activities of UB and LB associated with main activities, including raw and segmented data counts.

Main	Sub-Activity UB	Sub-Activity LB	No. Raw Data	No. Segmented Data
A1	UB1	LB3	14,410	2,684
A2	UB2	LB2	11,002	2,005
A3	UB2	LB2	15,550	2,930
A4	UB2	LB1	23,338	4,494
A5	UB1	LB3	12,740	2,386
A6	UB2	LB1	20,152	3,854
A7	UB3	LB2	27,202	4,922
A8	UB3	LB3	19,512	3,672
		Total	143,906	26,947

The final step involves a weighted combination to determine the probability of each activity by aggregating predictions from the three models using predefined weights, formulated in Eq. 5.10:

$$P(F_i) = P(A_i) + P(U_{i|j}) \times \bar{U}_{i|j} + P(L_{i|k}) \times \bar{L}_{i|k} \tag{5.10}$$

where $i \in \{A1...A8\}$, $j \in \{U1, U2, U3\}$, $k \in \{L1, L2, L3\}$, $P(A)$, $P(U)$, and $P(L)$ denote the predicted probabilities of the MA, MU, and ML models, respectively. $\bar{U}$ and $\bar{L}$ represent the mean accuracies of the MU and ML models, respectively. Here, $i|j$ and $i|k$

signify the corresponding combination of UB and LB sub-activities. For instance, for A1:

$$P(F_{A1}) = P(A_{A1}) + P(U_{A1|U1}) \times \bar{U}_{A1|U1} + P(L_{A1|L3}) \times \bar{L}_{A1|L3} \tag{5.11}$$

5.2.3 Classifier Selection

To assess the effectiveness of the proposed Hybrid Machine Learning (HML) network, the study initially concentrated on selecting the most suitable machine learning (MA) classifiers, considering both their accuracy and processing time, which are crucial for real-time embedded activity classification (see Fig. 5.2). Four classifiers are evaluated: KNN [74], DT [75], SVM [76], and RF [74]. The hyperparameters for these classifiers were examined and adjusted to determine the optimal configurations for the network. The optimal hyperparameters for the MA, MU, and ML models were detailed in Table 5.3, with variations observed across classifiers. For example, KNN and DT exhibited different hyperparameter configurations for MA, MU, and ML models, whereas others maintained consistent configurations across these models. In addition, two NNs were investigated: the CNN-LSTM, which is widely used in HAR [27], and the Multi-ResAtt [68], recognized for its high performance in multi-sensor fusion. It is also important to note that the architectures of CNN-LSTM and Multi-ResAtt networks were specifically redesign to reflect firefighting task characteristics rather than generic human activities.

5.3 Experimental Setup

5.3.1 Hardware Design

The findings of the study revealed that the heterogeneous IoF network exhibited improved data transmission throughput and range across various firefighting scenarios,

Table 5.3: Utilised classifiers and their respective hyperparameter for evaluating the performance of proposed HML-based network.

Classifier	Hyperparameter
KNN	MA: n_neighbours = 6; MU: n_neighbours = 7; ML: n_neighbours = 7
SVM	C = 5; kernel = {'rbf', 'poly', 'linear'}
DT	MA: max_depth = 10; MU: max_depth = 7; ML: max_depth = 7; criterion = 'entropy'
RF	n_estimators = 200; criterion = 'entropy'

CNN-LSTM	epoch = 100;
	batch = 5;
	3 1D-CNN layers [1024, 512, 1024];
	3 LSTM layers [1024, 512, 25];
	dense layer [ReLU, 64];
	dense layer [softmax, 8]

Multi-ResAtt	epoch = 100;
	batch = 5;
	5 parallel residual modules;
	1D average pooling;
	Bi-GRU + attention layer;
	dense layer [ReLU, 64];
	dense layer [softmax, 8]

although accompanied by elevated Wi-Fi power consumption. To mitigate this concern, the present study has replaced Wi-Fi with BLE for data transmission, utilising WBSN framework.

Figure 5.3 illustrates the overall system architecture of the proposed IoT-FAR integrated with the updated IoF. Table 5.4 depicts the components of the proposed work, including five sensor nodes (SNs) and a self-customised body node coordinator (BNC). The five SNs consist of four self-customised surface sEMG and IMU sensor bands (EMG-IMU), along with a Polar Verity Sense armband [166] for heart rate monitoring (HR-SN). These EMG-IMU bands are positioned on different parts of the firefighter's body, covering

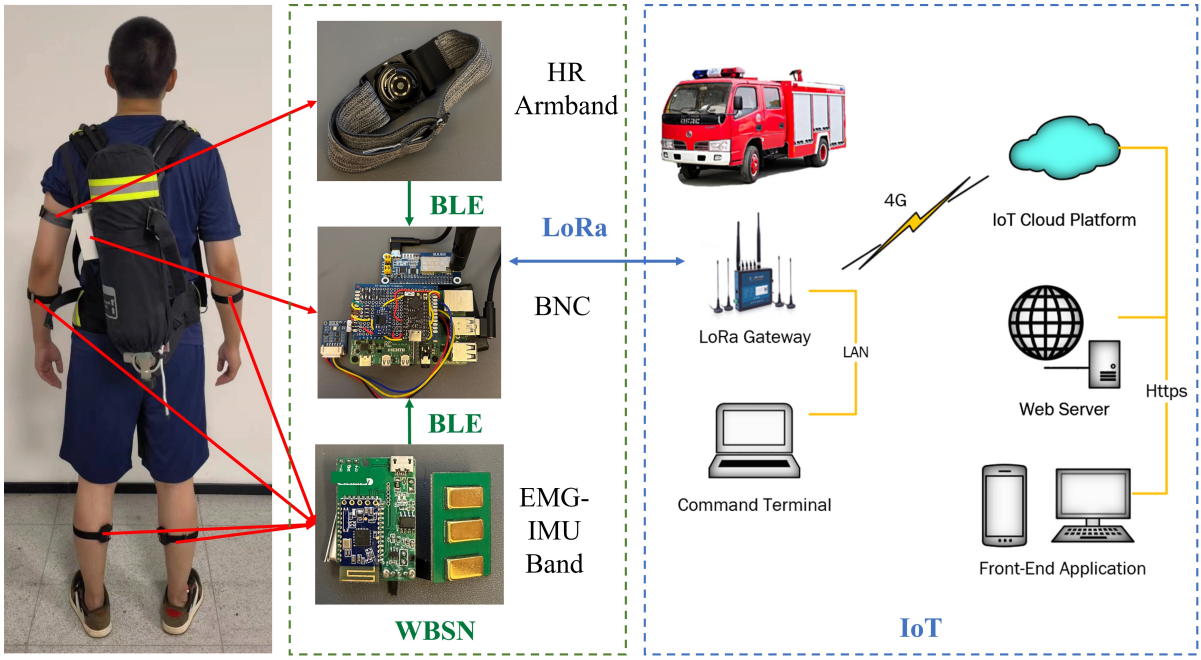

Figure 5.3: Overview of the proposed IoT-FAR, including the FAR and the IoF network.

the lower left forearm (LA), lower right forearm (RA), left shank (LS), and right shank (RS). The HR armband is placed on the upper left forearm (UA). Additionally, the BNC contains an IMU sensor for the FAR, which is placed on the SCBA and denoted as B, in addition to LA, RA, LS, and RS. The components of an EMG-IMU band include:

- MUP6050 module [167]: This 6-DoF IMU includes an accelerometer and a gyroscope to measure the firefighter's acceleration and angular velocity for capturing motion data.
- sEMG module [168]: Records sEMG signals from the brachioradialis and gastrocnemius muscles, for distinguishing tasks such as lifting hoses and breaking down doors.
- BLE 4.2 module (JDY-18) [169]: Enables seamless communication with the BNC at a sampling rate of 100 Hz.

The armband on the UA measures the firefighter's photoplethysmography (PPG)-based HR, serving as a physiological indicator of training intensity. The armband transmits data to the BNC at a sampling rate of 1 Hz. The BNC is the central component of the IoT-FAR system, housing the FAR model deployment. To ensure minimal interference with the firefighter's mobility, the BNC is composed of three modules and is affixed to the SCBA:

- RPi-Embedded Module: Configured with a Raspberry Pi (RPi) 4B+ with 4GB RAM [170], this module collects data from the five SNs via BLE connection and executes the FAR model.
- LoRaWAN Module: Features a LoRa wireless area network (WAN) module with a LoRaWAN gateway [171], establishing the LoRa connection between the indoor (WBSN) and outdoor (terminal).
- Multi-Sensor Board: This customized extension board, attached to the RPi, integrates the TinyPICO micro-processing unit [172], a BNO055 IMU (capturing motion data of the body torso) [169], and the BME688 environmental sensor (collecting humidity, temperature, pressure, and volatile organic compounds data) [173].

5.3.2 Building of the SFTAA Dataset

Eighteen volunteer firefighters from Huzhou Fire Brigade in Zhejiang province, China, participated in the study during SCBA endurance training activities. The firefighters had a mean age of 22±6 years (ranging from 19 to 28), a mean height of 174±10 cm (ranging from 166 to 184 cm), and a mean weight of 75±15 kg (ranging from 64 to 90 kg).

Table 5.4: Hardware specifications

Modules	Components	Specification
EMG-IMU	MPU6050	6-DOF IMU; Sampling rate: 100 Hz
	sEMG	Three dry electrodes (DRY+, DRY-, and GND)
	JDY-18	BLE 4.2
BNC	LoRaWAN terminal module	ASR6601 SoC; Frequency range: 398-525 MHz; Data rate: 0.814 Kbp
	Raspberry Pi 4B+	1.8 GHz Quad core Arm Cortex-A72; 4 GB RAM; 2.4 GHz Wi-Fi & BLE 5.0
	BNO055	9-DOF IMU
	BME688	Measuring humidity, temperature, pressure, and volatile organic compounds
	TinyPICO	240 MHz Dual-core Xtensa LX6 4 MB RAM 2.4 GHz Wi-Fi & BLE 4.2

The SCBA endurance training comprised seven specialized activities (A1 to A7) and one stationary activity (A8), as illustrated in Fig. 5.5. The details of these activities are outlined in Table 5.5. The experiments were conducted in controlled fire scenarios without actual fire and smoke, as shown in Fig. 5.4. On the left side of the large empty field, a regular vehicle tire was placed to simulate an obstacle that needed to be broken (see A1). On the right side, a 60 kg dummy was positioned to represent a victim awaiting rescue (see A2). A fire engine equipped with a water supply and hose was used to simulate an outdoor firefighting activity (see A3). In the center of the field, a fire training tower was used for firefighters to perform various activities (see A4, A5, and A6).

Each firefighter is instructed to complete the entire SCBA endurance training with a full oxygen level capacity at 28 mPa. Activities A1 to A6, considered as one cycle, should be performed continuously without any breaks in between. If the SCBA oxygen level remains above 8 mPa (not reaching the warning level), the firefighter is required

Figure 5.4: Experiment setup of the SCBA endurance training.

to initiate a new cycle. However, if the SCBA issues a warning alert at any point, the firefighter must stop the training immediately and proceed to the A8 activities. In this activity, the firefighter can choose to sit or squat, resting for approximately two to three minutes before removing the equipment.

Table 5.5: Details of firefighting SCBA endurance training activities

Activity	Description
A1	Use a hammer to hit a tire, causing it to move 5 meters, simulating a forceful break-in action.
A2	Drag a dummy for 20 meters to simulate the rescue of a trapped person.
A3	Move the nozzle with a water-supplied hose for 20 meters to simulate an outdoor firefighting task.
A4	Climb from the ground floor to the fourth floor while carrying two trays of hoses to simulate firefighting tasks in a high-rise building.
A5	Drag the hose from the ground floor to the fourth floor via window to simulate external replenishment tasks in indoor firefighting.
A6	Go down from the fourth floor to the ground floor while carrying two trays of hoses to simulate firefighting tasks on different floors.
A7	Perform the usual walking movement.
A8	Engage in stationary actions, including squatting or sitting during or after training to simulate waiting for peer rescue in dangerous situations.

In adherence to the training evaluation standard, each firefighter was required to complete a minimum of 20 activities, equivalent to at least three cycles. The duration

(a) (b) (c) (d)

(e) (f) (g) (h)

Figure 5.5: Illustration of the eight activities in the SCBA endurance training, including (a) A1, (b) A2, (c) A3, (d) A4, (e) A5, (f) A6, (g) A7 and (h) A8.

of the experiment for each firefighter varied based on their individual physical oxygen consumption ability. The results of the experiments revealed that only three out of the 18 firefighters were able to meet the training evaluation standard, highlighting the strenuous nature of the firefighting SCBA endurance training. Throughout the training sessions, a firefighter instructor was present to ensure safety. It is noteworthy that some participants exhibited signs of fatigue or lower physical fitness during the training. Notably, they chose to stand while performing the A8 activity, a decision deemed acceptable according to the instructor's guidelines. A camera is utilised to record the videos with the watermark of the timestamp. Then, by synchronising the system time of the BNC, the motion data collected with a timestamp can be matched with the specific frame in the video, to label what event the subject is doing. The data labelling was conducted by the two main researchers of this study and further validated by the firefighter training instructors. The SF-TAA dataset is now publicly available online at `https://github.com/HCI-Laboratory/`

Smart-Firefighting/tree/main/Firefighter-Activity-Recognition.

5.4 Results

Considering that the macro-averaging metric provides a more practical evaluation for real-world applications compared to micro-averaging and weighted-averaging metrics, this study adopted four evaluation metrics for the HML-based network performance assessment. These metrics include macro-average recall (MRC), macro-average precision (MPR), macro-averaged F1 score (MF1) and mean accuracy (MAC), defined as follows:

$$MAC = \frac{1}{N}\sum_{i=1}^{N}\frac{TP_i + TN_i}{TP_i + TN_i + FP_i + FN_i} \tag{5.12}$$

$$MRC = \frac{1}{N}\sum_{i=1}^{N}\frac{TP_i}{TP_i + FN_i} \tag{5.13}$$

$$MPR = \frac{1}{N}\sum_{i=1}^{N}\frac{TP_i}{TP_i + FP_i} \tag{5.14}$$

$$MF1 = \frac{2 \times MRC \times MPR}{MRC + MPR} \tag{5.15}$$

where N represents the number of classes (eight activities), and the variables TP_i, TN_i, FP_i, and FN_i denote the true positives, true negatives, false positives, and false negatives of class i, respectively.

A high-performance desktop PC, featuring an Intel Core i7-13700K 3.4 GHz CPU and NVIDIA RTX 4090 24 GB RAM GPU, was utilised for both model training and testing. The study adopted the cross-validation method to evaluate the individual model performances.

5.4.1 Preliminary Result on the Impact of SN Placement

To assess the impact of SN placement and its various combinations, the RF model was trained with different placements. The results, presented in Figure 5.6, indicate that the RF model trained with SN features on the B alone exhibited the lowest MAC of 90.77%. This result is reasonable as body movements are quite similar among these activities. Notably, the RF model trained with SN features on the RA demonstrated a higher MAC of 94.22%, indicating that activity recognition is more accurate depending on whether the firefighter is left-handed or right-handed, as all participants in the experiments were right-handed. On the other hand, the RF model trained with SN features on the B, RA, and LS (BRALS) showed a high MAC of 97.24%. While the RF model trained with SN features on all five positions (ALL) exhibited the highest MAC of 97.86%, the BRASL-type RF model appears to be the most practical solution, utilising only three SNs.

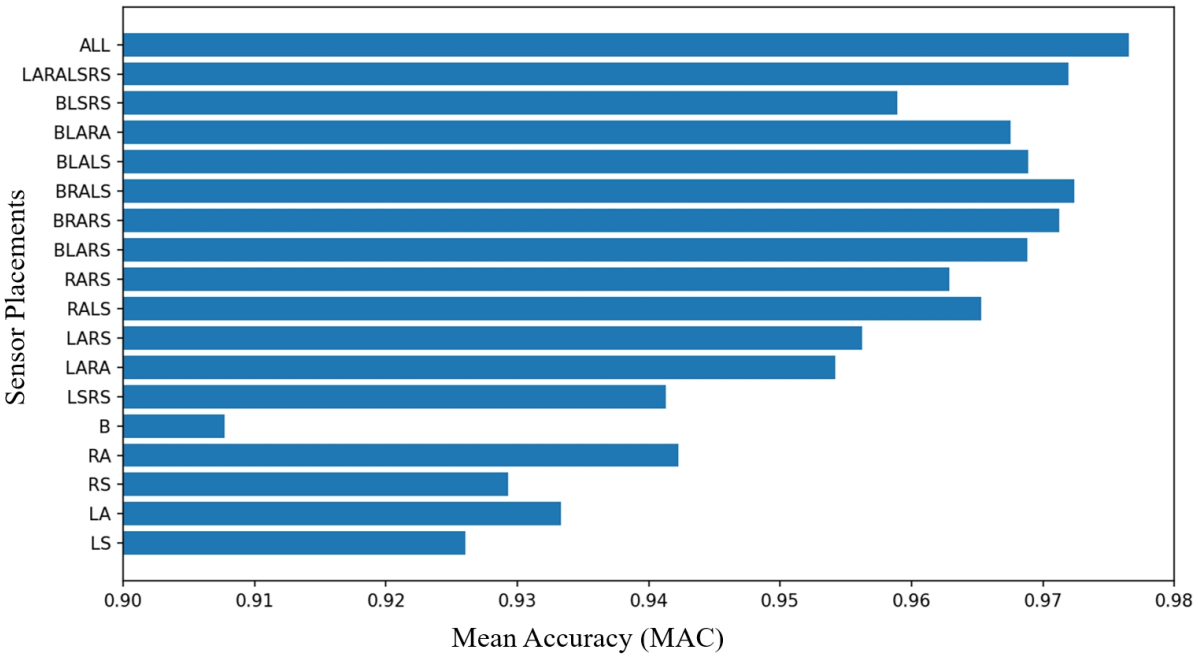

Figure 5.6: *AC* results of the trained RF models based on various combinations of sensor placements.

In addition, this study evaluates the effectiveness of integrating sEMG features. The

results in Table 5.6 indicate the best classification performance when the model is trained with both IMU and sEMG features. However, the MA-RF classifier trained exclusively with sEMG features exhibits poor overall performance. Further investigation into the underperformance of using only sEMG features in the trained RF model is conducted, and the corresponding confusion matrix (CF) is presented in Figure 5.7. The CF highlights a higher relative true prediction for activities A5 (MAC = 93.2%), A7 (MAC = 83.9%), and A8 (MAC = 82.3%) in comparison to A1 (MAC = 69.2%), A2 (MAC = 40.0%), A3 (MAC = 36.3%), A4 (MAC = 57.4%) and A6 (MAC = 6.25%). Figure 5.8 further showed the mean EMG signals for the RS, LS, RA and LA for different activities. The data reveals that sEMG data obtained from the LA and RA exhibit a high similarity pattern with lower variations, particularly for A2, A3, A4, and A6 activities, further justifying the above finding. Activities A7 and A8 are relatively simpler, as the trained models focus more on the features in the LB.

Table 5.6: Performance of the MA model using RF classifier (MA-RL) trained with IMU, sEMG, and combined IMU + sEMG features

Sensor	MRC	MPR	MF1	MAC
IMU	90.38	91.59	90.98	97.66
sEMG	54.99	56.81	55.89	83.72
sEMG + IMU	91.32	92.30	91.81	97.86

In summary, the results indicate a lower recognition rate for the U2 sub-activity (refer to Table 5.2). The analysis also reveals that, despite A1 and A5 exhibiting the same sub-activities of UB1 and LB3, the A1 activity presented relatively higher movement frequency compared to A5 which led to lower MAC. Furthermore, a significant observation emerges when comparing all firefighters' sEMG signals, showing a notable similarity in patterns across different activities. This similarity can be attributed to the long-term physical weight training that distinguishes firefighters from an average person. Therefore,

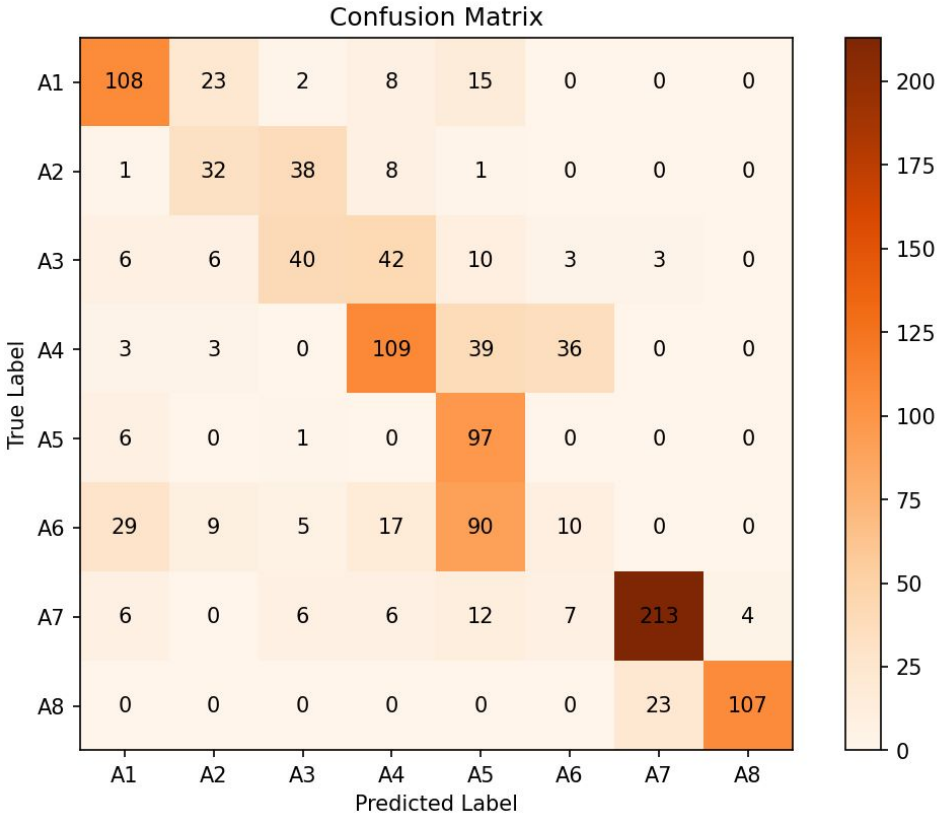

Figure 5.7: Confusion matrix for the MA-RF model trained with sEMG features.

this finding suggests that while sEMG features are effective in indicating the presence of activity, they are less effective in recognising the specific type of activity for firefighters.

5.4.2 Performance Evaluation of the MA, MU and ML Models

The performances of the MA, MU, and ML models are evaluated to determine the optimised combination of classifiers for constructing the proposed HML-based network. The results are depicted in Table 5.7. Generally, the MAC of different classifiers for the three models is higher than 90%, particularly with the highest performance in the MA-RF model (MAC = 97.86%). Similarly, the MA-RF model also shows the highest performance in terms of MRC and MPR evaluation metrics, with a slightly lower MRC compared to the MA-SVM-RBF model.

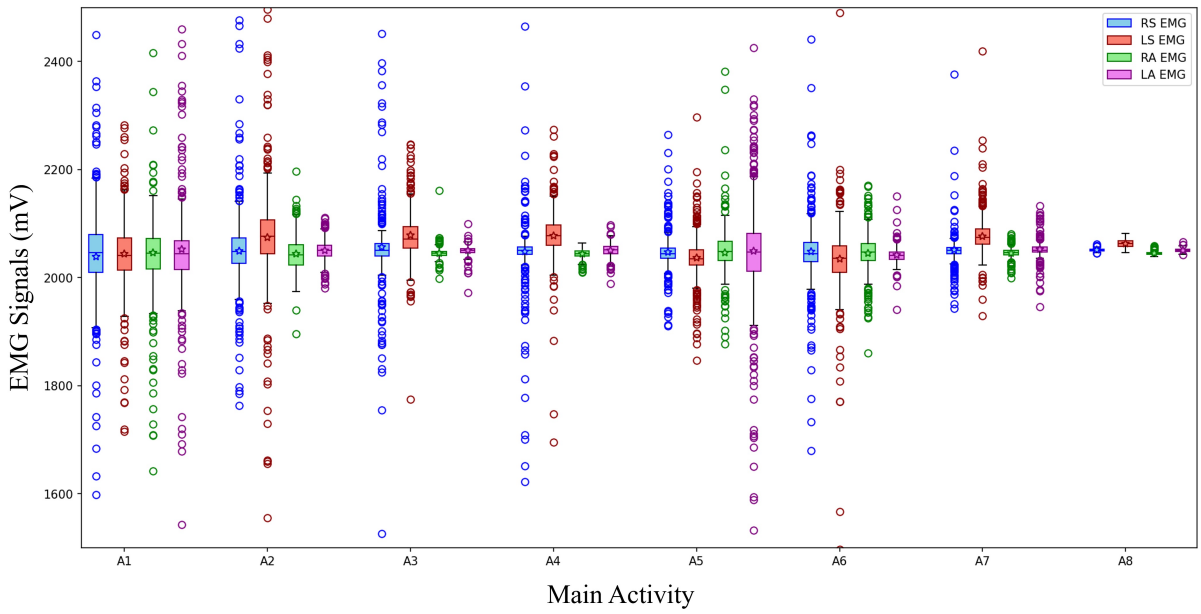

Figure 5.8: Boxplot of the standard deviation of sEMG data at RS, LS, RA and LA associated with A1 to A8 activities.

The findings suggest that the classification of sub-activities performs better, as demonstrated by the MU-RF and ML-RF models in terms of MRC, MPR, and MF1 evaluation metrics compared to the MA-RF model, consistent with the results presented in the existing study [82]. On the other hand, it is interesting to note that the Multi-ResAtt and CNN-LSTM classifiers exhibited lower performance with much higher complexity and processing cost compared to RF and SVM classifiers. This suggests that DL-based classifiers could be too overcomplex for classifying activities for firefighters, with a similar finding concluded in [26]. Based on the above analysis, the RF and SVM-RBF classifiers are selected for constructing the proposed HML-based network, with three different configurations depicted in Table 5.8.

5.4.3 Performance Evaluation of the HML-Based Networks

Table 5.9 illustrates the performance outcomes of the proposed networks based on HML alongside a comparative analysis with existing studies focusing on recognising com-

Table 5.7: Performance of the MA, MU and ML models which were trained with different classifiers

Model	Classifier	MRC	MPR	MF1	MAC
MA	RF	91.32	92.30	91.81	97.86
	SVM-RBF	91.83	88.87	90.33	97.55
	SVM-Poly	88.05	85.01	86.50	95.08
	SVM-Linear	88.61	85.32	86.93	96.07
	DT	77.55	78.06	77.80	93.38
	KNN	87.05	85.14	86.08	95.30
	Multi-ResAtt	88.90	86.99	87.93	97.15
	CNN-LSTM	86.62	85.87	86.24	96.59
MU	RF	95.47	95.84	95.65	97.02
	SVM-RBF	95.11	94.34	94.72	96.00
	SVM-Poly	93.50	92.57	93.03	94.61
	SVM-Linear	91.87	89.29	90.56	93.28
	DT	88.64	88.23	88.43	92.34
	KNN	93.09	92.11	92.60	94.34
	Multi-ResAtt	93.99	92.55	93.26	94.98
	CNN-LSTM	93.65	92.36	93.00	94.89
ML	RF	92.98	93.05	93.01	95.45
	SVM-RBF	90.78	89.09	89.93	92.67
	SVM-Poly	88.68	86.96	87.81	90.55
	SVM-Linear	81.95	80.38	81.16	86.10
	DT	85.45	85.96	85.70	90.18
	KNN	86.58	84.68	85.62	89.35
	Multi-ResAtt	89.92	88.64	89.28	92.99
	CNN-LSTM	90.30	89.48	89.89	93.42

plex activities. Among the three configurations of HML-based networks, the HML-SVM-RBF1-RF2 network demonstrates superior results, with a mean MAC of 98.29%, mean MRC of 93.48%, and mean MF1 of 92.19%, outperforming other configurations. Particularly, two main studies [57, 58] in firefighting activity recognition depicted comparatively lower performance, achieving mean MPR of 83.91% and 87.84% respectively, when compared with the proposed HML-SVM-RBF1-RF2 network. In the study performed by [54],

Table 5.8: Proposed HML-based network configuration for MA, MU and ML models

HML-Based Network	MA	MU	ML
HML-RF3	RF	RF	RF
HML-SVM-RBF3	SVM-RBF	SVM-RBF	SVM-RBF
HML-SVM-RBF1-RF2	SVM-RBF	RF	RF

focusing on physical tasks, exhibited marginally better mean MPR but lower mean MRC and MF1 compared to the proposed network. Similarly, a study by [53], covering 24 ADLs, showed similar classification performance. Conversely, while a study by [56] achieved a high mean MPR of 97.7%, its dataset was limited to only two subjects, significantly limiting its generalizability. Additionally, the study by [59] demonstrated acceptable performance in classifying 16 activities for construction workers, although the activities less related to firefighting tasks. Overall, the proposed HML-SVM-RBF1-RF2 network shows high performance in HAR, particularly those relevant to firefighting scenarios.

Table 5.9: Performance of the proposed HML-based network with the existing studies on complex activity recognition with different applications

Study	Application	Activities (Subjects)	Sensing Method	MRC	MPR	MF1	MAC
Lasek Jan & Gagolewski (2015)[57]	Firefighting	19 FAs (10)	7 6-DOF IMUs placed at legs, hands, arms, and back	/	83.91	/	/
Geng *et al.* (2016)[58]	Firefighting	7 ADLs (N/A)	4 RF transmitters at chest, forehead, right wrist, and right ankle	/	87.84	/	/
Qi *et al.* (2019)[54]	Gym setting	19 PAs (10)	Wrist sensor with ACC and Chest Sensor with ACC+ECG	89.75	91.69	90.78	/
Asuroglu (2022)[53]	Assisted Living	24 ADLs (52)	wrist worn ACC forehead, right wrist, and right ankle	91	90.9	91	91.3
Mastakouris *et al.* (2023)[56]	Assembly Work	5 CAs (2)	Wrist worn smartphone	/ 72.27	97.7 72.52	/ 63.29	/ 76.37
Mekruksavanich *et al.* (2023)[59]	Construction Work	16 CAs (13)	3 9-DOF IMUs placed at hip, upper arm, and the rear of the shoulder	/	/	88.67	88.64
HML-RF3	Firefighting	8 FAs (18)	4 6-DOF IMUs + sEMG placed at forearms and shanks; and 1 6-DOF IMU placed at the back	92.93	91.15	92.03	97.91
HML-SVM-RBF3				92.58	89.32	90.92	97.68
HML-SVM-RBF1-RF2*				93.48	90.94	92.19	98.29

Note: N/A: not available; FAs: firefighting activities; CAs: complex activities; PAs: physical activities; ACC: accelerometer; RF: radio frequency; ECG: electrocardiogram

Figure 5.9 illustrates the CF of the HML-SVM-RBF1-RF2 network. The HML-SVM-RBF1-RF2 model exhibits strong performance in overall activity recognition. Notably, the A8 activity is accurately predicted with only a 1.93% misclassification rate, highlighting the proposed network's capability to detect abnormal stationary activity behaviour. Conversely, the A3 activity shows the lowest accuracy (MAC), posing a significant challenge in distinguishing it from A2 and A7 activities due to high similarity. This underscores the importance of employing individual MU and ML models for classifying complex activities to achieve optimal recognition performance. Additionally, an intriguing observation reveals a 5.33% (246 out of 4612) misclassification of A7 into A3, despite substantial differences in upper body postures. This discrepancy is attributed to firefighters commonly placing the nozzle on their shoulders, resulting in weaker forearm muscle strength compared to other UB2 activities.

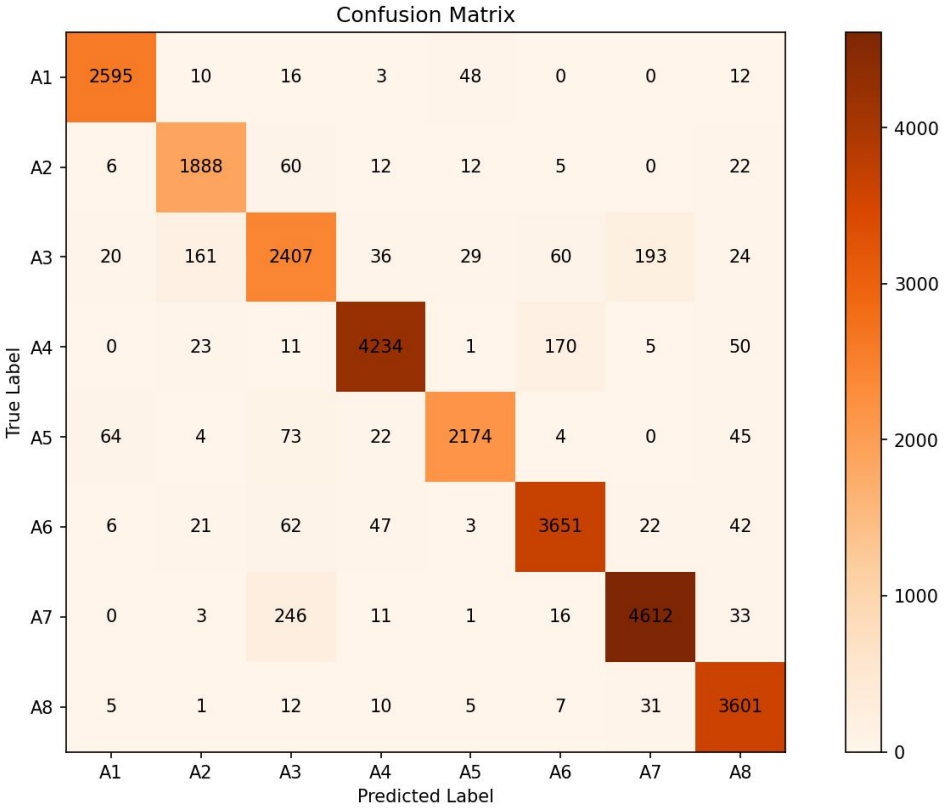

Figure 5.9: Confusion matrix for the proposed HML-SVM-RBF1-RF2 network.

5.4.4 Discussion on the Diversity in Activity Behaviours

HAR studies typically enforce standardised activity performance protocols to ensure consistent recognition accuracy. However, real-world scenarios often reveal substantial variations in participant behaviour, impacting recognition outcomes. In this study, firefighters occasionally exhibited signs of fatigue during training, leading to reduced FAR accuracy for specific firefighters. To address this variability, a detailed analysis was conducted using the leave-one-out cross-validation method with the HML-SVM-RBF1-RF2 network, as detailed in Fig. 5.10a and Table 5.10.

Table 5.10: Performance of HML-SVM-RBF1-RF2 network using leave-one-out cross validation method

Firefighter	MRC	MPR	MF1	MAC
F01	90.47	85.74	88.04	97.90
F02	90.24	82.76	86.34	96.79
F03	85.91	83.85	84.87	96.68
F04	97.41	96.08	96.74	99.18
F05	96.30	95.38	95.84	98.99
F06	91.16	88.97	90.02	97.31
F07	95.04	91.54	93.26	98.39
F08	96.13	89.15	92.51	98.94
F09	96.48	95.60	96.04	99.02
F10	93.99	94.38	93.96	98.57
F11	96.58	88.03	94.18	99.03
F12	85.23	86.58	85.90	96.58
F13	96.90	95.62	96.26	99.04
F14	97.78	97.02	97.40	99.45
F15	94.35	93.26	93.80	98.53
F16	95.61	94.86	95.23	99.08
F17	92.37	87.26	89.74	98.18
F18	90.72	90.76	90.74	97.64
Mean	93.48	90.94	92.27	98.29

The analysis highlighted that F03 and F12 demonstrated lower MRC values compared to others, with the average MRC across 18 subjects being 93.48%. Fig. 5.11 presents the confusion matrix for F12, revealing challenges in accurately predicting A3 and A5, which were often misclassified as A2 and A3, respectively. Subsequent video analysis compared

the execution of A2, A3, and A5 by both F12 (with the lowest MRC) and F14 (with the highest MRC). Fig. 5.12a depicts the incorrect rescuing behavior of F12, who pulled the dummy with one hand, while Fig. 5.12b shows the correct rescuing method. Additionally, Fig. 5.12c illustrates F12 incorrectly dragging the hose backward, contrary to the correct method demonstrated by F14 in Fig. 5.12d, where the hose was placed on the shoulder and moved forward.

In scenario A5, F12 mistakenly pulled the hose by moving his entire body backward (see Fig. 5.12e), instead of relying solely on upper body strength to draw the hose closer to the window while maintaining his position (see Fig. 5.12f). This incorrect method was noticeably similar to the A3, which deviated from the proper training standards, as confirmed by the firefighting instructors. Further analysis of firefighter performance, excluding F03 and F12, is illustrated in Fig. 5.10b. This analysis shows that most firefighters achieved over 90% in MRC, with the mean MRC value increasing by 0.61%. These findings underscore the impact of behavioral diversity on firefighting activity recognition.

Conversely, the misclassification of FAR presents an excellent opportunity to assess firefighter performance during training. This allows trainers and trainees to conduct thorough evaluations and reflections, facilitating detailed performance analysis. These results suggest that diverse behaviors pose challenges in accurately identifying human activities characterized by intricate movements, particularly tasks involving diverse and specific gestures, such as those performed by firefighters in real-world scenarios.

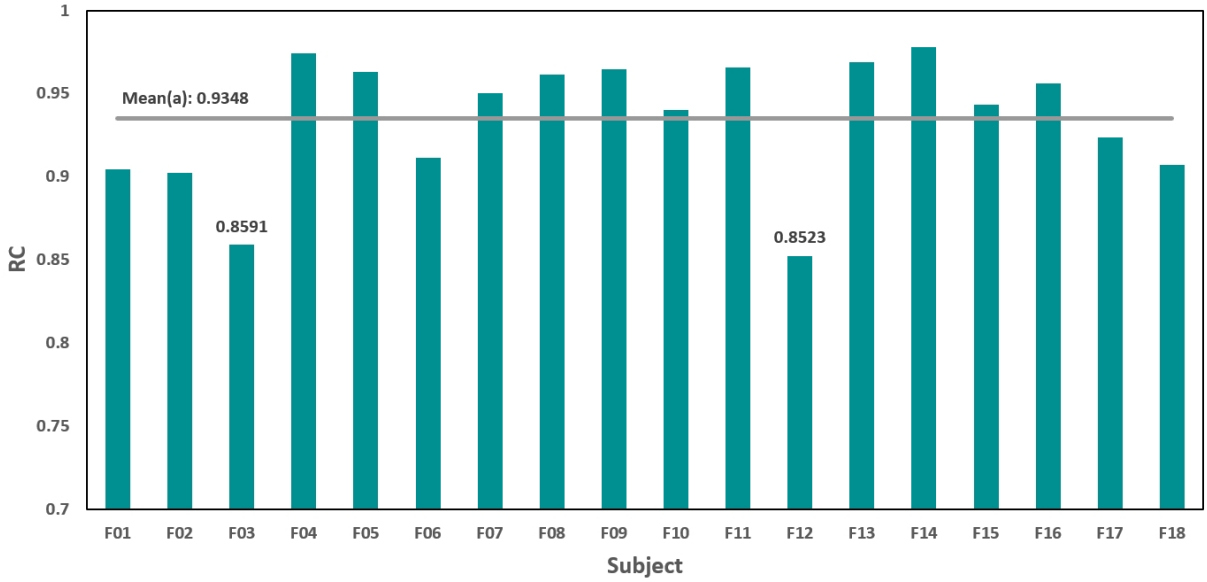

(a)

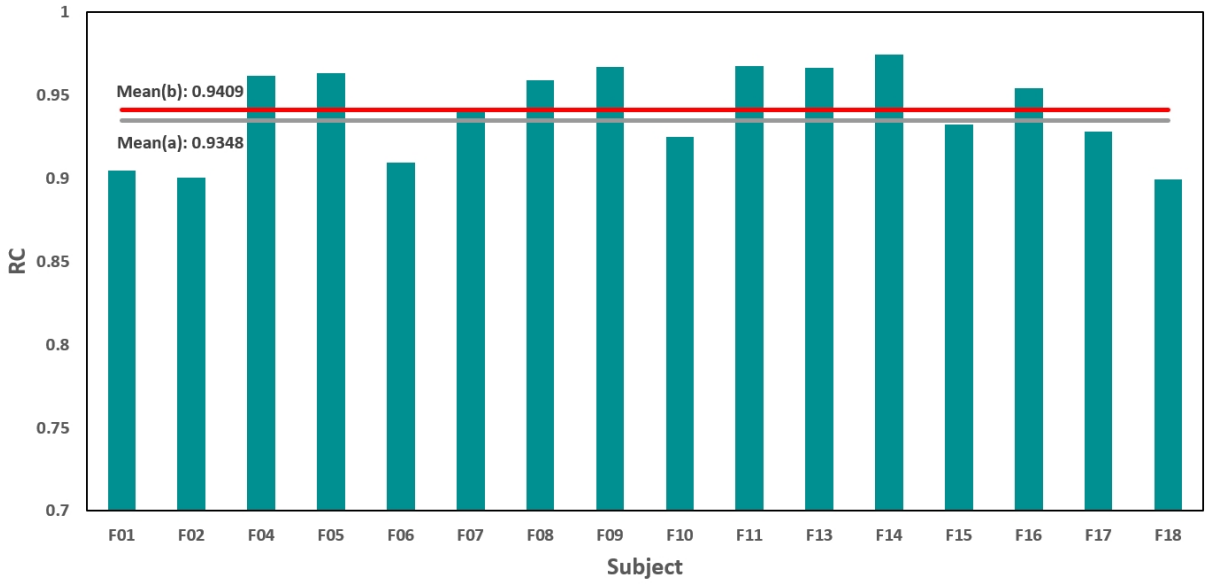

(b)

Figure 5.10: Performance of the HML-SVM-RBF1-RF2 network in MRC using leave-one-out cross-validation: (a) for all 18 subjects, and (b) for 16 subjects excluding F03 and F12.

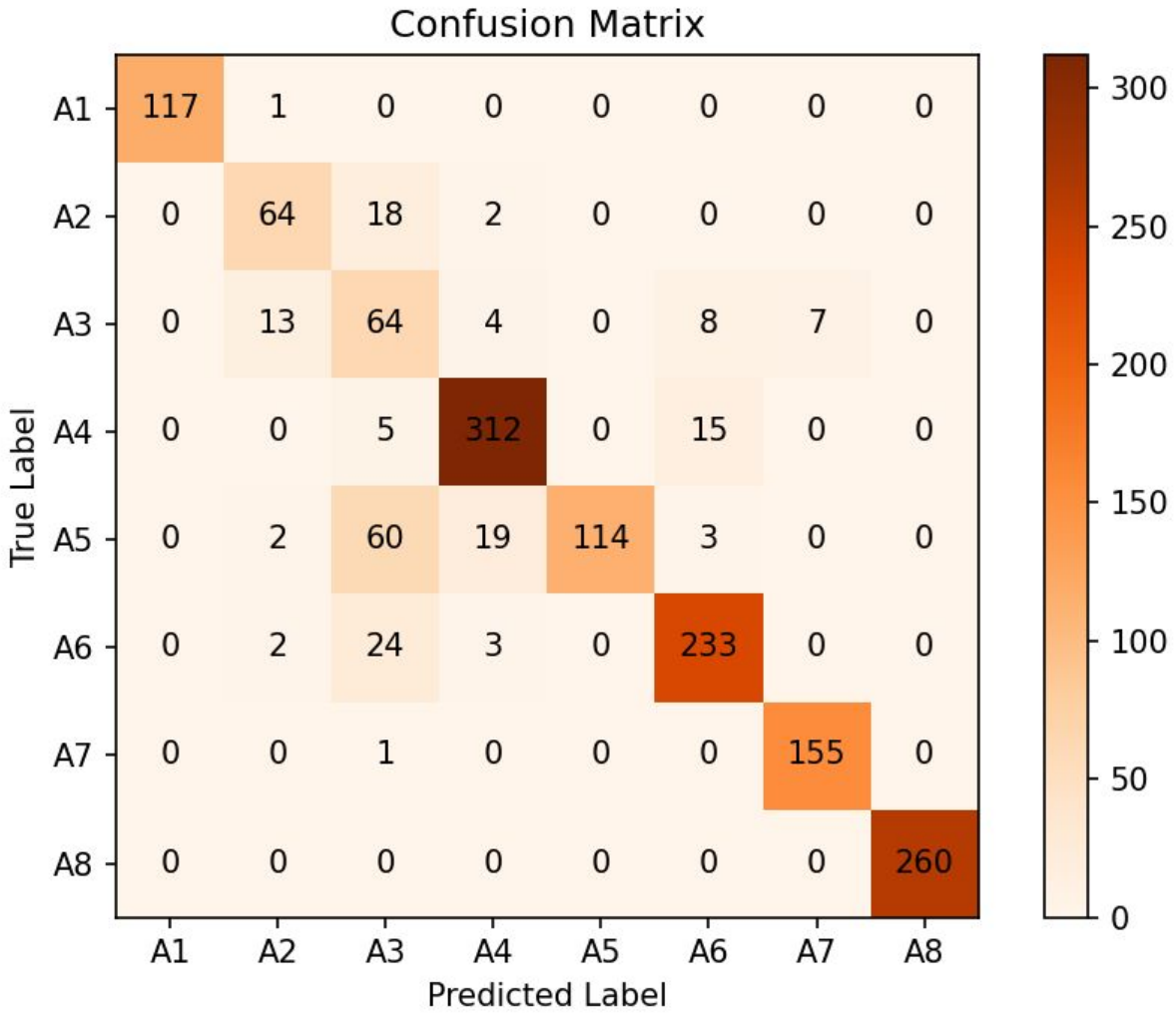

Figure 5.11: Confusion matrix for F12 using the proposed HML-SVM-RBF1-RF2 network.

Figure 5.12: Performance evaluation of various activities, including: (a) incorrect execution of A2 by F12, (b) correct execution of A2 by F14, (c) incorrect execution of A3 by F12, (d) correct execution of A3 by F14, (e) incorrect execution of A5 by F12, and (f) correct execution of A5 by F14.

5.5 Summary

This chapter proposes an IoT-FAR system, introduces a HML-based network for recognising firefighting SCBA endurance training activities, leveraging the integration of multiple models with multi-sensory wearable devices. The research utilises the SVM-RBF model in the MA and RF model in both MU and ML models to construct the proposed HML-SVM-RBF1-RF2 network, achieving the highest MAC of 98.29%. The results indicate that while integrating multiple sensors enhances recognition rates, it introduces computational complexity. The findings suggest that utilising sensors placed on the body and dominant hand is acceptable and highly sufficient for activity recognition with lower computational cost. However, sEMG features lack distinguishing patterns, necessitating further exploration for improved differentiation of training activities in real-world applications. The study also demonstrates the potential of using misclassification results as an evaluation tool for training activities.

Chapter 6

Conclusion and Future Work

This thesis introduces the development of a wearable FRAS for classifying specialised firefighting activities and detecting fall-related abnormal behaviours using multi-sensory fusion methods. Through the three studies presented, an effective IoT-based wearable FRAS was designed to enhance risk awareness on the fireground with activity monitoring and an early risk warning mechanism. This chapter comprehensively summarises the work conducted, discusses its limitations, and outlines potential future research directions.

6.1 Research Work Summary

This research explores the development of an advanced wearable FRAS for firefighters, deploying HAR and FDS algorithms using multi-sensory fusion. Three studies are conducted with ROs focused on improving FDS performance in accuracy and efficiency, exploring the PI-FDS algorithm on the edge, and developing effective FAR with an IoT framework to address the identified RQs. The details are as follows:

RQ1: *How can a reliable model be designed for assessing firefighter risk?*

This research begins with the development of a fall detection model as a preliminary step to assess the safety risks faced by firefighters. In response to RQ1, RS1 investigates the trade-off between fall event classification performance and the design of wearable sensing methods, including the placement of IMUs on different body parts

and the optimal number of IMUs for sensor fusion techniques. The results indicate that while utilising more IMUs can provide high classification accuracy, using only IMUs placed on the chest, elbows, and thighs yields acceptable performance, as validated by collaborating firefighters. A novel attitude-based feature extraction method is proposed to identify and use only the most informative features for fall event classification, significantly reducing processing time and allowing the deployment of the classification model on the device itself.

RQ2: *How can the PI-FDS model be designed for practical firefighting scenarios?*

To develop the practical PI-FDS system in firefighting scenarios, RS2 designs an IoT-based wearable system framework to improve data transmission between indoor and outdoor environments, enabling timely notification of any risks in firefighting contexts. Additionally, RS2 resolves the class imbalance issue of PI-FDS algorithm through a proposed dynamic thresholding approach named CIT method. Various ML methods are constructed and evaluated to find the optimal PI-FDS model that can be deployed on an edge device.

RQ3: *How can an efficient FAR model be designed to accurately distinguish between firefighting activities?*

RS3 addresses RQ3 by implementing a sensor fusion technique utilising IMUs and sEMG sensors to detect firefighting SCBA endurance training activities. The findings indicate that activity recognition performance is impacted by the accuracy of motion in completing the training tasks. The study shows that the proposed model can identify firefighters who completed tasks using incorrect motions, suggesting the potential to expand the model as a measurement standard for evaluating firefighter

training performance. The proposed HML-based network significantly improves HAR performance on distinguishing complex activities.

6.2 Research Contributions Summary

This research proposes a Firefighting Risk Assessment System (FRAS) framework, utilising a sensor fusion approach to differentiate firefighting activities and assess safety risks by detecting various fall events. The study also leads to the formation of two significant datasets:

- Simulated fall events dataset (see Chapter 3.3.2): Covering pre-impact fall data, especially the types of falls occurring during firefighting tasks, based on experiences from senior firefighters. (Available from: https://github.com/HCI-Laboratory/Smart-Firefighting/tree/main/Fall%20Detection.)

- Firefighting SCBA endurance training dataset (see Chapter 5.3.2): IMUs and surface electromyography (sEMG) data collected from firefighters during the training, which took place in multiple floors of different buildings. (Available from: https://github.co m/HCI-Laboratory/Smart-Firefighting/tree/main/Firefighter-Activity-Recognition.)

These datasets are valuable resources for the research community, facilitating the development of more reliable firefighter activity recognition models to enhance firefighter safety. Additionally, this research introduces an IoF network that integrates BLE for short-range communication and LoRa for long-range data transmission, addressing communication challenges in harsh fire environments. These contributions have advanced the

realisation of smart firefighting concepts, with a strong focus on improving firefighters safety.

6.3 Limitations and Future Research Directions

6.3.1 Improvement of Safety Risk Assessment Model

The FDS-based safety risk assessment model presented in this thesis is developed using simulated fall experiments to ensure firefighter safety. However, the dataset's validity is limited concerning real-world situations, as most falls occur unpredictably. Future research will explore multi-sensory methods to improve PI-FDS performance by utilising additional sensor data, such as physiological data (e.g., heart rate and blood pressure) and fireground environmental data (e.g., smoke concentration). Further work will also assess the hardware's energy efficiency and durability in fireground conditions, for instance, focusing on waterproofing and heat resistance.

6.3.2 High Stability of FRAS in Different Firefighting Scenarios

The FRAS algorithm is developed based on the SFTAA dataset. However, SCBA endurance training is a relatively straightforward programme conducted in non-realistic fire scenarios, lacking real fire and smoke. This limitation results in less discriminative patterns in sEMG and heart rate data, as it fails to simulate nervous and dangerous environments adequately. Future work plans to enrich the SFTAA dataset by including various training activities, especially in highly realistic simulated fire scenes. Further improvements in classification models are necessary to develop a high stability FRAS for practical use. In addition, expanding the IoT-FAR to integrate a large-scale firefighting network architecture, potentially spanning regions or even nationally, is to be explored,

in order to form a smart IoF infrastructure.

6.3.3 Firefighting Training Performance Assessment Metrics

This thesis discusses the diversity of firefighters' motion behaviours, identifying it as a main factor limiting the classification performance of complex FAR algorithms. Feedback from firefighters indicates that some activities during training experiments may be performed incorrectly due to a lack of physical strength, leading to improper training and potential safety risks in real firefighting scenarios. Future research will explore novel firefighting training performance assessment metrics using multi-sensory fusion approaches to improve firefighting skills.

References

[1] X. Zhang, M. Zhang, F. Meng, Y. Qiao, S. Xu, and S. Hour, "A low-power wide-area network information monitoring system by combining nb-iot and lora," *IEEE Internet of Things Journal*, vol. 6, no. 1, pp. 590–598, 2019.

[2] S. Ould, M. Guertler, P. Hanna, and N. S. Bennett, "Internet-of-things-enabled smart bed rail for application in hospital beds," *Sensors*, vol. 22, no. 15, 2022.

[3] *China Fire Protection Yearbook 2020*. Ministry of Emergency Management Publishing House, 2020.

[4] M. Fan, Q. Yang, S. Feng, C. Zhao, and j. Pu, "Research on causalites of firefighters in various firefighting and rescue tasks," *Industrial Safety and Environmental Protection*, vol. 41, no. 2, 2015.

[5] N. Brushlinsky, M. Ahrens, S. Sokolov, and P. Wagner, "World fire statistics," https://ctif.org/sites/default/files/2021-06/CTIF_Report26_0.pdf, 2021, (accessed on 05.08.2021).

[6] Z. Sun, "Research on safety safeguard measures for fire fighting and rescue," *Fire Daily*, (in Chinese).

[7] W. Fu, "Influencing factors and coping strategies of firefighter training lassitude," *Journal of Science and Technology*, vol. 7, 2022.

[8] H. Yuan, "Influencing factors and coping strategies of firefighter training lassitude," *Journal of China People's Police University*, vol. 30, no. 2, 2014.

[9] *China Fire Protection Yearbook 2018*. Yunnan People's Publishing House, 2018. [Online]. Available: https://books.google.co.jp/books?id=aFnMxQEACAAJ

[10] R. F. Fahy and J. L. Molis, "Firefighter fatalities in the us-2018," https://www.nfpa.org/-/media/Files/News-and-Research/Fire-statistics-and-reports/Emergency-responders/2019FFF.ashx, (accessed on 19.05.2021).

[11] A. Elliot and I. McGregor, "Fass: Firefighter audio safety systems," in *Proceedings of the 18th International Audio Mostly Conference*. New York, NY, USA: Association for Computing Machinery, 2023, p. 177–184.

[12] S. M. M. Islam and K. H. Talukder, "Exploratory analysis of smartphone sensor data for human activity recognition," *IEEE Access*, vol. 11, pp. 99 481–99 498, 2023.

[13] D. Chen, S. Yongchareon, E. M.-K. Lai, J. Yu, Q. Z. Sheng, and Y. Li, "Transformer with bidirectional gru for nonintrusive, sensor-based activity recognition in a multiresident environment," *IEEE Internet of Things Journal*, vol. 9, no. 23, pp. 23 716–23 727, 2022.

[14] J. Huang, S. Lin, N. Wang, G. Dai, Y. Xie, and J. Zhou, "Tse-cnn: A two-stage end-to-end cnn for human activity recognition," *IEEE Journal of Biomedical and Health Informatics*, vol. 24, no. 1, pp. 292–299, 2020.

[15] G. Vavoulas, M. Pediaditis, E. G. Spanakis, and M. Tsiknakis, "The mobifall dataset: An initial evaluation of fall detection algorithms using smartphones," in *13th IEEE International Conference on BioInformatics and BioEngineering*, 10-13 November 2013, pp. 1–4.

[16] C. Medrano, R. Igual, I. Plaza, and M. Castro, "Detecting falls as novelties in acceleration patterns acquired with smartphones," *PloS one*, vol. 9, p. e94811, 04 2014.

[17] T. Vilarinho, B. Farshchian, D. G. Bajer, O. H. Dahl, I. Egge, S. S. Hegdal, A. Lones, J. N. Slettevold, and S. M. Weggersen, "A combined smartphone and smartwatch fall detection system," in *2015 IEEE International Conference on Computer and Information Technology; Ubiquitous Computing and Communications; Dependable, Autonomic and Secure Computing; Pervasive Intelligence and Computing*, 2015, pp. 1443–1448.

[18] K. Desai, P. Mane, M. Dsilva, A. Zare, P. Shingala, and D. Ambawade, "A novel machine learning based wearable belt for fall detection," in *2020 IEEE International Conference on Computing, Power and Communication Technologies (GUCON)*, 2020, pp. 502–505.

[19] X. Chen, S. Jiang, and B. Lo, "Subject-independent slow fall detection with wearable sensors via deep learning," in *2020 IEEE SENSORS*, 25-28 October 2020, pp. 1–4.

[20] Y. Yan and Y. Ou, "Accurate fall detection by nine-axis imu sensor," in *2017 IEEE International Conference on Robotics and Biomimetics (ROBIO)*, 5-8 December 2017, pp. 854–859.

[21] C.-L. Lin, W.-C. Chiu, T.-C. Chu, Y.-H. Ho, F.-H. Chen, C.-C. Hsu, P.-H. Hsieh, C.-H. Chen, C.-C. K. Lin, P.-S. Sung, and P.-T. Chen, "Innovative head-mounted system based on inertial sensors and magnetometer for detecting falling movements," *Sensors*, vol. 20, no. 20, 2020. [Online]. Available: https://www.mdpi.com/1424-8220/20/20/5774

[22] T. Gu, L. Wang, Z. Wu, X. Tao, and J. Lu, "A pattern mining approach to sensor-based human activity recognition," *IEEE Transactions on Knowledge and Data Engineering*, vol. 23, no. 9, pp. 1359–1372, 2011.

[23] H.-L. Le, D.-N. Nguyen, T.-H. Nguyen, and H.-N. Nguyen, "A novel feature set extraction based on accelerometer sensor data for improving the fall detection system," *Electronics*, vol. 11, no. 7, 2022.

[24] P. Van Thanh, T. Nguyen, H. Nga, L. Thi, T. Ha, D. Lam, N. Chinh, and D.-T. Tran, "Development of a real-time supported system for firefighters in emergency cases," *International Conference on the Development of Biomedical Engineering in Vietnam*, 06 2016.

[25] P. Van Thanh, Q. B. Le, D. A. Nguyen, N. D. Dang, H. T. Huynh, and D. T. Tran, "Multi-sensor data fusion in a real-time support system for on-duty firefighters," *Sensors*, vol. 19, no. 21, 2019. [Online]. Available: https://www.mdpi.com/1424-8220/19/21/4746

[26] R. Ge, "Xgboost-based human activity recognition algorithm using wearable smart devices," in *Proceedings of the 4th International Conference on Computing and Data Science (CONF-CDS 2022)*, vol. 2, 03 2023, pp. 352–358.

[27] J. Zhu, H. Chen, and W. Ye, "A hybrid cnn–lstm network for the classification of human activities based on micro-doppler radar," *IEEE Access*, vol. 8, pp. 24 713–24 720, 2020.

[28] P. Turaga, R. Chellappa, V. S. Subrahmanian, and O. Udrea, "Machine recognition of human activities: A survey," *IEEE Transactions on Circuits and Systems for Video Technology*, vol. 18, no. 11, pp. 1473–1488, 2008.

[29] M. Abdel-Basset, H. Hawash, V. Chang, R. K. Chakrabortty, and M. Ryan, "Deep learning for heterogeneous human activity recognition in complex iot applications," *IEEE Internet of Things Journal*, vol. 9, no. 8, pp. 5653–5665, 2022.

[30] B. Fu, N. Damer, F. Kirchbuchner, and A. Kuijper, "Sensing technology for human activity recognition: A comprehensive survey," *IEEE Access*, vol. 8, pp. 83 791–83 820, 2020.

[31] W. Qi, H. Su, and A. Aliverti, "A smartphone-based adaptive recognition and real-time monitoring system for human activities," *IEEE Transactions on Human-Machine Systems*, vol. 50, no. 5, pp. 414–423, 2020.

[32] T. T. Alemayoh, J. Hoon Lee, and S. Okamoto, "Deep learning based real-time daily human activity recognition and its implementation in a smartphone," in *2019 16th International Conference on Ubiquitous Robots (UR)*, 2019, pp. 179–182.

[33] D. Garcia-Gonzalez, D. Rivero, E. Fernandez-Blanco, and M. R. Luaces, "A public domain dataset for real-life human activity recognition using smartphone sensors," *Sensors*, vol. 20, no. 8, 2020.

[34] Y. Li, L. Yu, J. Liao, G. Su, H. Ammarah, L. Liu, and S. Wang, "A single smartwatch-based segmentation approach in human activity recognition," *Pervasive and Mobile Computing*, vol. 83, p. 101600, 2022.

[35] S. M. M. Islam and K. H. Talukder, "Exploratory analysis of smartphone sensor data for human activity recognition," *IEEE Access*, vol. 11, pp. 99 481–99 498, 2023.

[36] R. Zhu, Z. Xiao, Y. Li, M. Yang, Y. Tan, L. Zhou, S. Lin, and H. Wen, "Efficient human activity recognition solving the confusing activities via deep ensemble learning," *IEEE Access*, vol. 7, pp. 75 490–75 499, 2019.

[37] B. Barshan and A. Yurtman, "Classifying daily and sports activities invariantly to the positioning of wearable motion sensor units," *IEEE Internet of Things Journal*, vol. 7, no. 6, pp. 4801–4815, 2020.

[38] H. Han, G. Kim, S. Choi, A. Basu, and S. W. Yoon, "Human activity and correlated posture monitoring using earlobe-worn wearable sensor system and deep learning algorithm," *IEEE Sensors Journal*, vol. 24, no. 1, pp. 533–542, 2024.

[39] G. Ascioglu and Y. Senol, "Activity recognition using different sensor modalities and deep learning," *Applied Sciences*, vol. 13, no. 19, 2023.

[40] D. Anguita, A. Ghio, L. Oneto, X. Parra, J. L. Reyes-Ortiz *et al.*, "A public domain dataset for human activity recognition using smartphones." in *Esann*, vol. 3, 2013, p. 3.

[41] J. R. Kwapisz, G. M. Weiss, and S. A. Moore, "Activity recognition using cell phone accelerometers," *SIGKDD Explor. Newsl.*, vol. 12, no. 2, p. 74–82, mar 2011. [Online]. Available: https://doi.org/10.1145/1964897.1964918

[42] A. Reiss and D. Stricker, "Introducing a new benchmarked dataset for activity monitoring," in *2012 16th International Symposium on Wearable Computers*, 2012, pp. 108–109.

[43] B. Barshan and M. C. Yüksek, "Recognizing daily and sports activities in two open source machine learning environments using body-worn sensor units," *The Computer Journal*, vol. 57, no. 11, pp. 1649–1667, 2014.

[44] P. Bharti, D. De, S. Chellappan, and S. K. Das, "Human: Complex activity recognition with multi-modal multi-positional body sensing," *IEEE Transactions on Mobile Computing*, vol. 18, no. 4, pp. 857–870, 2019.

[45] C. Zhu and W. Sheng, "Realtime recognition of complex human daily activities using human motion and location data," *IEEE Transactions on Biomedical Engineering*, vol. 59, no. 9, pp. 2422–2430, 2012.

[46] S. Cheng, E. Bolívar-Nieto, and R. D. Gregg, "Real-time activity recognition with instantaneous characteristic features of thigh kinematics," *IEEE Transactions on Neural Systems and Rehabilitation Engineering*, vol. 29, pp. 1827–1837, 2021.

[47] R. Chavarriaga, H. Sagha, A. Calatroni, S. T. Digumarti, G. Tröster, J. del R. Millán, and D. Roggen, "The opportunity challenge: A benchmark database for on-body sensor-based activity recognition," *Pattern Recognition Letters*, vol. 34, no. 15, pp. 2033–2042, 2013.

[48] K. Kang, K. Rhee, and H.-C. Shin, "A precise muscle activity onset/offset detection via emg signal," in *2021 International Conference on Information Networking (ICOIN)*, 2021, pp. 633–635.

[49] S. S. Bangaru, C. Wang, and F. Aghazadeh, "Data quality and reliability assessment of wearable emg and imu sensor for construction activity recognition," *Sensors*, vol. 20, no. 18, 2020.

[50] A. Vijayvargiya, P. Singh, R. Kumar, and N. Dey, "Hardware implementation for lower limb surface emg measurement and analysis using explainable ai for activity recognition," *IEEE Transactions on Instrumentation and Measurement*, vol. 71, pp. 1–9, 2022.

[51] O. W. Samuel, M. G. Asogbon, Y. Geng, A. H. Al-Timemy, S. Pirbhulal, N. Ji, S. Chen, P. Fang, and G. Li, "Intelligent emg pattern recognition control method for upper-limb multifunctional prostheses: Advances, current challenges, and future prospects," *IEEE Access*, vol. 7, pp. 10 150–10 165, 2019.

[52] H. Zheng, Y. Chen, Y. Li, Z. Wang, J. Chen, and X. Zhu, "High-accuracy and fine-granularity human activity recognition method based on body rfid skeleton," *IEEE Transactions on Consumer Electronics*, vol. 70, no. 1, pp. 1040–1051, 2024.

[53] T. Aşuroğlu, "Complex human activity recognition using a local weighted approach," *IEEE Access*, vol. 10, pp. 101 207–101 219, 2022.

[54] J. Qi, P. Yang, M. Hanneghan, S. Tang, and B. Zhou, "A hybrid hierarchical framework for gym physical activity recognition and measurement using wearable sensors," *IEEE Internet of Things Journal*, vol. 6, no. 2, pp. 1384–1393, 2019.

[55] V. S. Nguyen, H. Kim, and D. Suh, "Attention mechanism-based bidirectional long short-term memory for cycling activity recognition using smartphones," *IEEE Access*, vol. 11, pp. 136 206–136 218, 2023.

[56] A. Mastakouris, G. Andriosopoulou, D. Masouros, P. Benardos, G.-C. Vosniakos, and D. Soudris, "Human worker activity recognition in a production floor environment through deep learning," *Journal of Manufacturing Systems*, vol. 71, pp. 115–130, 2023.

[57] J. Lasek and M. Gagolewski, "The winning solution to the aaia'15 data mining competition: Tagging firefighter activities at a fire scene," in *2015 Federated Conference on Computer Science and Information Systems (FedCSIS)*, 2015, pp. 375–380.

[58] Y. Geng, J. Chen, R. Fu, G. Bao, and K. Pahlavan, "Enlighten wearable physiological monitoring systems: On-body rf characteristics based human motion classification using a support vector machine," *IEEE Transactions on Mobile Computing*, vol. 15, no. 3, pp. 656–671, 2016.

[59] S. Mekruksavanich, P. Jantawong, N. Hnoohom, and A. Jitpattanakul, "Wearable-based activity recognition of construction workers using lstm neural networks," in *2022 37th International Technical Conference on Circuits/Systems, Computers and Communications (ITC-CSCC)*, 2022, pp. 1–4.

[60] T. Blecha, R. Soukup, P. Kaspar, A. Hamacek, and J. Reboun, "Smart firefighter protective suit - functional blocks and technologies," in *2018 IEEE International Conference on Semiconductor Electronics (ICSE)*, 15-17 August 2018, pp. C4–C4.

[61] M. Meina, A. Janusz, K. Rykaczewski, D. Slezak, B. Celmer, and A. Krasuski, "Tagging firefighter activities at the emergency scene: Summary of aaia'15 data mining competition at knowledge pit," in *2015 Federated Conference on Computer Science and Information Systems (FedCSIS)*, 2015, pp. 367–373.

[62] N. Zhang, Y. Song, D. Fang, Z. Gao, and Y. Yan, "An improved deep convolutional lstm for human activity recognition using wearable sensors," *IEEE Sensors Journal*, vol. 24, no. 2, pp. 1717–1729, 2024.

[63] R. Nair, M. Ragab, O. Mujallid, K. Mohammad, R. Mansour, and G. Viju, "Impact of wireless sensor data mining with hybrid deep learning for human activity recognition," *Wireless Communications and Mobile Computing*, vol. 2022, 03 2022.

[64] J. Zhang, Y. Liu, and H. Yuan, "Attention-based residual bilstm networks for human activity recognition," *IEEE Access*, vol. 11, pp. 94 173–94 187, 2023.

[65] R. Huan, C. Jiang, L. Ge, J. Shu, Z. Zhan, P. Chen, K. Chi, and R. Liang, "Human complex activity recognition with sensor data using multiple features," *IEEE Sensors Journal*, vol. 22, no. 1, pp. 757–775, 2022.

[66] O. Barut, L. Zhou, and Y. Luo, "Multitask lstm model for human activity recognition and intensity estimation using wearable sensor data," *IEEE Internet of Things Journal*, vol. 7, no. 9, pp. 8760–8768, 2020.

[67] J. Zhang, Y. Liu, and H. Yuan, "Attention-based residual bilstm networks for human activity recognition," *IEEE Access*, vol. 11, pp. 94 173–94 187, 2023.

[68] M. A. A. Al-qaness, A. Dahou, M. A. Elaziz, and A. M. Helmi, "Multi-resatt: Multilevel residual network with attention for human activity recognition using wearable sensors," *IEEE Transactions on Industrial Informatics*, vol. 19, no. 1, pp. 144–152, 2023.

[69] Y. Wang, X. Wang, H. Yang, Y. Geng, H. Yu, G. Zheng, and L. Liao, "Mhagnn: A novel framework for wearable sensor-based human activity recognition combining multi-head attention and graph neural networks," *IEEE Transactions on Instrumentation and Measurement*, vol. 72, pp. 1–14, 2023.

[70] S. Mekruksavanich, A. Jitpattanakul, K. Sitthithakerngkiet, P. Youplao, and P. Yupapin, "Resnet-se: Channel attention-based deep residual network for complex activity recognition using wrist-worn wearable sensors," *IEEE Access*, vol. 10, pp. 51 142–51 154, 2022.

[71] M.-K. Yi, W.-K. Lee, and S. O. Hwang, "A human activity recognition method based on lightweight feature extraction combined with pruned and quantized cnn for wearable device," *IEEE Transactions on Consumer Electronics*, vol. 69, no. 3, pp. 657–670, 2023.

[72] J. Liang, L. Zhang, C. Han, C. Bu, H. Wu, and A. Song, "A collaborative compression scheme for fast activity recognition on mobile devices via global compression ratio decision," *IEEE Transactions on Mobile Computing*, pp. 1–14, 2023.

[73] X. Yao, X. Shi, and F. Zhou, "Human activities classification based on complex-value convolutional neural network," *IEEE Sensors Journal*, vol. 20, no. 13, pp. 7169–7180, 2020.

[74] E. Uzunhisarcikli, E. Kavuncuoğlu, and A. T. Özdemir, "Investigating classification performance of hybrid deep learning and machine learning architectures on activity recognition," *Computational Intelligence*, vol. 38, no. 4, pp. 1402–1449, 2022.

[75] B. Vidya and S. P, "Wearable multi-sensor data fusion approach for human activity recognition using machine learning algorithms," *Sensors and Actuators A: Physical*, vol. 341, p. 113557, 2022.

[76] Q. Mascret, M. Bielmann, C.-L. Fall, L. J. Bouyer, and B. Gosselin, "Real-time human physical activity recognition with low latency prediction feedback using raw imu data," in *2018 40th Annual International Conference of the IEEE Engineering in Medicine and Biology Society (EMBC)*, 2018, pp. 239–242.

[77] M. E. Issa, A. M. Helmi, M. A. A. Al-Qaness, A. Dahou, M. Abd Elaziz, and R. Damaševičius, "Human activity recognition based on embedded sensor data fusion for the internet of healthcare things," *Healthcare*, vol. 10, no. 6, 2022.

[78] H. Yuan, S. Chan, A. P. Creagh, C. Tong, A. Acquah, D. A. Clifton, and A. Doherty, "Self-supervised learning for human activity recognition using 700,000 person-days of wearable data," *NPJ Digital Medicine*, vol. 7, no. 1, p. 91, 2024.

[79] S. A. Khowaja, P. Khuwaja, F. A. Dharejo, S. Raza, I. H. Lee, R. A. Naqvi, and K. Dev, "Refuseact: Representation fusion using self-supervised learning for activity recognition in next generation networks," *Information Fusion*, vol. 102, p. 102044, 2024.

[80] Y. Dong, R. Zhou, C. Zhu, L. Cao, and X. Li, "Hierarchical activity recognition based on belief functions theory in body sensor networks," *IEEE Sensors Journal*, vol. 22, no. 15, pp. 15 211–15 221, 2022.

[81] F. Samie, L. Bauer, and J. Henkel, "Hierarchical classification for constrained iot devices: A case study on human activity recognition," *IEEE Internet of Things Journal*, vol. 7, no. 9, pp. 8287–8295, 2020.

[82] J. V. Jeyakumar, A. Sarker, L. A. Garcia, and M. Srivastava, "X-char: A concept-based explainable complex human activity recognition model," *Proc. ACM Interact. Mob. Wearable Ubiquitous Technol.*, vol. 7, mar 2023.

[83] E. Casilari, J.-A. Santoyo-Ramon, and J.-M. Cano-Garcia, "Analysis of public datasets for wearable fall detection systems," *Sensors*, vol. 17, no. 7, 2017. [Online]. Available: https://www.mdpi.com/1424-8220/17/7/1513

[84] N. Noury, A. Fleury, P. Rumeau, A. Bourke, G. O. Laighin, V. Rialle, and J. Lundy, "Fall detection - principles and methods," in *2007 29th Annual International Conference of the IEEE Engineering in Medicine and Biology Society*, 2007, pp. 1663–1666.

[85] A. Iazzi, M. Rziza, and R. Oulad Haj Thami, "Fall detection system-based posture-recognition for indoor environments," *Journal of Imaging*, vol. 7, no. 3, 2021. [Online]. Available: https://www.mdpi.com/2313-433X/7/3/42

[86] C. Rougier and J. Meunier, "Demo: Fall detection using 3d head trajectory extracted from a single camera video sequence," *Journal of Telemedicine and Telecare*, vol. 11, 01 2005.

[87] S. Gasparrini, E. Cippitelli, S. Spinsante, and E. Gambi, "A depth-based fall detection system using a kinect® sensor," *Sensors*, vol. 14, no. 2, pp. 2756–2775, 2014.

[88] B. Jansen and R. Deklerck, "Context aware inactivity recognition for visual fall detection," in *2006 Pervasive Health Conference and Workshops*, 29 November - 1 December 2006, pp. 1 – 4.

[89] G. Diraco, A. Leone, and P. Siciliano, "An active vision system for fall detection and posture recognition in elderly healthcare," in *2010 Design, Automation Test in Europe Conference Exhibition (DATE 2010)*, 8-12 March 2010, pp. 1536–1541.

[90] B. Kwolek and M. Kepski, "Human fall detection on embedded platform using depth maps and wireless accelerometer," *Computer Methods and Programs in Biomedicine*, vol. 117, no. 3, pp. 489–501, 2014.

[91] D.-W. Lee, K. Jun, K. Naheem, and M. S. Kim, "Deep neural network–based double-check method for fall detection using imu-l sensor and rgb camera data," *IEEE Access*, vol. 9, pp. 48 064–48 079, 2021.

[92] B. Kwolek and M. Kepski, "Improving fall detection by the use of depth sensor and accelerometer," *Neurocomputing*, vol. 168, pp. 637–645, 2015. [Online]. Available: https://www.sciencedirect.com/science/article/pii/S0925231215007572

[93] S. Chen, W. Yang, Y. Xu, Y. Geng, B. Xin, and L. Huang, "Afall: Wi-fi-based device-free fall detection system using spatial angle of arrival," *IEEE Transactions on Mobile Computing*, pp. 1–1, 2022.

[94] Y. Hu, F. Zhang, C. Wu, B. Wang, and K. J. R. Liu, "Defall: Environment-independent passive fall detection using wifi," *IEEE Internet of Things Journal*, vol. 9, no. 11, pp. 8515–8530, 2022.

[95] Y. Wang, S. Yang, F. Li, Y. Wu, and Y. Wang, "Fallviewer: A fine-grained indoor fall detection system with ubiquitous wi-fi devices," *IEEE Internet of Things Journal*, vol. 8, no. 15, pp. 12 455–12 466, 2021.

[96] K. Nishio, T. Kaburagi, Y. Hamada, T. Matsumoto, S. Kumagai, and Y. Kurihara, "Construction of an aggregated fall detection model utilizing a microwave doppler sensor," *IEEE Internet of Things Journal*, vol. 9, no. 3, pp. 2044–2055, 2022.

[97] M. Mubashir, L. Shao, and L. Seed, "A survey on fall detection: Principles and approaches," *Neurocomputing*, vol. 100, p. 144–152, 01 2013.

[98] A. Ramachandran, A. Ramesh, and A. Karuppiah, "Evaluation of feature engineering on wearable sensor-based fall detection," in *2020 International Conference on Information Networking (ICOIN)*, 7-10 January 2020, pp. 110–114.

[99] L. Zhu, P. Zhou, A. Pan, J. Guo, W. Sun, L. Wang, X. Chen, and Z. Liu, "A survey of fall detection algorithm for elderly health monitoring," in *2015 IEEE Fifth International Conference on Big Data and Cloud Computing*, 26-28 August 2015, pp. 270–274.

[100] M. Waheed, H. Afzal, and K. Mehmood, "Nt-fds—a noise tolerant fall detection system using deep learning on wearable devices," *Sensors*, vol. 21, no. 6, 2021. [Online]. Available: https://www.mdpi.com/1424-8220/21/6/2006

[101] D. Liang, G. Zhao, Y. Guo, and L. Wang, "Pre-impact & impact detection of falls using wireless body sensor network," in *Proceedings of 2012 IEEE-EMBS International Conference on Biomedical and Health Informatics*, 2012, pp. 763–766.

[102] A. Wertner, P. Czech, and V. Pammer-Schindler, "An open labelled dataset for mobile phone sensing based fall detection," in *Proceedings of the 12th EAI International Conference on Mobile and Ubiquitous Systems: Computing, Networking and Services on 12th EAI International Conference on Mobile and Ubiquitous Systems: Computing, Networking and Services*. ICST (Institute for Computer Sciences, Social-Informatics and Telecommunications Engineering), 2015, p. 277–278.

[103] G. Vavoulas, C. Chatzaki, T. Malliotakis, M. Pediaditis, and M. Tsiknakis, "The mobiact dataset: Recognition of activities of daily living using smartphones," in *Proceedings of the International Conference on Information and Communication Technologies for Ageing Well and e-Health - ICT4AWE, (ICT4AGEINGWELL 2016)*, 21-22 April 2016, pp. 143–151.

[104] D. Micucci, M. Mobilio, and P. Napoletano, "Unimib shar: A dataset for human activity recognition using acceleration data from smartphones," *Applied Sciences*, vol. 7, no. 10, 2017. [Online]. Available: https://www.mdpi.com/2076-3417/7/10/1101

[105] J. A. Santoyo-Ramon, E. Casilari-Perez, and J. Cano-Garcia, "Analysis of a smartphone-based architecture with multiple mobility sensors for fall detection," *PLoS ONE*, vol. 11, 2018.

[106] P. V. Er and K. K. Tan, "Non-intrusive fall detection monitoring for the elderly based on fuzzy logic," *Measurement*, vol. 124, pp. 91–102, 2018. [Online]. Available: https://www.sciencedirect.com/science/article/pii/S0263224118302859

[107] N. Jia, "Detecting human falls with a 3-axis digital accelerometer," *A forum for the exchange of circuits, systems, and software for real-world signal processing*, vol. 43, 2009.

[108] P. Tsinganos and A. Skodras, "On the comparison of wearable sensor data fusion to a single sensor machine learning technique in fall detection," *Sensors*, vol. 18, no. 2, 2018.

[109] M. Selvaraj, V. Baltzopoulos, A. Shaw, C. Maganaris, J. Cullen, T. O'Brien, and P. Kot, "Stair fall risk detection using wearable sensors," in *2018 11th International Conference on Developments in eSystems Engineering (DeSE)*, 2018, pp. 108–112.

[110] O. Ojetola, E. Gaura, and J. Brusey, "Data set for fall events and daily activities from inertial sensors," in *Proceedings of the 6th ACM Multimedia Systems Conference*. New York, NY, USA: Association for Computing Machinery, 2015, p. 243–248.

[111] E. Casilari, J. A. Santoyo-Ramón, and J. M. Cano-García, "Umafall: A multisensor dataset for the research on automatic fall detection," *Procedia Computer Science*, vol. 110, pp. 32–39, 2017, 14th International Conference on Mobile Systems and Pervasive Computing (MobiSPC 2017) / 12th International Conference on Future Networks and Communications (FNC 2017) / Affiliated Workshops.

[112] A. Sucerquia, J. D. López, and J. F. Vargas-Bonilla, "Sisfall: A fall and movement dataset," *Sensors*, vol. 17, no. 1, 2017.

[113] L. Martinez-Villasenor, H. Ponce, J. Brieva, E. Moya-Albor, J. Nunez-Martínez, and C. Penafort-Asturiano, "Up-fall detection dataset: A multimodal approach," *Sensors*, vol. 19, no. 9, 2019. [Online]. Available: https://www.mdpi.com/1424-8220/19/9/1988

[114] F. Luna-Perejon, L. Munoz-Saavedra, J. Civit-Masot, A. Civit, and M. Dominguez-Morales, "Ankfall—falls, falling risks and daily-life activities dataset with an ankle-placed accelerometer and training using recurrent neural networks," *Sensors*, vol. 21, no. 5, 2021. [Online]. Available: https://www.mdpi.com/1424-8220/21/5/1889

[115] Y. Su, D. Liu, and Y. Wu, "A multi-sensor based pre-impact fall detection system with a hierarchical classifier," in *2016 9th International Congress on Image and Signal Processing, BioMedical Engineering and Informatics (CISP-BMEI)*, 2016, pp. 1727–1731.

[116] I. Kiprijanovska, H. Gjoreski, and M. Gams, "Detection of gait abnormalities for fall risk assessment using wrist-worn inertial sensors and deep learning," *Sensors*, vol. 20, no. 18, 2020. [Online]. Available: https://www.mdpi.com/1424-8220/20/18/5373

[117] J. Shi, D. Chen, and M. Wang, "Pre-impact fall detection with cnn-based class activation mapping method," *Sensors*, vol. 20, no. 17, 2020. [Online]. Available: https://www.mdpi.com/1424-8220/20/17/4750

[118] F. Hussain, F. Hussain, M. Ehatisham-ul Haq, and M. A. Azam, "Activity-aware fall detection and recognition based on wearable sensors," *IEEE Sensors Journal*, vol. 19, no. 12, pp. 4528–4536, 2019.

[119] H.-L. Le, D.-N. Nguyen, T.-H. Nguyen, and H.-N. Nguyen, "A novel feature set extraction based on accelerometer sensor data for improving the fall detection system," *Electronics*, vol. 11, no. 7, 2022.

[120] P. Vallabh, R. Malekian, N. Ye, and D. C. Bogatinoska, "Fall detection using machine learning algorithms," in *2016 24th International Conference on Software, Telecommunications and Computer Networks (SoftCOM)*, 2016, pp. 1–9.

[121] G. Anania, A. Tognetti, N. Carbonaro, M. Tesconi, F. Cutolo, G. Zupone, and D. De Rossi, "Development of a novel algorithm for human fall detection using wearable sensors," in *SENSORS, 2008 IEEE*, 2008, pp. 1336–1339.

[122] Y. Wu, Y. Su, R. Feng, N. Yu, and X. Zang, "Wearable-sensor-based pre-impact fall detection system with a hierarchical classifier," *Measurement*, vol. 140, pp. 283–292, 2019.

[123] F. A. S. Ferreira de Sousa, C. Escriba, E. G. Avina Bravo, V. Brossa, J.-Y. Fourniols, and C. Rossi, "Wearable pre-impact fall detection system based on 3d accelerometer and subject's height," *IEEE Sensors Journal*, vol. 22, no. 2, pp. 1738–1745, 2022.

[124] Z. Zhong, F. Chen, Q. Zhai, Z. Fu, J. P. Ferreira, Y. Liu, J. Yi, and T. Liu, "A real-time pre-impact fall detection and protection system," in *2018 IEEE/ASME International Conference on Advanced Intelligent Mechatronics (AIM)*, 2018, pp. 1039–1044.

[125] H. Jung, B. Koo, J. Kim, T. Kim, Y. Nam, and Y. Kim, "Enhanced algorithm for the detection of preimpact fall for wearable airbags," *Sensors*, vol. 20, p. 1277, 02 2020.

[126] M. Li, G. Xu, B. He, X. Ma, and J. Xie, "Pre-impact fall detection based on a modified zero moment point criterion using data from kinect sensors," *IEEE Sensors Journal*, vol. 18, no. 13, pp. 5522–5531, 2018.

[127] J. Xiao, W. Ren, X. Huang, and H. Wang, "A surface electromyography-based pre-impact fall detection method," in *2018 Chinese Automation Congress (CAC)*, 2018, pp. 681–685.

[128] A. Leone, G. Rescio, A. Caroppo, and P. Siciliano, "An emg-based system for pre-impact fall detection," in *2015 IEEE SENSORS*, 2015, pp. 1–4.

[129] G. Mezzina, F. Aprigliano, S. Micera, V. Monaco, and D. D. Venuto, "Eeg/emg based architecture for the early detection of slip-induced lack of balance," in *2019 IEEE 8th International Workshop on Advances in Sensors and Interfaces (IWASI)*, 2019, pp. 9–14.

[130] J. K. Lee, S. N. Robinovitch, and E. J. Park, "Inertial sensing-based pre-impact detection of falls involving near-fall scenarios," *IEEE Transactions on Neural Systems and Rehabilitation Engineering*, vol. 23, no. 2, pp. 258–266, 2015.

[131] G. Zhao, Z. Mei, D. Liang, K. Ivanov, Y. Guo, Y. Wang, and L. Wang, "Exploration and implementation of a pre-impact fall recognition method based on an inertial body sensor network," *Sensors*, vol. 12, no. 11, pp. 15 338–15 355, 2012.

[132] J. Liu and T. E. Lockhart, "Development and evaluation of a prior-to-impact fall event detection algorithm," *IEEE Transactions on Biomedical Engineering*, vol. 61, no. 7, pp. 2135–2140, 2014.

[133] N. Otanasap, "Pre-impact fall detection based on wearable device using dynamic threshold model," in *2016 17th International Conference on Parallel and Distributed Computing, Applications and Technologies (PDCAT)*, 2016, pp. 362–365.

[134] S. Liang, T. Chu, D. Lin, Y. Ning, H. Li, and G. Zhao, "Pre-impact alarm system for fall detection using mems sensors and hmm-based svm classifier," in *2018 40th Annual International Conference of the IEEE Engineering in Medicine and Biology Society (EMBC)*, 2018, pp. 4401–4405.

[135] L. Wang, M. Peng, and Q. Zhou, "Pre-impact fall detection based on multi-source cnn ensemble," *IEEE Sensors Journal*, vol. 20, no. 10, pp. 5442–5451, 2020.

[136] A. Celik, K. N. Salama, and A. M. Eltawil, "The internet of bodies: A systematic survey on propagation characterization and channel modeling," *IEEE Internet of Things Journal*, vol. 9, no. 1, pp. 321–345, 2022.

[137] Z. Qian, Y. Lin, W. Jing, Z. Ma, H. Liu, R. Yin, Z. Li, Z. Bi, and W. Zhang, "Development of a real time wearable fall detection system in the context of internet of things," *IEEE Internet of Things Journal*, pp. 1–1, 2022.

[138] S. U. R. Aqeel-ur Rehman, I. U. Khan, M. Moiz, and S. Hasan, "Security and privacy issues in iot," *International Journal of Communication Networks and Information Security (IJCNIS)*, vol. 8, no. 3, pp. 147–157, 2016.

[139] L. Gutiérrez-Madroñal, L. La Blunda, M. F. Wagner, and I. Medina-Bulo, "Test event generation for a fall-detection iot system," *IEEE Internet of Things Journal*, vol. 6, no. 4, pp. 6642–6651, 2019.

[140] K. J. O'Donovan, R. Kamnik, D. T. O'Keeffe, and G. M. Lyons, "An inertial and magnetic sensor based technique for joint angle measurement," *Journal of Biomechanics*, vol. 40, no. 12, pp. 2604–2611, 2007. [Online]. Available: https://www.sciencedirect.com/science/article/pii/S0021929007000103

[141] R. Mahony, T. Hamel, and J.-M. Pflimlin, "Nonlinear complementary filters on the special orthogonal group," *IEEE Transactions on Automatic Control*, vol. 53, no. 5, pp. 1203–1218, 2008.

[142] S. Madgwick, "An efficient orientation filter for inertial and inertial / magnetic sensor arrays," *Report x-io and University of Bristol (UK)*, vol. 25, pp. 113–118, 2010.

[143] C. Li, G. Teng, and Y. Zhang, "A survey of fall detection model based on wearable sensor," in *2019 12th International Conference on Human System Interaction (HSI)*, 25-27 June 2019, pp. 181–186.

[144] "Bno055 inertial measurement unit. available online:," https://item.taobao.com/item.htm?spm=a230r.1.14.16.282a69630O3V2r&id=541798409353&ns=1&abbucket=5#detail, (accessed on 10.05.2021).

[145] J. Antonio Santoyo-Ramón, E. Casilari, and J. Manuel Cano-García, "A study of the influence of the sensor sampling frequency on the performance of wearable fall detectors," *Measurement*, vol. 193, p. 110945, 2022.

[146] "Seeeduino xiao mcu. available online:," https://detail.tmall.com/item.htm?id=612336208350&spm=a1z09.2.0.0.48d12e8d1z1cxA&_u=ajtqea1c090, (accessed on 03.06.2021).

[147] "Tca9548a i2c multiplexer. available online:," https://detail.tmall.com/item.htm?id=555889112029&spm=a1z09.2.0.0.48d12e8d1z1cxA&_u=ajtqea191ec, (accessed on 19.05.2021).

[148] "Jdy-18 bluetooth low energy 4.2 module. available online:," https://detail.tmall.com/item.htm?id=561783372873&spm=a1z09.2.0.0.48d12e8d1z1cxA&_u=ajtqea15f8b, (accessed on 01.06.2021).

[149] "3.7v 400mah lthium-ion battery. available online:," https://item.taobao.com/item.htm?id=619553965700&ali_refid=a3_430008_1006:1102265936:N:%2BblvRi4iO%2FgjtUw1Rz5DMnH2RFqSzBpj:1cecdd7aee090b757014f8c1916c98e1&ali_trackid=1_1cecdd7aee090b757014f8c1916c98e1&spm=a230r.1.0.0, (accessed on 22.05.2021).

[150] Q. Li, J. A. Stankovic, M. A. Hanson, A. T. Barth, J. Lach, and G. Zhou, "Accurate, fast fall detection using gyroscopes and accelerometer-derived posture information," in *2009 Sixth International Workshop on Wearable and Implantable Body Sensor Networks*, 3-5 June 2009, pp. 138–143.

[151] F. Wu, H. Zhao, Y. Zhao, and H. Zhong, "Development of a wearable-sensor-based fall detection system," *International Journal of Telemedicine and Applications*, vol. 2015, pp. 1–11, 02 2015.

[152] S. Ahn, J. Kim, B. Koo, and Y. Kim, "Evaluation of inertial sensor-based pre-impact fall detection algorithms using public dataset," *Sensors*, vol. 19, no. 4, 2019. [Online]. Available: https://www.mdpi.com/1424-8220/19/4/774

[153] S. S. Saha, S. S. Sandha, and M. Srivastava, "Machine learning for microcontroller-class hardware: A review," *IEEE Sensors Journal*, vol. 22, no. 22, pp. 21 362–21 390, 2022.

[154] "Usr-lg220 lora gateway. available from:," https://www.pusr.com/products/industrial-lora-gateways-usr-lg220.html.

[155] T. von Marcard, B. Rosenhahn, M. J. Black, and G. Pons-Moll, "Sparse inertial poser: Automatic 3d human pose estimation from sparse imus," *Computer Graphics Forum*, vol. 36, no. 2, pp. 349–360, 2017.

[156] Y. Huang, M. Kaufmann, E. Aksan, M. J. Black, O. Hilliges, and G. Pons-Moll, "Deep inertial poser: Learning to reconstruct human pose from sparse inertial measurements in real time," *ACM Trans. Graph.*, vol. 37, no. 6, 2018.

[157] X. Yi, Y. Zhou, M. Habermann, S. Shimada, V. Golyanik, C. Theobalt, and F. Xu, "Physical inertial poser (pip): Physics-aware real-time human motion tracking from sparse inertial sensors," 2022.

[158] J. Hislop, M. Isaksson, J. McCormick, and C. Hensman, "Validation of 3-space wireless inertial measurement units using an industrial robot," *Sensors*, vol. 21, no. 20, 2021. [Online]. Available: https://www.mdpi.com/1424-8220/21/20/6858

[159] A. Saha, S. Rajak, J. Saha, and C. Chowdhury, "A survey of machine learning and meta-heuristics approaches for sensor-based human activity recognition systems," *Journal of Ambient Intelligence and Humanized Computing*, 05 2022.

[160] N. Mozaffari, J. Rezazadeh, R. Farahbakhsh, S. Yazdani, and K. Sandrasegaran, "Practical fall detection based on iot technologies: A survey," *Internet of Things*, vol. 8, p. 100124, 2019.

[161] D. Bhattacharya, D. Sharma, W. Kim, M. F. Ijaz, and P. K. Singh, "Ensem-har: An ensemble deep learning model for smartphone sensor-based human activity recognition for measurement of elderly health monitoring," *Biosensors*, vol. 12, no. 6, 2022.

[162] J. Zhang, J. Li, and W. Wang, "A class-imbalanced deep learning fall detection algorithm using wearable sensors," *Sensors*, vol. 21, no. 19, 2021.

[163] M. B. Rasheed, N. Javaid, T. A. Alghamdi, S. Mukhtar, U. Qasim, Z. A. Khan, and M. H. B. Raja, "Evaluation of human activity recognition and fall detection using android phone," in *2015 IEEE 29th International Conference on Advanced Information Networking and Applications*, 2015, pp. 163–170.

[164] O. Dehzangi and V. Sahu, "Imu-based robust human activity recognition using feature analysis, extraction, and reduction," in *2018 24th International Conference on Pattern Recognition (ICPR)*, 2018, pp. 1402–1407.

[165] S. M. Lundberg and S.-I. Lee, "A unified approach to interpreting model predictions," in *Proceedings of the 31st International Conference on Neural Information Processing Systems*. Curran Associates Inc., 2017, p. 4768–4777.

[166] Polar Verity Sense. Accessed: Apr. 21, 2023 [Online], Available: https://www.polar.com/en/products/accessories/polar-verity-sense/.

[167] MPU 6050. Accessed: Apr. 21, 2023 [Online], Available: https://invensense.tdk.com/products/motion-tracking/6-axis/mpu-6050/.

[168] J. Song, A. Zhu, Y. Tu, H. Huang, M. A. Arif, Z. Shen, X. Zhang, and G. Cao, "Effects of different feature parameters of semg on human motion pattern recognition using multilayer perceptrons and lstm neural networks," *Applied Sciences*, vol. 10, no. 10, 2020.

[169] X. Chai, R. Wu, M. Pike, H. Jin, W.-Y. Chung, and B.-G. Lee, "Smart wearables with sensor fusion for fall detection in firefighting," *Sensors*, vol. 21, no. 20, 2021.

[170] Raspberry Pi 4B. Accessed: May. 10, 2023 [Online], Available: https://www.raspberrypi.com/products/raspberry-pi-4-model-b/.

[171] X. Chai, B.-G. Lee, M. Pike, R. Wu, D. Chieng, and W.-Y. Chung, "Pre-impact firefighter fall detection using machine learning on the edge," *IEEE Sensors Journal*, vol. 23, no. 13, pp. 14 997–15 009, 2023.

[172] TinyPICO. Accessed: Apr. 29, 2023 [Online], Available: https://www.tinypico.com/.

[173] BME688. Accessed: Apr. 30, 2023 [Online], Available: https://www.adafruit.com/product/5046.

Appendix A

Wearable Prototype

Figure A.1 shows the wearable prototype we developed for FDS studies. The simulated fall events dataset is conducted based on this system.

Figure A.1: First version of the wearable prototype with wired connections developed in 2021.

Figure A.2 presents a new wearable prototype we designed with conductive fabrics to replace the fragile wired connections. However, after conducting some tests, we found that this design is still unstable; for example, sensor nodes may drop out during movement and wearing the processing unit at the back is uncomfortable and inconvenient.

Figure A.3 presents the final IoT-FAR system we designed with four IMU-EMG sensor nodes, an HR armband, and a coordinator unit. The SFTAA dataset is conducted based on this wearable prototype.

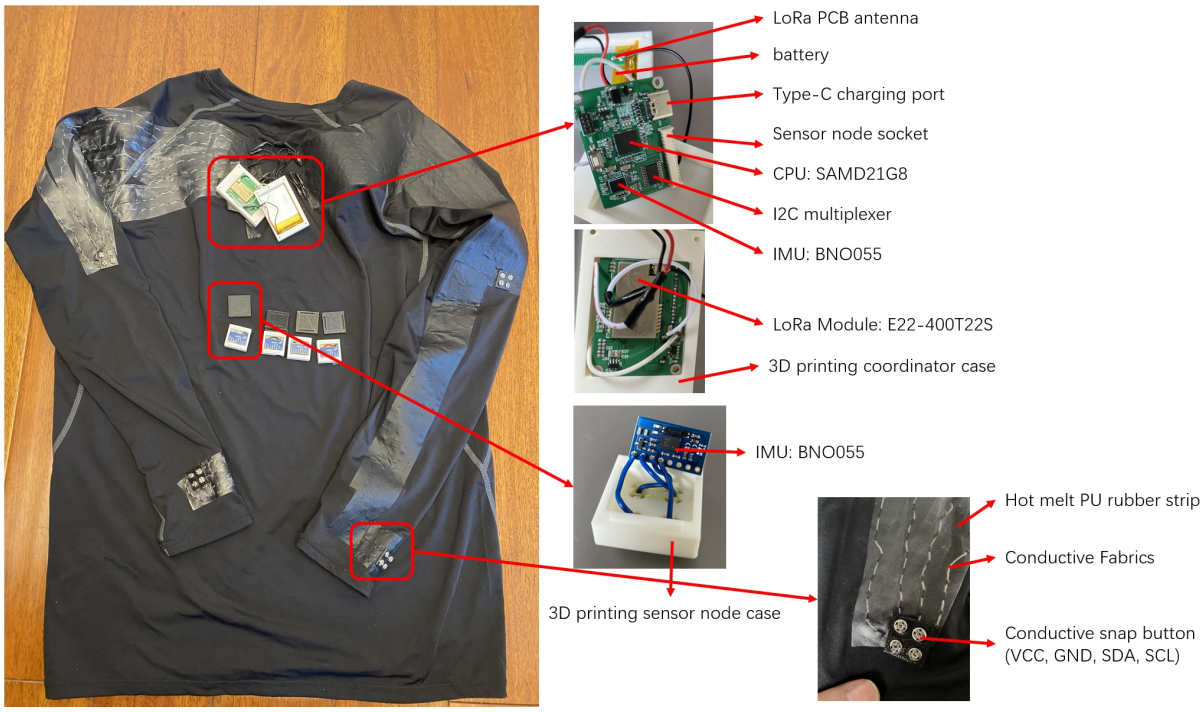

Figure A.2: Interim version of the wearable prototype with conductive fabrics developed in 2022.

(a) (b)

Figure A.3: Final version of the wearable prototype with wireless IoT design developed in 2023.

Appendix B

Experiments

Figure B.1: Experiments for SFTAA dataset collection in Nantaihu Fire Brigade, Huzhou, Zhejiang, China.

Figure B.2: The firefighter performs SCBA training with a safety supervisor.

Figure B.3: Firefighting rescue training with real fire and smoke.

Figure B.4: Firefighting training with real fire and smoke.

Figure B.5: Environmental experiment during the firefighting training with real fire and smoke.

Figure B.6: The environment of the fireground after firefighting is completed.

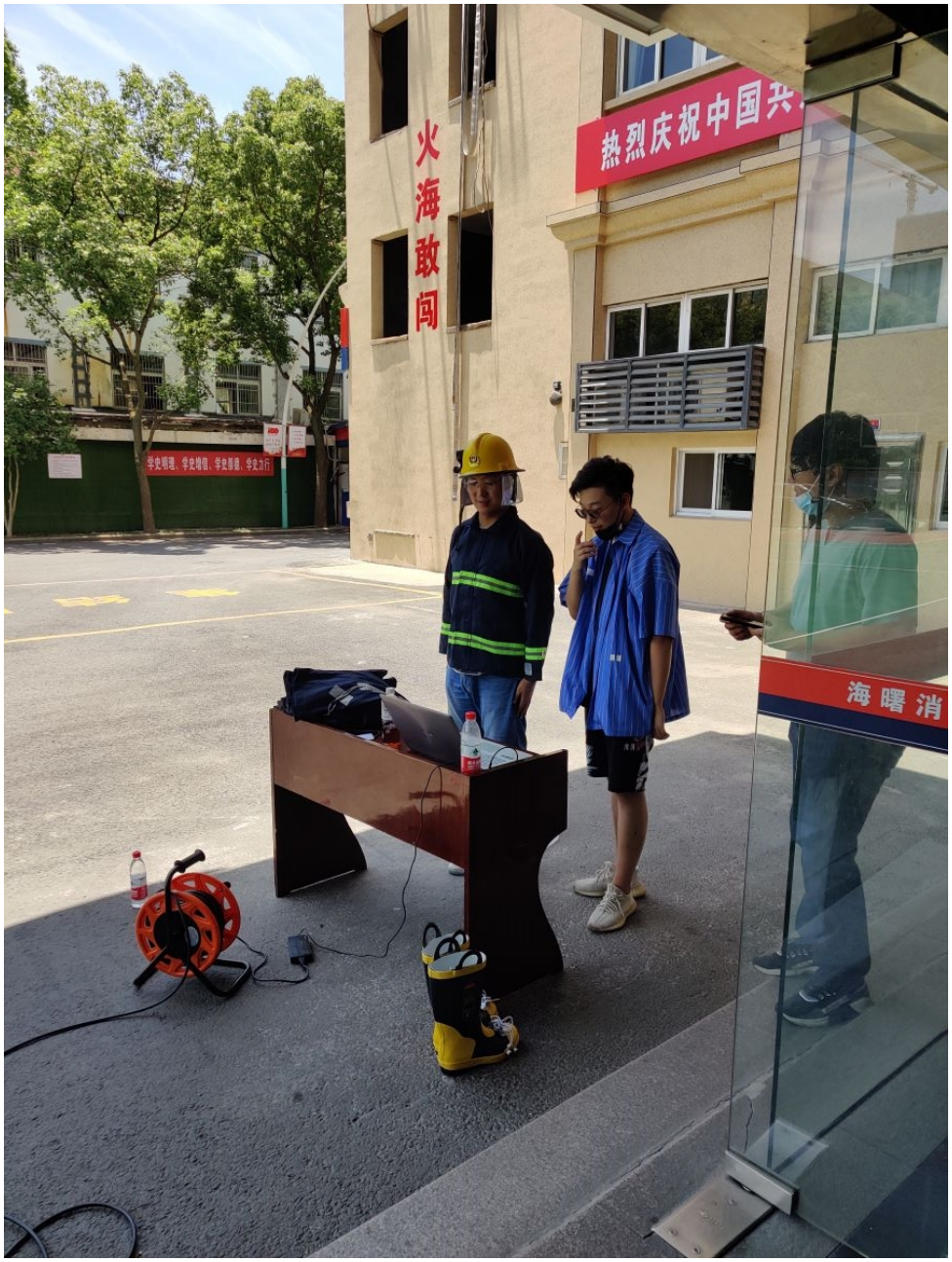

Figure B.7: Carrying out the simulated fall events data collection in Haishu Fire Brigade, Ningbo, China.

Figure B.8: Experiment of a simulated low visibility environment with a simulated smoke generator.

Figure B.9: Firefighter using an infrared thermal imager in low visibility environment.